SEQUENTIAL MEASUREMENT OF MULTIDIMENSIONAL TRANSDUCERS

J. R. SKLAR

Temp # 77829

TECHNICAL REPORT 431

OCTOBER 29, 1964

MASSACHUSETTS INSTITUTE OF TECHNOLOGY

RESEARCH LABORATORY OF ELECTRONICS

CAMBRIDGE, MASSACHUSETTS

The Research Laboratory of Electronics is an interdepartmental laboratory in which faculty members and graduate students from numerous academic departments conduct research.

The research reported in this document was made possible in part by support extended the Massachusetts Institute of Technology, Research Laboratory of Electronics, by the JOINT SERVICES ELECTRONICS PROGRAMS (U. S. Army, U. S. Navy, and U. S. Air Force) under Contract No. DA36-039-AMC-03200(E); additional support was received from the National Science Foundation (Grant GP-2495), the National Institutes of Health (Grant MH-04737-04), and the National Aeronautics and Space Administration (Grants NsG-334 and NsG-496).

The research reported in this document was also performed at Lincoln Laboratory, a center for research operated by the Massachusetts Institute of Technology, with the support of the United States Air Force under Contract AF19(628)-500.

MASSACHUSETTS INSTITUTE OF TECHNOLOGY

RESEARCH LABORATORY OF ELECTRONICS

Technical Report 431

LINCOLN LABORATORY

Technical Report 360

October 29, 1964

SEQUENTIAL MEASUREMENT OF MULTIDIMENSIONAL TRANSDUCERS

J. R. Sklar

This report is based on a thesis submitted to the Department of Electrical Engineering, M. I. T., September 23, 1964, in partial fulfillment of the requirements for the degree of Doctor of Philosophy.

Abstract

Although the problem of decoding tree-encoded messages in communications and that of measuring the parameters which describe a multidimensional transducer appear very different at first, striking similarities arise upon closer scrutiny. These similarities are most evident when each successive transducer output depends on an additional transducer parameter. Because of these similarities and because sequential decoding has been so successful in decoding tree-encoded messages, a study of the application of sequential decoding algorithms to measurements was undertaken.

This report analyzes a sequential algorithm suggested by R. M. Fano, Massachusetts Institute of Technology, and describes its application to measurement problems. From the analysis, bounds to the average number of computations needed to estimate one parameter are obtained. A bound is also derived for the probability of estimating at least one parameter of a set incorrectly. It will become apparent that when an attempt is made to differentiate between parameter values that produce too small an effect on the output, relative to the noise, the sequential method will fail. This difficulty determines a limit to the precision obtainable with the sequential method. This critical level may be likened to the computational cutoff rate in the corresponding communication problem.

A series of simulation experiments was performed to test the hypotheses and results of the theory. These experiments consisted of estimating the characteristic impedance values of the sections of a transmission line constructed of many short segments. This problem displays many of the features characteristic of geophysical layer determination. Although the theoretical and simulated measurement problems were not identical, the theoretical and experimental results agree, at least qualitatively. Thus it appears that further research is warranted on the application of sequential decoding to actual measurement problems.

TABLE OF CONTENTS

CONTENTS

SEQUENTIAL MEASUREMENT OF MULTIDIMENSIONAL TRANSDUCERS

I. INTRODUCTORY REMARKS

A. Introduction

One of the traditional areas of interest to the electrical engineer has been the design of measurement equipment. Historically, he first concentrated on measuring a single unknown parameter, trying to do so with a minimum of interference from other quantities. Then as time went on, it became necessary to measure two unknowns simultaneously and the complexity of measurement techniques increased. Today, the number of unknowns in measurement problems is typically even larger. We are therefore forced to develop techniques applicable to the measurement of a large number of parameters from data which depend on many of them simultaneously.

The interpretation of the data from such measurements is quite complicated. In particular, the data required to measure one parameter may depend on some of the other parameters whose values are not determined. Ideally, we could quantize the values of the parameters to some acceptable degree of precision, form all possible combinations of values for the system parameters, and determine from the instrument's internal relations the output for each such combination. Then we could compare the actual output with each of these postulated outputs, and choose as the measurement result that set of system parameters which produces the most favorable comparison. However, if each parameter takes on D values and there are N parameters, the number of combinations is D^N, which is extremely large even for relatively small values of D and N. It is therefore desirable to develop procedures not characterized by this exponential growth in computational load.

In this report, we consider such a problem. More specifically, we define a class of multidimensional measurement problems endowed with a so-called tree structure, and consider in detail an algorithm designed to determine the N unknown parameters by a number of computations that grows only linearly with N. The particular algorithm analyzed was introduced by Fano[1] for sequentially decoding tree-encoded messages transmitted over communication channels. We shall show how this technique can also be applied to measurements.

B. Measurement Problem

In most measurement problems, an observer attempts to assign estimated values to a set of unknown system parameters. We assume throughout the report that the observer knows which parameters characterize the system being measured and that he also knows the range of these parameters. With this information, the observer will be able to construct a general model of the system being measured and then, by estimating the unknown parameters, he will be able to

characterize it completely. Perhaps it is required that the estimates of the parameters satisfy some precision criterion. Generally, there is noise corrupting the measurement, thereby making the job more difficult. If this noise is too severe, it may be impossible to estimate the parameters with less than some specific error. Hopefully, analysis of the particular measurement problem permits the observer to determine in advance whether a specified measurement technique will satisfy the precision criterion.

A model of the system being measured, together with the measuring equipment, can be constructed as in Fig. 1. The probe signal, under the observer's control, enters the system which is described by the unknown parameters, and reacts with it. The result of the reaction is an output which is usually corrupted by noise before it becomes available to the observer. This distorted output then becomes available for processing, and the observer has the option of choosing the processing technique that will provide the best possible measurement.

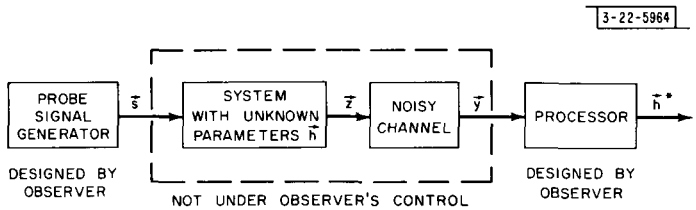

Fig. 1. Generalized measurement equipment.

In the cases of principal interest, the output depends on several parameters simultaneously. Assigning estimated values to these parameters (under a maximum likelihood criterion) involves finding the set of parameter values which maximizes the probability of the output, conditioned on these values. Since several parameters determine the output, one must find the maximum of a function of several variables. This search is known as a multidimensional "hill climb." Since the sequential decoding algorithms used for decoding tree-encoded messages perform such a hill climb in an efficient manner, the possibility of using an analogous procedure here suggests itself.

In the remainder of this report, we restrict our attention to additive noise, since it is the type most frequently encountered in measurement problems. On the basis of this assumption, we adopt the following terminology as illustrated in Fig. 1. Let $\vec{s}$ be a vector† with enough components to represent the probe signal; let $\vec{h}$ be a similar vector describing the unknown parameters; let $\vec{z}$ be the output of the system being measured when the probe signal $\vec{s}$ is applied; and let $\vec{y}$ be the output available to the observer as a noisy version of $\vec{z}$. If $\vec{n}$ is a vector describing the noise, the additive noise assumption implies

$$\vec{y} = \vec{z} + \vec{n} \quad .$$

C. Communication Problem

Since the motivation for the application of a sequential algorithm to measurements arose from certain similarities between measurement problems and communication problems, we shall

† In its most general sense, a vector can be regarded as an ordered set of quantities. Thus a vector of sample values can be used to represent a time signal and a vector of arbitrary numbers can be used to represent a set of parameters.

discuss the communication problem briefly. The general communication system is shown in Fig. 2. A message source is generating messages that must be transmitted to a user over a noisy channel. Because of the noise, the transmitted signal does not arrive at the receiver exactly as transmitted, but is corrupted by an unwanted effect imposed upon it by the channel. Thus errors are made in conveying the source message to the user.

Fig. 2. Generalized communication system.

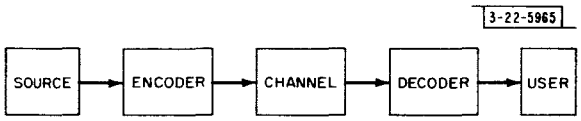

It is the communication engineer's job to design the encoder in such a way that the error probability is as low as possible. Shannon, in his classic paper,[2] considered this problem and introduced a measure of the information content of a message. By using this measure, he defined a rate of transmission in bits per second, and proved that, by proper encoding, communication over a noisy channel with as low a probability of error as desired is possible, provided that the rate of transmission does not exceed a fixed quantity, the channel capacity, which is determined by the noise characteristics of the channel. The proof was purely one of existence, and did not show explicitly how to construct good codes.

Since Shannon's paper appeared, information theorists have concerned themselves with the search for coding techniques[3] that permit communication with low error probability, and are also relatively simple to implement. The first codes investigated were called block codes and were designed to use on a binary channel. In these codes, a sequence of nR binary information symbols is encoded into a block of n binary symbols to be transmitted over the channel. Here R, the transmission rate, is the ratio of the number of information bits to the total number of transmitted bits. Shannon proved that there are block codes which yield an error probability that decreases exponentially with n, the block length. The rate at which this exponential decrease takes place indicates the quality of the code.

Although it was possible to prove the existence of good block codes from ensemble average arguments, it was difficult to find codes which had sufficient mathematical structure so that they could be encoded and decoded easily. Much of the difficulty arose from the fact that the block length n must be quite large to insure that the error probability be low. Thus the number of code words 2^{nR} must also be large for the communication to continue at a reasonable rate. Typically, 10^{30} code words might be used. Ideally, we could compare the received sequence of symbols with the transmitted sequence for each of these code words and, by some measure of distance, ascertain which code word is closest to the received word. However, the large number of comparisons makes this procedure undesirable, particularly since this number grows exponentially with block length. Those long codes which, because of mathematical structure, are simply decoded, suffer from a significantly higher error probability than theory shows can be obtained.

Several years ago, Wozencraft[4] proposed a sequential decoding procedure for decoding binary convolutionally encoded messages. As long as the rate did not exceed a particular quantity R_{comp} which is strictly less than the channel capacity, Wozencraft showed that the average number of computations needed to discard an incorrect symbol grew slowly with the constraint length (analogous to block length). In addition, under the same rate restriction, this overall encoding-decoding system gave the same error exponent as that for random block codes. Later this technique was generalized by Reiffen[5] for nonbinary alphabets. Recently, Fano[1] suggested an

alternate algorithm to sequentially decode tree-encoded messages. This method could be analyzed more completely than that of Wozencraft, and was shown to require an average number of computations per digit that is independent of constraint length.[6] These sequential decoding techniques will be described in more detail later.

D. Measurements Vs Communications

If the measurement problem discussed in Sec. I-B. is compared with the communication problem, some striking similarities appear. In both problems, a known vector quantity† reacts with an unknown vector quantity to produce a noise-free data vector. In both cases, there is a noise effect which prevents the user from observing the data vector directly and thereby determining uniquely and at once the values of the set of unknowns. In both instances, he can perform an exhaustive search to find the best estimate for these quantities; however, as previously discussed, this technique is unattractive. The only real difference lies in the form of the reaction between the known and the unknown vectors.

The transformation from the message symbols to the transmitted symbols carried out in the encoder for communications, and the transformation from the probe signal to the noise-free data vector in the measurement problem, may both be represented by the general transformation $T(\vec{s}, \vec{h})$. In the representation of the communications encoder, let $\vec{s}$ be the vector of encoding parameters and $\vec{h}$ the sequence of message symbols; in the representation of the system undergoing measurement, let $\vec{s}$ represent the probe signal and $\vec{h}$ the unknown parameters. Then in both communications and measurements, $\vec{s}$ and T are known to the user and it is his task to determine $\vec{h}$. Thus an additional similarity exists between the measurement and the communication problems.

However, it is at this point that a subtle difference arises. For in communications, the choice of T is at the disposal of the user, whereas in measurements, T, although known, is specified by the form of the system being measured. Thus the particular communication problem analogous to the general measurement problem is the study of a particular encoding technique where the objective of the study is to develop an efficient decoding procedure and to ascertain how well this procedure will operate.

Despite this difference, it is clear that the number of similarities is sufficiently large to suggest that an efficient communication technique might apply to measurement problems as well. More specifically, we have indicated above that the sequential decoding technique has permitted the multidimensional search, required to decode tree-encoded messages in communications, to be completed with a reasonable number of computations. We have also indicated that a similar multidimensional search occurs in interpreting measurement data. Thus the possibility of using a sequential method in measurement problems arises.

E. Objectives

In this report, we investigate the possibility of using a sequential processing method for measurements. First, we discuss the class of measurement problems which appear amenable to the application of a sequential method. In this connection, we shall discuss measures by which we can compare hypothesized noise-free output sequences ($\vec{z}$ in Fig. 1) with actual data vectors ($\vec{y}$ in Fig. 1); we shall define a tree structure which is required for the sequential method

† Again we refer to a vector in its most general sense.

to apply to a measurement problem; we shall suggest a further requirement, called the differential bias assumption, that guarantees the usefulness of the sequential method; and we shall introduce examples which seem to satisfy the above two requirements.

After describing the methods suggested by Wozencraft[4] and Fano[1] for sequential decoding, we analyze the Fano technique in detail. We show that the average number of computations to decode one branch of the tree is bounded by a constant. We also demonstrate that the probability of incorrectly estimating a parameter decreases exponentially with the number of available output samples dependent upon that parameter. For the case of white, Gaussian noise, graphs will be presented which show how the decoder's operation depends on the various quantities which are used to describe the decoder and on the noise level. It will become apparent that when we try to differentiate between parameter values that produce too small an effect on the output, relative to the noise, the sequential method will fail. Thus there is a parameter analogous to R_{comp}, the rate above which the sequential method fails in communications.

Finally, the results of a simulation of the sequential method used on a particular simplified measurement problem will be presented. It will be seen that the simulated behavior is very similar to the calculated behavior, thereby lending support to the assumptions made in analyzing the sequential method as applied to the measurement problem. The simulation results are for a model of the geophysical exploration problem, and a clearer understanding of the difficulties inherent in this problem came about through the simulation. Some thoughts in this area, particularly in connection with quantizing the unknown parameters, will be presented. Finally, some suggestions for future research will be made.

II. APPLICATION OF SEQUENTIAL METHOD TO MEASUREMENTS

A. Introduction

In this section, we consider specifically the application of a sequential method to measurements. First, we discuss metrics which must be used to define precisely the fit of a hypothesis to the data. Then we set forth the two requirements sufficient to prove that the Fano algorithm will be applicable. Next, we consider two examples toward which the sequential method may be applied. Finally, we describe the Wozencraft and Fano algorithms.

B. Metrics

In Sec. I-B, we considered estimating a set of parameters $\vec{h}$, by comparing the output vector $\vec{z}$, resulting from a particular $\vec{h}^*$ vector, to the received $\vec{y}$ vector. To carry out an algorithm, this notion must be made precise. We consequently define a quantity, hereafter denoted a metric,† which specifies the degree to which a fit is made.

Before specifying the particular metric that will be considered in this report, we recall the difference between maximum likelihood and maximum a posteriori estimation. Suppose there is a set of alternatives $\{a_i\}$, each occurring with the a priori probability $p(a_i)$. We are trying to choose which alternative produced the datum d. First, we could calculate the probability of each alternative, conditional on the datum $p(a_i/d)$, and choose as the estimate that alternative which maximized this function. This is referred to as maximum a posteriori estimation, since $p(a_i/d)$ is the a posteriori probability of the alternatives. We note that the calculation is made from Bayes rule,[7]

† The term metric is convenient but not strictly proper, since we do not require these metrics to have the mathematical properties of reflexivity, symmetry, and triangle inequality satisfaction.

$$p(a_i|d) = \frac{p(d|a_i)\, p(a_i)}{\sum_i p(d|a_i)\, p(a_i)} \quad .$$

Thus the a priori probabilities are used to carry out the a posteriori estimation method.

Generally, however, the a priori probabilities are not known explicitly. We must then take care not to introduce bias into the metric by the use of uncertain values for the a priori probabilities. The maximum likelihood approach should therefore be considered.

A maximum likelihood estimate is that value of the unknown parameter which maximizes the probability $p(d/a_i)$ of the datum, conditional on the parameter value. The maximum likelihood method has the benefit of being independent of the a priori knowledge, and thus is more convenient to implement. It is important to note that the maximum likelihood method is equivalent to the a posteriori probability method if the a priori probabilities are equal.

Discussions of the appropriateness of each technique are common in the statistical literature[7] and it could serve little purpose to continue them here. Suffice it to say, however, that if one's ability to perform a measurement depended critically on the a priori probabilities, then one would have little confidence in the result.

Because we seldom have reliable a priori information available in a measurement problem, and for the other reasons cited above, we restrict ourselves in this report to a maximum likelihood approach. Consequently, the decoding metric should be a monotone function of $p_{\vec{n}}(\vec{y}/\vec{z})$, the probability density function of the noise vector.† It is also desirable to define the metric in such a way that independent contributions to the total are additive. A metric with these properties is proportional to $\log p_{\vec{n}}(\vec{y}/\vec{z})$. If the noise samples are indeed independent and identically distributed, this becomes

$$\log p_{\vec{n}}(\vec{y}\,|\,\vec{z}) = \sum_j \log p_n(y_j|z_j) \quad .$$

On correct paths, the expected value of this metric is

$$\int p_{\vec{n}}(\vec{y}\,|\,\vec{z}) \log p_{\vec{n}}(\vec{y}\,|\,\vec{z})\, d(\vec{y}\,|\,\vec{z}) = -H(\vec{N})$$

where $H(\vec{N})$ is the entropy of the noise vector.

We shall see in the discussion of the Fano algorithm that the metric should increase on correct paths, while it should decrease on all others. Therefore, the metric for that algorithm will be chosen to be

$$M_k = \sum_{j=1}^{k} R + \ln p_n(y_j|z_j)$$

$$= kR + \sum_{j=1}^{k} d_j$$

† The subscript $\vec{n}$ specifies the noise probability density function.

where d_j is the incremental contribution to the metric due to the noise and R is a constant bias to be chosen later. If R exceeds the noise entropy, this metric will, on the average, be composed of positive increments on the incorrect path. If R is not chosen too large, and if the noise is not too great, it will be shown that the metric will, on the average, decrease on all incorrect paths.

C. Tree Structures

In the coupled parameter measurement problem, the observer has available the noisy data vector $\vec{y}$ and the probe signal $\vec{s}$ as well as some qualitative information about their relationship. This qualitative description is to be made explicit through the estimation of the unknown parameters designated by $\vec{h}$.

A general estimation procedure for this complex problem might consist of guessing values for all N components of $\vec{h}$ and comparing the resultant $\vec{z}$ vector with the received data vector $\vec{y}$. Then by varying the $\vec{h}$ components until all possible vectors are tested, the observer can choose the best fit to the data vector $\vec{y}$. As mentioned in the introduction, this would require an unrealistic number of attempts for any sizable number of $\vec{h}$ components.

Occasionally, it may be possible to find the best fit by guessing an $\vec{h}$ vector and then adjusting the guess, a component at a time, until the fit cannot be improved. However, this procedure has the pitfall of local maxima at which a poor fit gets poorer, no matter how the $\vec{h}$ components are individually varied. Another difficulty arising with this method is the so-called "plateau" problem whereby, for most guesses, the adjustment of any $\vec{h}$ parameter gives a negligible change in the fit.

In the class of problems to which the sequential algorithm applies, there is a structure known as a tree structure which permits these problems to be circumvented and is defined as follows. Suppose that each $\vec{h}$ is quantized to D levels so that there are D^N possible $\vec{h}$ vectors. Also suppose the components of $\vec{z}$ and $\vec{h}$ can be ordered so that

$$z_1 = f_1(h_1, \vec{s})$$

$$z_2 = f_2(h_1, h_2, \vec{s})$$

$$\vdots$$

$$z_i = f_i(h_1, h_2, \ldots, h_i, \vec{s}) \quad .$$

Then a tree can be constructed having nodes which represent the set of all $\vec{h}$ vectors having a common initial part. In this tree, a node at depth i represents all $\vec{h}$ vectors identical in the first i components. Since z_i is dependent only on the first i $\vec{h}$ components, a one-to-one correspondence exists between the D^i nodes at depth i and the D^i sets of $\vec{h}$ vectors where each set consists of the D^{N-i} vectors with a common prefix.

Once this tree structure is assumed, it becomes possible to perform the hill climb on an incremental basis. That is, one can estimate h_1 on the basis of y_1, and then, conditional on this value for h_1, consider h_2 using y_2 for comparison as well as y_1, etc. If the estimates are correct, these comparisons will continue to be satisfactory. However, if an error occurs at one stage due to a large noise sample, and if the effect of this incorrect hypothesis is to make the succeeding hypothesized $\vec{z}$ components different from the true $\vec{z}$ components, the error will

become apparent at later stages. When such evidence appears, the estimation of additional parameters should be halted, and the processor should concentrate instead on correcting the error. The sequential decoding algorithms are formalized procedures for making and correcting these estimates and will be discussed later in this section. First, however, we present examples of practical measurement interest which possess the tree structure defined above.

D. Example I. Impulse Response of Discrete Linear Filter

As a relatively simple example illustrating the use of a sequential measurement procedure, we consider a linear, time-invariant, time- and amplitude-discrete filter. Because of the linear aspect of this problem, linear regression techniques can be used to estimate the components of the filter in a much less complex manner than the sequential one. However, the linear filter is simple and familiar enough to be described easily. For completeness, the linear regression technique is briefly discussed in Appendix B.

It is assumed that the amplitude of the filter impulse response is quantized to one bit (two levels) and that a necessary and sufficient description of the filter is given by its response to an input pulse of unit amplitude. In addition, the input signal amplitude is also quantized to one bit and is time discrete in synchronism with the filter response. Gaussian noise samples are added to the filter output and the result is transmitted to the user, whose task is to determine the filter response given the input signal and the noisy output.

Part of the user's problem is to determine a satisfactory or perhaps even optimum (in some sense) input signal subject to some total energy constraint. Of course, the most obvious input is a sequence of unit pulses spaced sufficiently far apart to guarantee that the filter response has ended before a second response due to a second input pulse has begun. With such an input, since the symbols are independently disturbed by the noise, the only reasonable strategy is to determine the filter response components independently on the basis of the output components influenced by them. No sequential procedure suggests itself here and indeed none can logically be proposed, since there is no output component influenced by more than one component of the filter response.

However, because he may want to put energy into the filter more rapidly than this procedure allows under a peak-power constraint, the user may prefer to use a more complex input of shorter total duration than is permitted, if outputs are not to overlap. In this instance, a natural sequential procedure occurs and it is this procedure which will be discussed in the remainder of this section.

The system under consideration consists of an input signal $\vec{s}$, a filter response $\vec{h}$, an undisturbed filter output $\vec{z}$, a noise sequence $\vec{n}$, and a system output $\vec{y}$. The components of $\vec{s}$ and $\vec{h}$ take on the values (+1) and (−1), the components of $\vec{z}$ take on integral values, and $\vec{n}$ and $\vec{y}$ take on values in the continuum. For simplicity, we assume that the duration of $\vec{h}$ is known to be M units and that of $\vec{s}$ is N units.

Before describing the sequential procedure, the ideal measurement technique will be discussed. The undisturbed output $\vec{z}$ is an M + N − 1 component time-discrete signal and can therefore be plotted as a vector in an M + N − 1 dimensional vector space. The noisy output $\vec{y}$ can also be plotted in this same space and, if the noise level is not very high, will be a point not far from $\vec{z}$. Now it is the user's task to determine from $\vec{y}$ which of the 2^M possible vectors is the actual filter response. Since the input signal $\vec{s}$ is known, the user could theoretically compute the 2^M $\vec{z}$ vectors corresponding to the 2^M possible $\vec{h}$ vectors by convolving the known $\vec{s}$ with each one of them. Then the maximum likelihood filter response is that corresponding to the $\vec{z}$

closest to the output signal $\vec{y}$. The effect of choosing $\vec{s}$ is to move the 2^M $\vec{z}$ vectors in the output space; optimally, $\vec{s}$ should be choosen to minimize the probability of confusion between them. Practically, however, this method of measurement is not feasible, since the number of computations 2^N grow exponentially with the response duration.

We immediately note the similarity between this ideal procedure and that existing for the decoding of convolutionally encoded messages. In that case, too, the ideal method is impractical because of the exponential growth in the number of computations with constraint length. The sequential decoding procedure is designed to avoid this exponential growth and it would not seem surprising that it could be applied to obtain the same advantage in this measurement problem.

The key to the operation of a sequential procedure is the so-called tree structure. In the measurement problem the structure arises as follows. The input-output relationship for the filter is given by the well-known convolution integral (summation is due to the synchronous time-discrete input and filter response).

$$z_j = \sum_{i=0}^{j} h_i s_{j-i} \quad .$$

The indexing convention implies that only positive indices are meaningful. Therefore, we may write the first few equations as

$$z_o = h_o s_o$$

$$z_1 = h_o s_1 + h_1 s_o$$

$$z_2 = h_o s_2 + h_1 s_1 + h_2 s_o \quad , \quad \text{etc.}$$

Consequently, the two hypotheses for h_o lead to two hypotheses for z_o. Given each hypothesis for h_o, the two hypotheses for h_1 lead to two hypotheses for z_1, etc. The tree is therefore constructed by considering each path through the tree as a separate filter response and calculating for each branch the undisturbed filter output that would occur for the corresponding filter response. This is illustrated in Fig. 3.

After M postulates have been made, the entire filter response is determined. However, $N - 1$ components of $\vec{z}$ have not been compared with the corresponding components of $\vec{y}$. Although no choice remains, these components do contain information about the filter response components; therefore, they should be used in the measurement procedure. Consequently, there will be $N\vec{z}$ components corresponding to the last branch of the tree. We shall call this set of components the remainder set.

In the next section, we discuss a problem toward which the sequential procedure might realistically be applied.

E. Example II. Reflection Study of Geophysical Layers

In the simplified linear filter problem discussed in the preceding section, the applicability of the sequential measurement technique came about through the dispersive nature of the filter. The first M successive output pulses each depend on a filter response component that had not affected the previous output pulses. Thus a tree structure arose and the sequential procedure became feasible. However, because the outputs are linear functions of the unknown parameter,

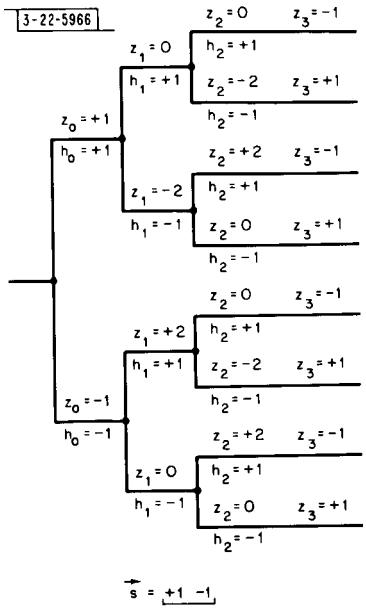

Fig. 3. Tree structure for a 3-component filter and a specific 2-component input.

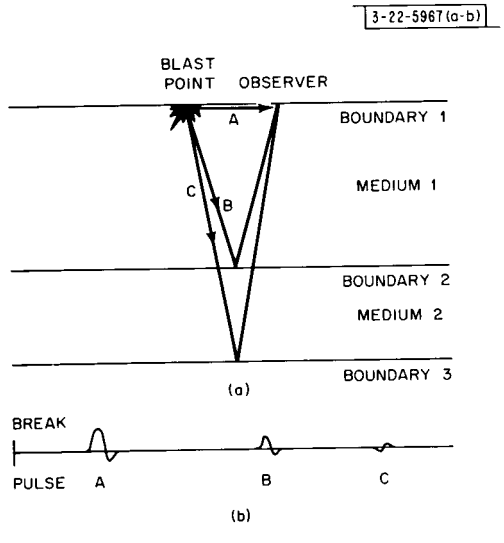

Fig. 4. Reflections from layered structures.

Note: The pulses are labeled in accordance with the path they followed.

the sequential method is inferior to a linear regression technique which is much less complex to instrument.

Of more practical interest is a problem in which the outputs are not linear fuctions of the unknown parameters, and we choose the geophysical exploration problem as an example for this discussion. Other examples might include radar investigation of targets with range extent and telephone line measurements by pulsed inputs. The geophysical problem was chosen partly because of the readiness with which the sequential technique could be adopted. However, it appears that all the information available to the observer is not utilized in geophysical work because of a lack of suitable data-processing techniques.

For about fifty years, artificially generated seismic waves have been used in the investigation of layered structures beneath the earth's surface. Although initially refraction studies were carried out exclusively, improvements in technique since World War II have brought about a broad changeover to reflection methods. Indeed, in many areas of geological exploration, such as in petroleum prospecting, the change is almost complete.

Generally speaking, the earth's structure is one of multiple layers of varying materials and of varying thicknesses. A seismic wave, initiated by the detonation of several pounds of explosive, travels downward through the earth's crust and is reflected, in part, at each boundary. Since the initial blast is pulse-like, pulses from the succeeding layers will arrive at the surface at later times which depend specifically on the propagating media, the location of the layers, and the location of the observation point. This is illustrated in Fig. 4(a-b). By observing the arrival times and amplitudes of these pulses, it is possible to deduce the layered structure of the subterrain.

The seismic waves propagate through the layers in a manner governed by the wave equation for an acoustic wave in an elastic medium. These waves travel with a velocity that depends on the medium, and at a boundary they are partially reflected and partially transmitted. It does not seem appropriate to discuss the pertinent equations in great detail, since there are many formal presentations available.[8] We may say, however, that the equations and their solution are perfectly analogous to those obtained in the study of electromagnetic plane waves traveling through dielectric media.

In particular, we can define a characteristic impedance of a medium Z_o, which is related to the velocity of propagation v and the medium's density ρ by

$$Z_o = \rho v \quad .$$

If a pulse of amplitude A propagating in a medium with characteristic impedance Z_{01} strikes perpendicularly to the boundary of a second medium with characteristic impedance Z_{02}, there will be a reflected pulse of amplitude

$$\frac{Z_{02} - Z_{01}}{Z_{02} + Z_{01}} \cdot A$$

and a transmitted pulse of amplitude

$$\frac{2Z_{02}}{Z_{02} + Z_{01}} \cdot A \quad .$$

On the basis of these amplitudes, it is possible to calculate the entire response of a given structure to an initial wave in terms of its amplitude and the various acoustic impedances. Note that

multiple reflections may simultaneously arrive at the observer and these must be accounted for in the calculation.

In the geophysical problem, however, the acoustic impedances are the objective of the measurement. At some time after the blast, the observed signal will be a very complex function of the many geophysical parameters. However, we shall soon see that there is a tree structure that simplifies the processing and makes a sequential technique the natural one.

Note, first, that the first response to the observer is a reflection from the first boundary and that its time of arrival indicates the thickness of the first layer while the amplitude, relative to the amplitude of the initial disturbance, permits the acoustic impedance of the second layer (assuming that of the first is known) to be determined. The next response is from the second boundary and gives information of the second layer's thickness and the third's impedance. Thus the layers may be considered sequentially and, as the measurement process continues, the effects of earlier layers may be removed from later data points.

From the above description of the seismic reflection problem, we can abstract a simplified model which was simulated as a basis for testing the sequential measurement technique.[9] Consider a transmission line of L sections each of the same length. Let the impedance of each section be one of the two quantities Z_A or Z_B. Let the reflected output of the line be available to the observer disturbed by Gaussian white noise of variance σ^2. Then the observer's objective is to determine the $\{Z_{on}\}$. In doing so, he may choose any input that best satisfies his objective.

Before proceeding to a more detailed description of sequential decoding, a few more remarks relative to the geophysical exploration problem are in order. When studying the data processing methods in this area, one is struck by the dearth of precise techniques. Indeed, long-term amplitude information is being generally discarded in favor of automatic volume control which permits a constant amplitude on the seismograph record without a need to calibrate. The chief argument for this approach has been that the amplitude of the test pulse generated by the blast is too variable. Only recently has the usefulness of the amplitude ratios been noted.[10] In addition, the majority of the seismographic data gathered in search of petroleum has been reduced by eye. Consequently, the skill of the reducer is of prime importance and any oversight by him could result in the waste of an expensive seismic survey.

Thus there is a strong need for automatic, precise data reduction techniques. Perhaps the sequential measurement technique will provide the basis for a practical, efficient method to process data from the seismic exploration of layered geophysical structures.

F. Sequential Decoding (According to Wozencraft)

In the preceding sections, we discussed sequential algorithms in general and indicated some typical problems to which they may apply. We next describe in detail the two procedures which have received the most attention. Although the bulk of this work will be concerned with an algorithm similar to that of Fano, we include for completeness a brief description of the sequential decoding technique introduced by Wozencraft[4] and generalized by Reiffen.[5]

The objective in the measurement problem is to determine which of the $\vec{z}$ vectors is "closest" to the $\vec{y}$ vector that has been received. The notion of closeness can be made explicit by defining a metric which is additive and increases with the size of the noise samples according to $\log p_{\vec{n}}(\vec{y}/\vec{z})$ where $p_{\vec{n}}(\vec{y}/\vec{z})$ is the probability density function of the noise vector. Suppose first that in terms of this quantity, one considers "radii" of constant metric around the received vector $\vec{y}$. Then one may ask if any of the vectors lies within a radius r_1 of $\vec{y}$. This question could

be answered by postulating the first j components of $\vec{h}$, computing the portion of the $\vec{z}$ vector determined by this subset of $\vec{h}$ components, and determining the portion of the total metric calculable on the basis of the partial hypothesis. Certainly, if the partial metric D_j exceeds r_1, the total metric will also. We will see later that the average number of computations is reduced if r_1 is varied as the depth into the tree increases. Therefore, those $\vec{z}$ vectors very distant from the received $\vec{y}$ will be eliminated from consideration before many of the components are tried. Since most of the 2^M $\vec{z}$ vectors are very different from $\vec{y}$, the number of computations will be greatly reduced and it is this reduction that permits, on the average, a linear rather than exponential growth in computation with N. If the D_j does not exceed r_1, then another component of $\vec{h}$ is postulated.

Suppose that none of the $\vec{z}$ vectors are within r_1 of $\vec{y}$. In that case, the procedure suggests repeating the procedure for $r_2 > r_1$. Eventually, the sphere will be enlarged sufficiently to include one of the $\vec{z}$ vectors and this one is considered the undisturbed filter output, and the corresponding filter response becomes the measurement result. It may happen that more than one $\vec{z}$ vector falls within an increased value of the radius and as a result the wrong response could be determined. This event is one of the possibilities for error and it will be assumed conservatively that whenever it does happen, an error results.

Clearly, the number of computations can be decreased, if the radii considered above are changed as the procedure successively postulates more $\vec{h}$ components. Since it is unlikely that a cumulative metric will increase very rapidly for small values of j and then very slowly for larger values in order that the total metric remains below r_k, a set of criterion functions $r_k(j)$ should be used which increase monotonically. This reduces the number of computations by causing any short path with rapidly increasing cumulative metric to be dropped from further consideration before the partial distance becomes equal to the maximum allowable distance. Of course, the correct path may have a metric which first increases rapidly and then much more slowly. Although such a path may be rejected under this procedure for the k^{th} criterion function, $r_k(j)$, it will prove to be acceptable for some other criterion function $r_{k'}(j)$, $k' > k$.

In the analysis of this technique, the number of computations for rejecting the incorrect branches at a node have been bounded, but the number for accepting the correct branch have not. The analysis of the Fano procedure permits a complete bound to the number of computations.

G. Sequential Decoding (According to Fano)

To determine the $\vec{z}$ vector closest to the received $\vec{y}$ vector, another related procedure, similar to that developed by Fano[1] for sequential decoding, can also be used. In this procedure, the paths through the encoding tree are also tested for cumulative distance, but the thresholding strategy differs greatly. A metric is used which tends to increase when the decoder is on the correct path and decrease when the incorrect path is followed. With such a measure, the analogous procedure is to postulate successive branches, to compute the total measure and then to compare this with a threshold. If the total measure crosses under the threshold, the branch is considered unacceptable and other branches from the previous node are tried until an acceptable branch is found stemming from it.

If this cannot be done, the procedure is to back off another node and to test branches stemming from it against a threshold that is just satisfactory. When the metric is chosen in such a way that the variation on the correct path will eventually put the total measure on the acceptable side

of the threshold, this search will eventually be successful. If the total does not cross the threshold, the threshold is adjusted by a multiple of a basic increment to just keep the current total metric satisfactory. This practice of following the total metric as closely as possible with the threshold serves to minimize the number of computations with a small loss in error exponent.

As indicated in Sec. II-B, the Fano algorithm requires a metric that increases on the correct path and decreases on incorrect ones. We have seen that the metric for n observation intervals

$$M_n = nR + \sum_{i=1}^{n} d_i$$

where d_i is the incremental contribution and R is a constant bias, has the desired properties.

The decoder will consider branches stemming from a node in order of decreasing metric. It will record previous decisions by means of a vector variable i(1), i(2), . . . , i(n) where i(n) is the order number of the branch selected by the decoder at depth n in the tree. Such a vector description of the decoder position requires the use of the first j vector components to determine the position at depth j.

The algorithm will best be described in connection with the flow chart of Fig. 5. Every time a branch of the tree is tested, the decoder is situated at the point marked "start." First the increment to the metric corresponding to the branch under test is computed and added to the cumulative metric M_n. The quantity M_{n+1} is then compared with the current threshold T. If $M_{n+1} \geq T$, the branch is deemed satisfactory to the decoder which then follows loop A and proceeds to test a new branch beyond the one just tested. When the successful branch is under test for the first time, the threshold is raised until it obtains its maximum permissible value below M_{n+1}. If the branch has been tested previously, the threshold should remain at the original level.

The remainder of the flow chart deals with unsatisfactory branches. Since the branches stemming from a node are tested in order of decreasing metric, the failure of one branch immediately implies the failure of all branches at that node for the present threshold. Therefore, the decoder must return to a previous node to seek a satisfactory branch. Before testing, if branches

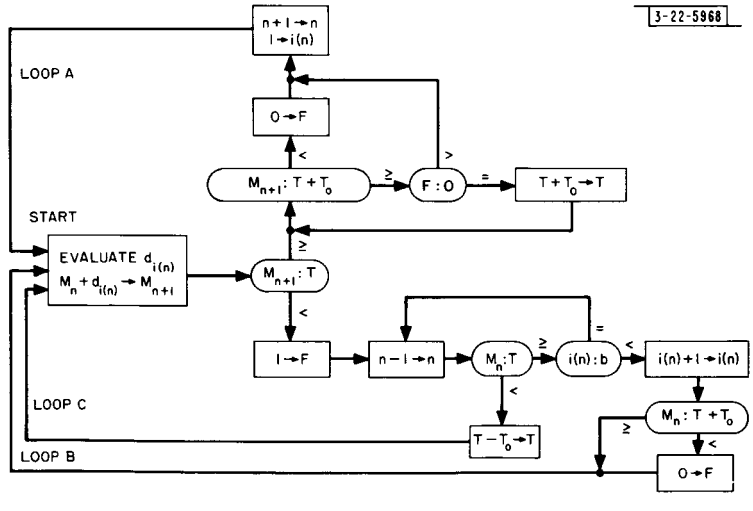

Fig. 5. Flow chart of the sequential decoding procedure (A → B indicates: set B equal to A).

from that node are satisfactory, it is necessary to test the cumulative metric at the node itself. If $M_n < T$, the decoder lowers the threshold by T_o and then searches to see if there is a path remaining above the new threshold setting. If $M_n \geq T$, other less likely branches are tested to see if they lead to paths remaining above T.

The decoder must take care not to raise the threshold on a path that has already been tested. The procedure operates by testing thresholds in order of decreasing value, and if one proves unsatisfactory, no higher threshold should be used until virgin territory is reached. We see in Fig. 5 that F = 0 whenever a new path is followed and that F = 1 whenever one is being retraced. F is set to one whenever a path falls below a threshold T'. If the threshold is then lowered to $T' - T_o$, the decoder will continue to retrace branches already investigated until it finds one that exceeds $T' - T_o$ but is below T'. This is the first new branch to be tested and F is reset to zero. If the decoder does not lower the threshold, but instead backs up to an earlier node with several paths above T', it will search a <u>new</u> path only if one remains below $T' + T_o$. Otherwise, the decoder would have raised the threshold to $T' + T_o$ when it reached this node for the first time.

The operation of the algorithm will be best understood by the reader if he follows its operation in typical cases in detail. Figure 6 is a sequence of display photographs resulting from the simulation of the decoder operating on a model of a geophysical exploration problem of the type discussed in Sec. II-E. These photographs illustrate the more important cases that occur during the decoder's operation. This display follows the acceptance of a choice in loop A of the decoder before the threshold is raised for this newly accepted branch.

H. Differential Bias Assumption

In Sec. I-D, we noted a basic difference in the freedom available in communications for introducing redundancy and that available in measurements. In communications, there is the freedom to design the encoder in a way that will make the set of possible transmitted sequences as different among themselves as possible. Once such an encoder is chosen, certain parameters are chosen to optimize the encoder's performance. The analysis of this performance is usually based on the average behavior over the ensemble of parameter values. We are thus guaranteed that there is at least one set of parameters which would provide this average behavior.

In measurements, however, this possibility does not exist. Although we have the freedom to choose the probe signal, the set of possible transmitted sequences is highly constrained by the device being measured. Consequently, it could well happen that the various hypothesized parameter vectors produce almost identical sequences of noise-free outputs, no matter how the probe signal is chosen. In such a case, measurements that would distinguish among the vectors would be difficult.

The notion of coding in communications is different from that in measurements. In both areas, coding is essential, since there must be some redundancy in the noise-free data to indicate to the decoder when it has erred. Unless an incorrect hypothesis at some point leads the decoder to a node in the tree at which every hypothesized output differs from the correct output for that tree depth, the decoder will never be able to ascertain its error. Otherwise there would always be some incorrect path through the tree identical in its output sequence to the correct output sequence. In communications, this characteristic of the tree code is obtained by reducing the rate and picking the code words at each node independently and at random. In measurements, the characteristic must be provided by the device under measurement itself.

-22-5439 (a-d)

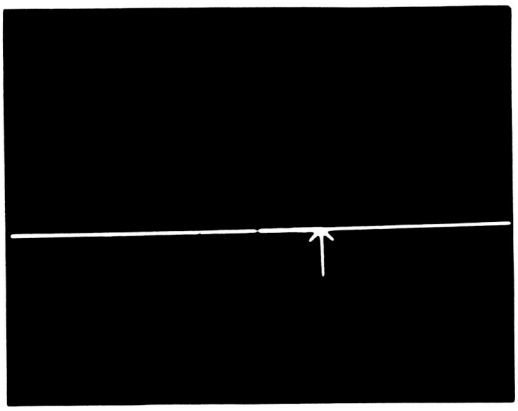

1. Decoder is in initial state.

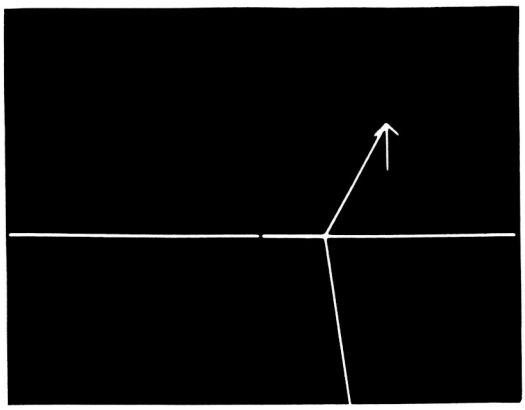

2. Metric values for alternatives at first node are computed. Path corresponding to highest is chosen.

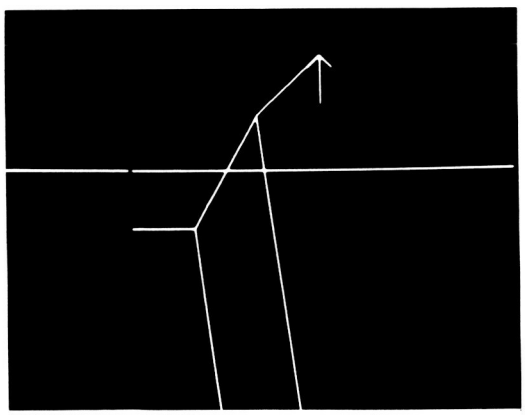

3. Repeated at node 2. Threshold has been raised.

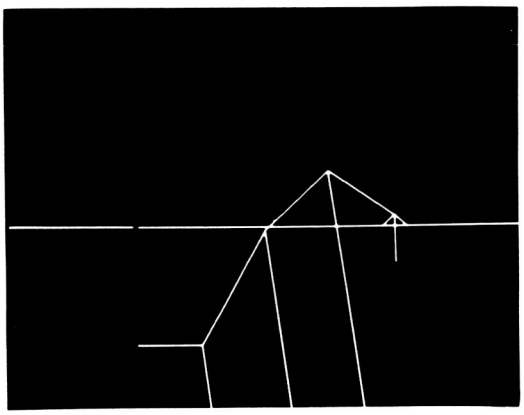

4. At node B, both metric increments are negative, but one remains above threshold.

Fig. 6. Oscillographic simulation output.

-22-5440 (a-d)

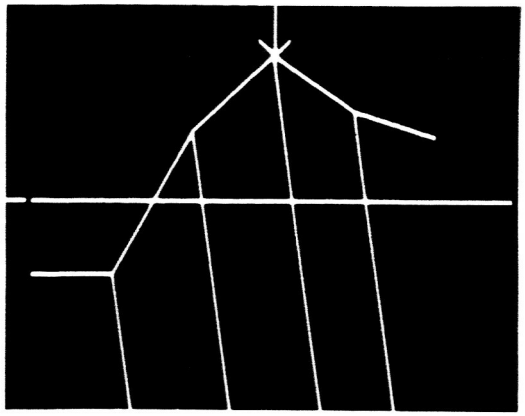

5. Metric increments at node 4 were computed; both caused metric to fall below threshold. Decoder then returned to node 3, found that untested branch fell below threshold, and then lowered threshold.

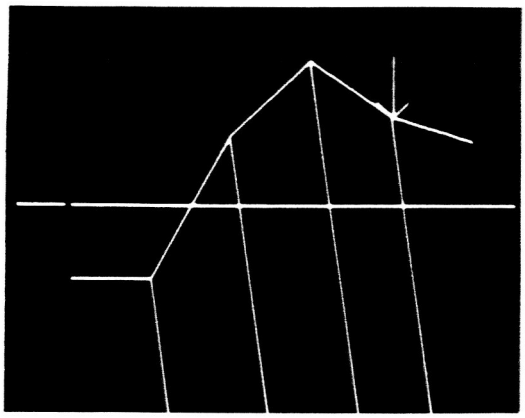

6. With lowered threshold, decoder retraces.

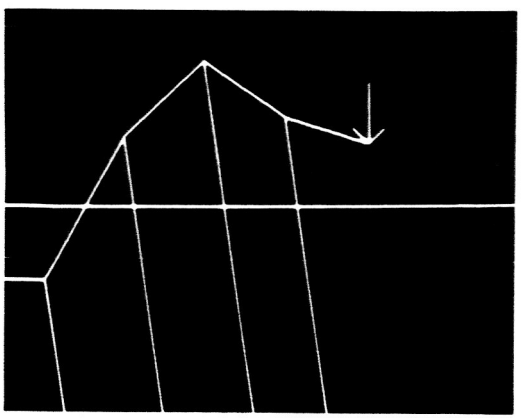

7. Branch at node 4 is successsfully chosen.

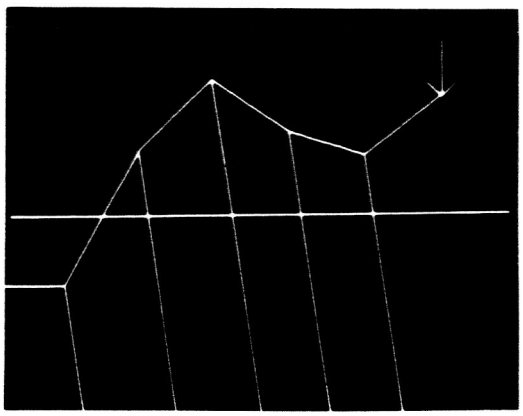

8. Branch at node 5 is chosen.

Fig. 6. Continued.

-22-5441 (a-d)

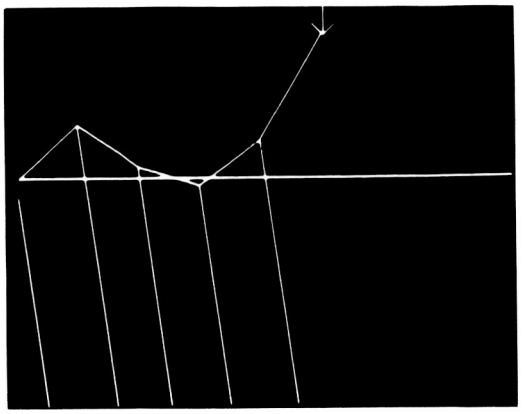

9. Branch at node 6 is chosen. Threshold is raised.

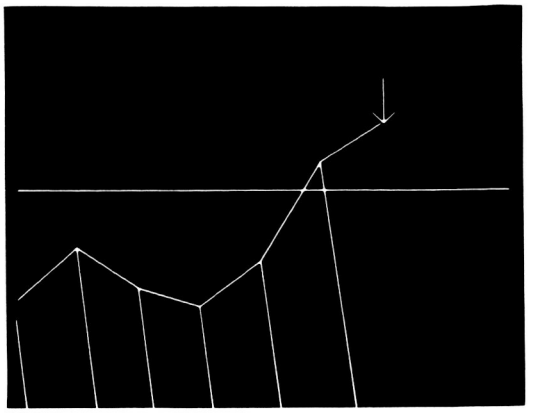

10. Branch at node 7 is chosen. Threshold is raised.

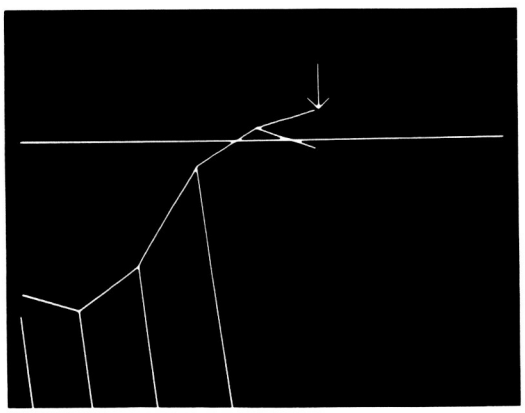

11. Branch at node 8 is chosen. Threshold is raised. Dropping signal-to-noise ratio is becoming apparent.

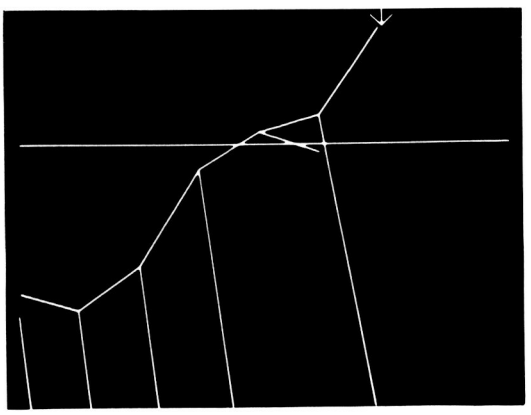

12. Branch at node 9 is chosen.

Fig. 6. Continued.

-22-5442 (a-d)

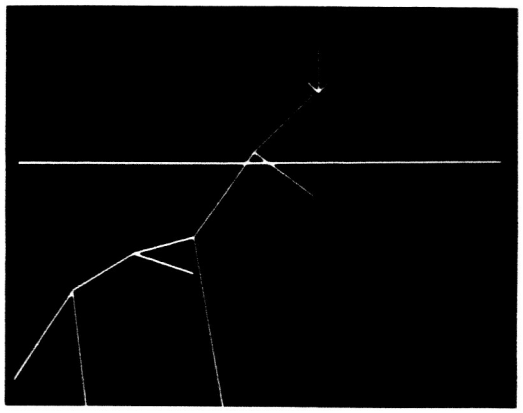

13. Branch at node 10 is chosen. This branch is incorrect. Threshold is raised.

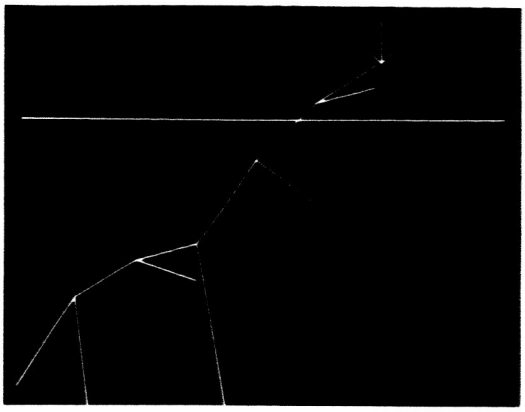

14. Branch at node 11 is chosen. Threshold is raised. Although on incorrect path, metric is increasing.

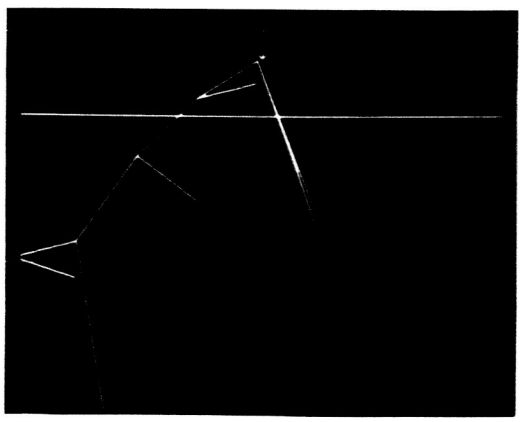

15. Alternatives at node 12 are computed. Both cause metric to fall below threshold.

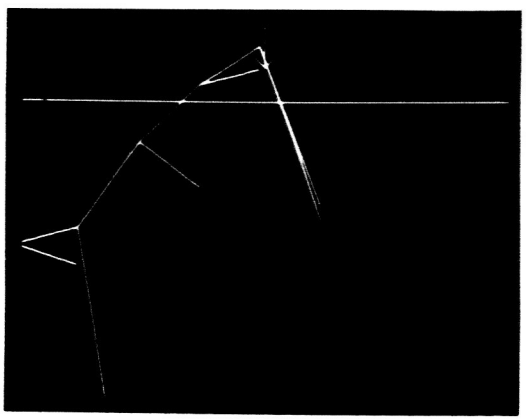

16. Decoder returns to node 11, where it tries untested branch with highest metric increment.

Fig. 6. Continued.

-22-5443 (a-d)

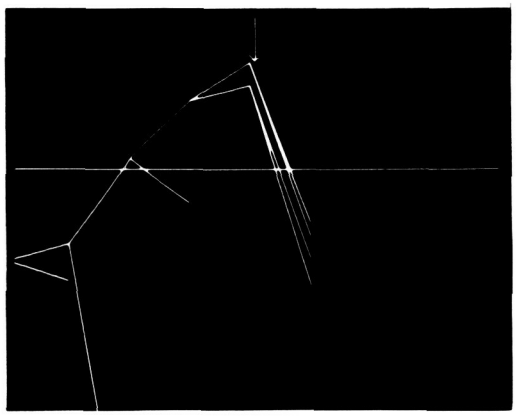

17. Alternative metric values for this choice are computed, both falling below threshold. Again decoder returns to node 11 where it finds no more untested branches. It returns to node 10, finds metric below threshold, lowers it, and then tries branch from node 11 with highest metric value.

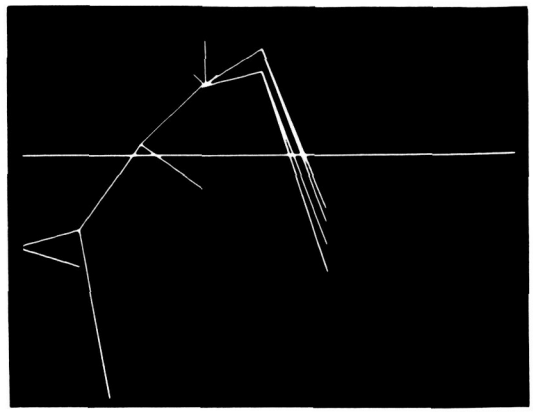

18. At node 12, it finds that both alternatives fall below threshold. Decoder returns to node 11.

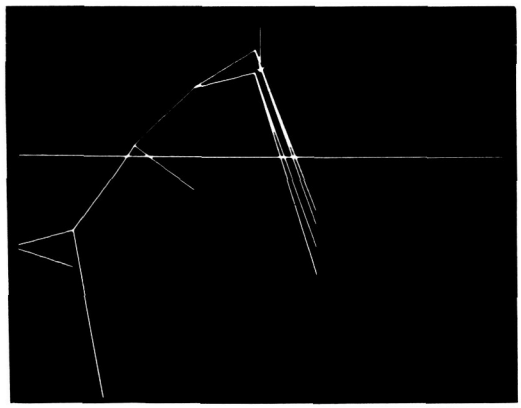

19. Decoder tries untested branch at node 11 with highest metric increment.

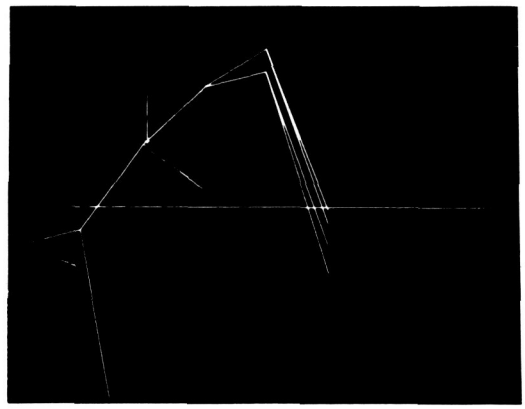

20. At node 12, both alternatives fell below threshold. Returning to node 11, decoder found no more untested branches and therefore lowered threshold. Then it returned to node 10 to begin search with this new threshold value.

Fig. 6. Continued.

-22-5444 (a-d)

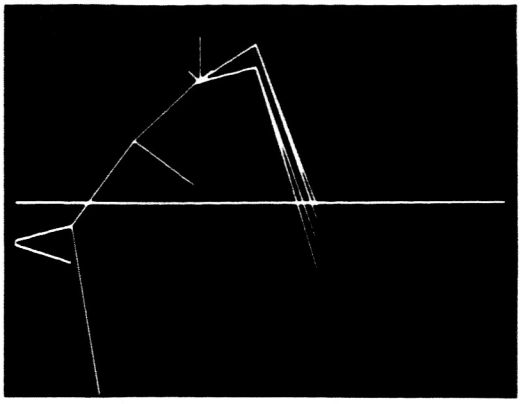

21. Search moves to node 11. Threshold remains fixed.

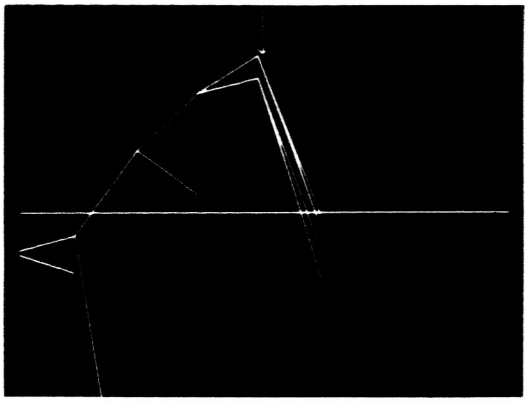

22. Branch at node 12 is chosen. Threshold remains fixed.

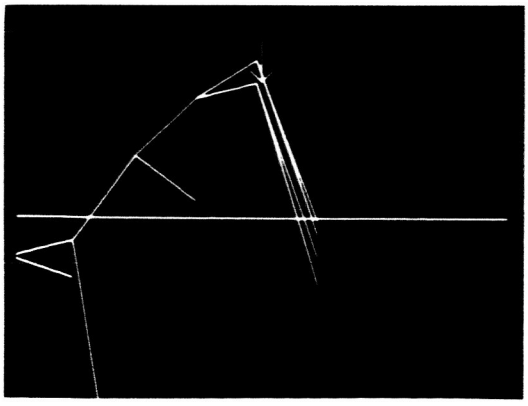

23. Both alternatives fell below threshold causing untested (with current threshold) branch with highest metric increment to be checked.

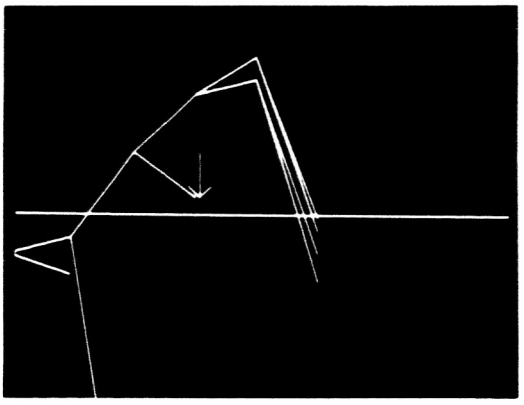

24. Both alternatives fell below threshold. No untested branches remained at node 11. Decoder then returned to try untested branch at node 10 with highest metric increment. This is correct path at last.

Fig. 6. Continued.

-22-5445 (a-d)

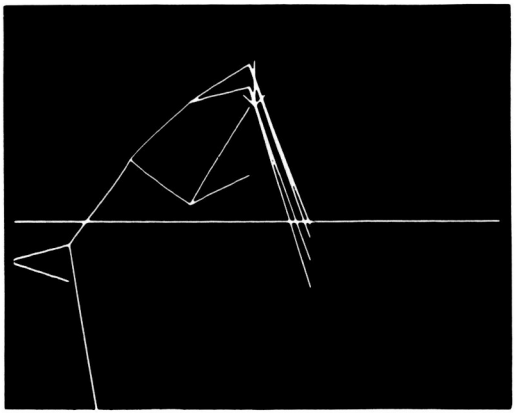

25. Branch at node 11 is chosen.

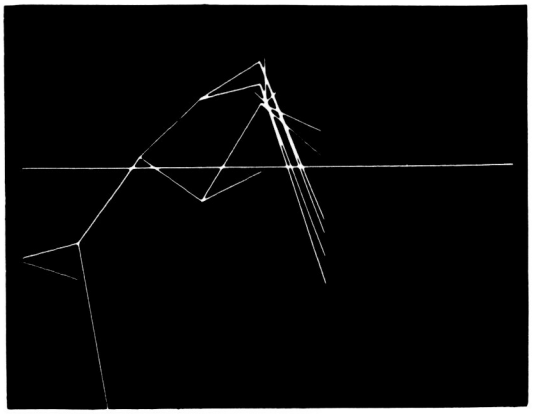

26. Branch at node 12 is chosen.

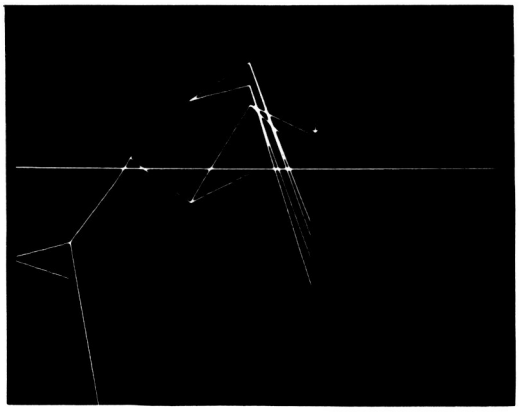

27. Branch at node 12 fell below threshold which was raised just after display 26. Threshold was lowered again.

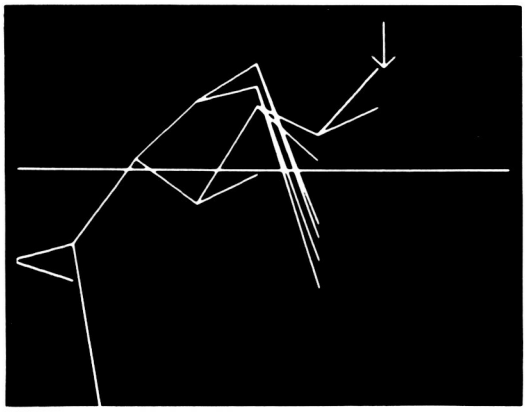

28. Branch at node 13 is chosen. Decoder is on right track.

Fig. 6. Continued.

The constraints imposed by the system under measurement become important in another way also. When analyzing the operation of the sequential algorithm, it will be necessary to consider the behavior of the metric along incorrect paths as well as its behavior on correct paths. Since the metric on the correct path is a function only of the noise samples, its components are independent. However, the metric on the various incorrect paths is a function not only of the noise samples, but also of the particular incorrect $\vec{z}$ values which occur along the incorrect path being considered. Thus, in the analysis of the metric on the incorrect path, we must take into account these $\vec{z}$ values. Clearly, such a procedure would be cumbersome since, in general, every incorrect path would have to be considered separately.

In the analysis of sequential decoding as applied to communications, this problem is avoided by a mathematical artifice known as ensemble averaging. Instead of considering the behavior of the metric on the set of incorrect paths for a particular code, we consider the average behavior on the set of incorrect paths for an ensemble of codes. Over such an ensemble, the output symbols along incorrect paths are independent, and therefore it is possible to consider all the incorrect paths simply. From such a result, a particular code that gives results at least as good as the average is guaranteed.

An analogous procedure is not plausible in measurements. Even if we could consider an ensemble of unknown parameters and thereby obtain independence, it is senseless to say there is a set of unknown parameters which could be measured at least as well as an average. In actuality, we are trying to measure a particular set of parameters and do not care if there is another set of parameters on which we could do a better job. We might also consider the ensemble of input signals, but the constraints imposed by the transformation are usually too strong to permit any simplifications to result among the incorrect output vectors.

Because the device being measured is not under the observer's control, we have seen that it is possible for two distinct hypothesis vectors to produce similar output vectors and for dependencies to exist among output values along a path. Both these features give rise to difficulties which must be overcome to proceed with the analysis. Consequently, we shall make an assumption, referred to as the differential bias assumption, which will permit the analysis to be completed and which, in addition, is reasonable from an intuitive viewpoint. Generally, this assumption implies that once an error is made in the decoding, a bias will be produced in later hypothesized outputs which acts in the same way that the addition of an extra noise source would. This appearance of additional noise in the data will indicate to the decoder that an error was made and that a retracing procedure should be started. The differential bias assumption itself will be defined precisely in Sec. III-E.

III. AVERAGE NUMBER OF COMPUTATIONS

A. Introduction

In this section, we shall compute an upper bound to the average number of times the decoder follows loop A of Fig. 5 in decoding a branch of the tree. This computation is similar to that done by Fano.[6] Since loop A must be taken for the decoder to move forward, the number of times the decoder follows it is within a factor of two of the total number of computations. Therefore, we shall henceforth define a computation as one pass around loop A. Note from Fig. 5 that loop A is traversed when the decoder is accepting a node one level deeper than the current depth. Thus threshold settings discussed in the next section are compared with the value of the metric at such a node.

We shall see that when there is a sufficient difference between the correct and incorrect noise-free data points as seen by the observer, it is possible to decode a branch of the tree with a number of computations that is independent of the depth of the node under consideration. In addition, we shall see that as this difference grows, the bound on the computations will decrease rapidly.

The bounds that will be derived are computed with the bias constant R discussed in Sec. II-B as a parameter. The effects of various values for this quantity are shown by means of curves derived for the Gaussian noise case.

B. Splitting $\overline{N}$

In the consideration of $\overline{N}$, the average number of computations required per branch of the decoding tree, it is desirable to consider separately the average number of computations made in each of three circumstances. Before defining these classes, we shall introduce the notion of a reference node and illustrate in a typical case the role it plays in the computation. Any node along the correct path can be regarded as the so-called reference node. In the computation of $\overline{N}$, we consider all paths stemming from this node and calculate the average number of branches along such paths that must be considered. Once this has been done, the next reference node and all paths stemming from it must be considered in the same way. Since each node along the correct path has a similar set of incorrect paths stemming from it, we can consider the total number of computations on incorrect paths stemming from the reference node and the total number of computations on the correct branch stemming from the reference node as the total number of computations per branch.

In the remainder of this section, we shall refer to an incorrect node as a node along an incorrect path stemming from the reference node. All other incorrect nodes will be considered when the correct node from which they stem is considered to be the reference node.

If we recall from Sec. II-G that the threshold takes on values quantized by increments of T_o, we shall find it convenient to define T_1 as the highest value of the threshold still below the value of the metric at the reference node. In addition, since the decoder operates only on metric changes, we can choose its reference to be arbitrary. For convenience, we assume that $T = 0$ at the reference node.

It will be convenient to divide the number of computations to decode one branch into three parts. First, there will be one computation each time the decoder returns to the reference node and tests the correct branch. Let $\overline{N}_c$ denote the average number of such computations. Second, there are those computations required to consider incorrect nodes when the threshold is set at T_1 and at various levels above T_1. Denote this average number by $\overline{N}_i^+$. Finally, there are those computations required to consider all incorrect nodes when the threshold is set at various levels below T_1. We let $\overline{N}_i^-$ be the average number of computations in this category.

Although it is possible that all the incorrect nodes with metric above a particular threshold will be considered by the decoder, many may not because of the specific way in which the metric varies along the path they are on. To be conservative, we neglect the existence of such metric variations and bound the desired result by one obtained by considering them all. Thus

$$\overline{N} \leqslant \overline{N}_c + \overline{N}_i^+ + \overline{N}_i^- \tag{1}$$

where $\bar{N}_c$ is the average number of computations on the correct branch, $\bar{N}_i^+$ is the average number along incorrect paths when the threshold is set at some value above T_1, and $\bar{N}_i^-$ is the quantity along incorrect paths when the threshold is set at some value below T_1.

In the calculation of $\bar{N}$, we neglect the fact that in measurement problems of interest the tree is of finite depth and instead we assume that the depth is infinite. Clearly, this is an upper bound to the average number of computations required for a finite tree, since the additional depths of an infinite tree provide more branches that the decoder may have to investigate.

In particular, if the size of the tree is increased, there will be more possibilities in which an event causing error could occur. Thus the number of computations to decode one branch increases as the size of the tree beyond it increases, and in the limit the tree can grow to infinite size.

Once the infinite-depth tree is assumed, it may be noted that the average number of computations to decode the correct branch stemming from a reference node is independent of the reference node's depth. This is because the number of computations depends on the behavior of the metric along paths stemming from the reference node, and the composition of the set of such paths is independent of the reference node.

C. Events Contributing to Partial Averages

We consider $\bar{N}_c$ first. Since succeeding branches on the correct path will be considered when the nodes from which they stem are regarded as reference nodes, we need consider only the first branch. This branch will, of course, be considered at least once and it will be reconsidered once for each threshold below T_1, below which the correct path falls. In particular, the decoder will not return to the reference node if the total metric does not fall below T_1, but will do so once for each different threshold value below T_1 used by the decoder.

Define P(T) as the probability that the total metric falls below T somewhere along the correct path. Using this quantity, we can bound $\bar{N}_c$ as

$$\bar{N}_c \leq 1 + \sum_{j=0}^{\infty} P(T)_{T=T_1-jT_o} \quad . \tag{2}$$

As will be seen later, and is heuristically obvious, P(T) decreases with decreasing T. Therefore,

$$\bar{N}_c \leq 1 + \sum_{j=0}^{\infty} P(T)_{T=-jT_o} \quad . \tag{3}$$

Next we consider nodes along incorrect paths stemming from the reference node which are considered when the threshold is set at a value, $T^* \geq T_1$. It is possible that all incorrect nodes above such a threshold will be considered once for each threshold value above or at T_1. The incorrect nodes in this category may or may not be considered by the decoder, depending on the behavior of the metric on the correct path and on the manner in which the metric varies along incorrect paths. To be conservative, we assume that all nodes above $T^* \geq T_1$ will be considered. This is illustrated in Fig. 7(a). The incorrect path's metric exceeds that of the correct path at the reference node and an error results. Then the threshold is eventually raised to $T_1 + 2T_o$. Before the decoder returns to the reference node, one computation on the incorrect path will be made with the threshold at $T_1 + 2T_o$, two at $T_1 + T_o$, and two with it at T_1.

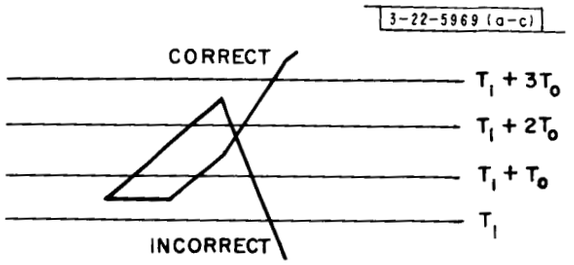

(a)

(a) Error when metric increases on correct path.

(b) Error when metric decreases on correct path.

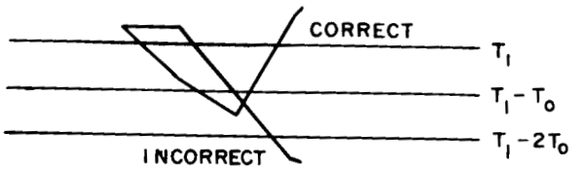

(b)

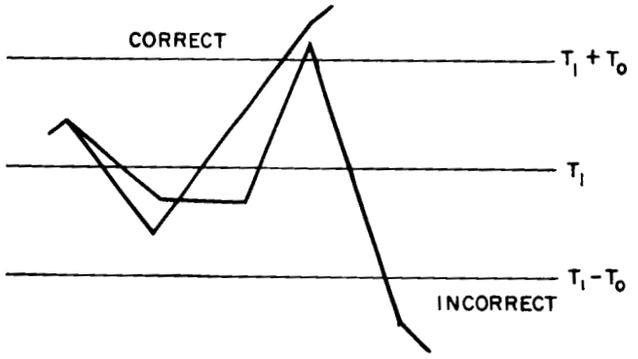

(c)

(c) Error when metric decreases on both correct and incorrect paths.

Fig. 7. Typical metric behavior.

Therefore, we see that if $\overline{N}(T^*)$ is defined as the average number of nodes along incorrect paths at which the total metric equals or exceeds T^*, $\overline{N}_i^+$ is upper bounded by the sum

$$\overline{N}_i^+ \leq \sum_{j=0}^{\infty} \overline{N}(T^*)_{T^*=T_1+jT_o} \quad . \tag{4}$$

We shall see later that $\overline{N}(T^*)$ increases with decreasing T^* so that

$$\overline{N}_i^+ \leq \sum_{j=-1}^{\infty} \overline{N}(T^*)_{T^*=jT_o} \quad . \tag{5}$$

Finally, we consider $\overline{N}_i^-$, the number of computations made on incorrect paths for threshold settings below T_1. Such branches will be considered only if the correct path falls below T_1 at some depth. In fact, these branches will be reconsidered once for <u>each</u> threshold value $T^* < 0$, for which the correct path falls below $T^* + T_o$. This may be illustrated as in Fig. 7(b). In this example, one incorrect node will be tried with the threshold at T_1, one at $T_1 - T_o$, and two at $T_1 - 2T_o$.

Consequently, if we define $\overline{N}(T^*/T)$ as the average number of nodes on an incorrect path exceeding T^* when the correct path falls below T, we can upper bound $\overline{N}_i^-$ by the sum

$$\overline{N}_i^- \leq \sum_{j=0}^{\infty} \overline{N}(T^* \mid T)_{\substack{T^*=T_1-(j+1)T_o \\ T=T_1-jT_o}} P(T)_{T=T_1-jT_o} \tag{6}$$

$$\leq \sum_{j=0}^{\infty} \overline{N}(T^* \mid T)_{\substack{T^*=-(j+2)T_o \\ T=-jT_o}} P(T)_{T=-jT_o} \tag{7}$$

where we have again used the monotone properties of $P(T)$ and $\overline{N}(T^*)$ which will be discussed later.†

The reader may note that if the correct path falls below $T \leq T_1$, some incorrect nodes may be considered with the threshold setting above T_1. Such a case is illustrated in Fig. 7(c). Since the metric on the correct path fell below T_1 and also fell below that of the incorrect path shown, the incorrect path was tried by the decoder. At one point, node A will be considered for $T^* = T_1 + T_o$. Such a computation would be included in $\overline{N}_i^+$ (and also $\overline{N}_i^-$) despite the fact that this path would be taken only if the metric on the correct path falls below T_1.

D. Chernoff Bounds to Probabilities

The average number of computations has been upper bounded by three sums involving two quantities $P(T)$ and $\overline{N}(T^*)$, the probability of the correct path falling below T and the average number of incorrect nodes above T^*, respectively. In this section, these quantities are upper bounded by means of the well-known Chernoff bound.[11]

This bound states that if x is a random variable, $F(x)$ is its cumulative distribution function, and $\gamma(r)$ is the corresponding moment generating function,

† A slight improvement in the bound can be obtained if this monotone condition is not imposed until the summation is performed.

$$\gamma(r) = \int e^{rx}\, dF(x)$$

then

$$F(x) \leq \gamma(r)\, e^{-rx} \quad , \quad \text{any } r \leq 0 \tag{8}$$

and

$$1 - F(x) \leq \gamma(r)\, e^{-rx} \quad , \quad \text{any } r \geq 0 \quad . \tag{9}$$

These inequalities have been extremely valuable in the analysis of sequential decoding of tree encoded messages and we shall find them very useful here as well.

Let $P_k(T) = Pr(M_k < T)$ be the probability that the value of the metric M_k at the k^{th} node beyond the reference node on the correct path is smaller than some value T. We observe that on the correct path the metric increment is $R + \ln p_n(n_j)$, where $n_j = y_j - z_j$. Thus the behavior of the metric on a correct path depends only on the noise samples.

Let $\gamma_c^{(k)}(r)$ be the moment generating function of the metric on a correct path of length k. That is,

$$\gamma_c^{(k)}(r) = \int \cdots \int \prod_{j=1}^{k} p_n(n_j) \exp\left\{ r \sum_{j=1}^{k} [R + \ln p_n(n_j)] \right\} dn_1 \cdots dn_k \tag{10}$$

where $p_n(n_i)$ is the probability density function of the noise. Then the Chernoff bound implies that

$$P_k(T) \leq \gamma_c^{(k)}(r)\, e^{-nT} = \exp\{\mu_c^{(k)}(r) - rT\} \quad , \quad r \leq 0 \tag{11}$$

where

$$\mu_c^{(k)}(r) = \ln \gamma_c^{(k)}(r) \quad .$$

Next we turn to $\bar{N}(T^*)$ which was defined in Sec. III-C as the total number of incorrect nodes above T^*. Let $P_k(T^*)$ be the probability that the value of the metric M_k^* at the k^{th} node along a particular incorrect path stemming from the reference node exceeds a value T^*. This quantity depends on the particular incorrect path under consideration.

We now note that if we consider D quantization levels there is a total of $(D-1)D^{k-1}$ completely incorrect paths of length k stemming from the reference node. Let $P_k^m(T^*)$ be the largest $P_k(T^*)$ of those computed for all these incorrect paths. Then the average number of incorrect nodes at depth k exceeding T^* is given by

$$\bar{N}_k(T^*) = \sum_{i=1}^{(D-1)D^{k-1}} \Pr \left(\begin{array}{l} \text{metric on } i^{th} \text{ incorrect path of length} \\ k \text{ exceeds } T^* \end{array} \right) \quad .$$

Since $P_k(T^*) \leq P_k^m(T^*)$ for all incorrect paths it follows that

$$\bar{N}_k(T^*) \leq P_k^m(T^*) \cdot (D-1)D^{k-1} \quad . \tag{12}$$

But the Chernoff bounding procedure allows us to upper bound $P_k^m(T^*)$. Note that

$$p_n(y_j | z_j^*) = p_n(y_j - z_j^*) = p_n(z_j - z_j^* + n_j) \quad .$$

Let $\gamma_i^{(k)}(t)$ be the moment generating function of the metric along the incorrect path of length k giving rise to $P_k^m(T^*)$

$$\gamma_i^{(k)}(t) = \int \cdots \int \prod_{j=1}^{k} p_n(n_j) \exp\left\{t \sum_{j=1}^{k} [R + \ln p_n(z_j - z_j^* + n_j)]\right\} \quad dn_1 \cdots dn_k \tag{13}$$

where $p_n(n_j)$ is the probability density for the j^{th} one of the k independent noise samples, z_j is the j^{th} noise-free output on the correct path, and z_j^* is the j^{th} noise-free output on the incorrect path giving rise to the maximum $P_k(T^*)$, $P_k^m(T^*)$. Then by the Chernoff bound

$$P_k^m(T^*) \leqslant \gamma_i^{(k)}(t)\, e^{-tT^*} \quad , \quad \text{for any } t \geqslant 0 \tag{14}$$

so that combining Eqs. (12) and (14)

$$\overline{N}_k(T^*) \leqslant (D-1)\, D^{k-1}\, \gamma_i^{(k)}(t)\, e^{-tT^*} \quad . \tag{15}$$

$\overline{N}(T^* \mid T)$ can be bounded using a similar technique. Let

$$P_{k|n}(T^* \mid T) = P_r(M_k^* \geqslant T^* \mid M_n < T)$$

be the conditional probability that the value of the metric M_k^* at the k^{th} node along a particular incorrect path stemming from the reference node exceeds a value T^* when the metric M_n at the n^{th} node along the correct path falls below T. This quantity depends on the particular incorrect path under consideration.

As before, we note that there are a total of $(D-1)\, D^{k-1}$ completely incorrect paths stemming from the reference node. Let $P_{k|n}^m(T^* \mid T)$ be the largest $P_{k|n}(T^* \mid T)$ of those computed for all these incorrect paths. Then the same procedure can be employed by assuming that

$$P_{k|n}(T^* \mid T) \leqslant P_{k|n}^m(T^* \mid T) \quad . \tag{16}$$

for all incorrect paths. Therefore, the average number of nodes along incorrect paths of length k above T^*, given that the correct path is below T at depth n, is bounded by

$$\overline{N}_{k|n}(T^* \mid T) \leqslant P_{k|n}^m(T^* \mid T) \cdot (D-1)\, D^{k-1} \quad . \tag{17}$$

If we now multiply both sides of this inequality by $P_n(T)$ we obtain

$$P_n(T)\, \overline{N}_{k|n}(T^* \mid T) \leqslant P_r(M_n < T, M_k^* \geqslant T^*) \cdot (D-1)\, D^{k-1} \quad . \tag{18}$$

It is worthy of note that the right-hand side of this expression is also an upper bound to the joint probability that $M_n < T$ on the correct path and that there is at least one node at distance k along some incorrect path stemming from the reference node for which $M_k^* \geqslant T^*$. This bound is due to the fact that the probability of a union of events is upper bounded by the sum of probabilities of the individual events.

To further bound this joint probability, we can employ the Chernoff bound in two dimensions. Note as before that

$$p_n(y_j \mid z_j) = p_n(y_j - z_j) = p_n(n_j)$$

and

$$p_n(y_j|z_j^*) = p_n(y_j - z_j^*) = p_n(z_j - z_j^* + n_j)$$

when

$$n_j = y_j - z_j \quad .$$

Let $\gamma_i^{(n,k)}(r,t)$ be the joint moment generating function of the metric on the correct path of length n together with the metric on the incorrect path of length k leading to the maximum $P_{k|n}(T^*|T)$, $P_{k|n}^m(T^*|T)$. That is,

$$\gamma_i^{(n,k)}(r,t) = \int \cdots \int \prod_{j=1}^{k} p_n(n_j) \exp\left\{ r \sum_{j=1}^{n} [R + \ln p_n(n_j)] + t \sum_{j=1}^{k} [R + \ln p_n(z_j - z_j^* + n_j)] \right\} dn_1 \cdots dn_k \tag{19}$$

if $k \geq n$, $t \geq 0$, and $r \leq 0$, and

$$\gamma_i^{(n,k)}(r,t) = \int \cdots \int \prod_{j=1}^{n} p_n(n_j) \exp\left\{ r \sum_{j=1}^{n} [R + \ln p_n(n_j)] + t \sum_{j=1}^{k} [R + \ln p_n(z_j - z_j^* + n_j)] \right\} dn_1 \cdots dn_k \tag{20}$$

if $k \leq n$, $t \geq 0$, and $r \leq 0$. Then

$$\Pr(M_n < T, M_k^* > T^*) \leq \gamma_i^{(n,k)}(r,t) \exp\{-rT - tT^*\} \tag{21}$$

for $t \geq 0$ and $r \leq 0$.

Before proceeding further in the calculation, we make an assumption about the incorrect paths in order that all possible incorrect paths will not have to be considered individually.

E. Differential Bias Assumption

The calculation of the moment generating functions defined in Eqs. (19) and (20) is complicated by the dependencies that exist between the metric values on the correct path and those on the incorrect path, and by dependencies existing along incorrect paths. Indeed, it does not appear that their computation is tractable without some simplifying assumption. In this connection, it may be noted that for an incorrect decision to be discovered, its consequences must produce an observable discrepancy between the true noise-free data vector and the hypothesized noise-free data vector. Because of the analog nature of the noise effects under consideration, this discrepancy must appear as an arithmetic difference in at least some of the vector components depending

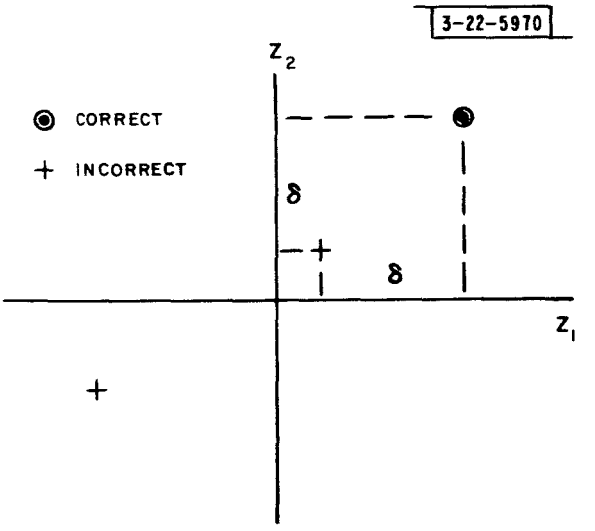

Fig. 8. Differential bias assumption.

on differing hypotheses. Thus the effect of an erroneous decision is to produce a bias in the data. With these remarks as motivation, we make the following assumption†:

> On all incorrect paths, each incorrect output value z_i^* differs from the corresponding correct output value z_i by at least a constant δ. More precisely, $|z_i - z_i^*| > \delta$ for all incorrect branches.

We shall see that under this condition, the moment generating functions can be calculated without regard to the dependencies existing along incorrect paths.

A geometric interpretation of this assumption is readily obtained. Consider the noise-free data vector of each possible tree path of length n as a point in n-dimensional Euclidean space. The above assumption implies that the components of each incorrect point differ by at least δ from the corresponding components of the correct point. This is illustrated for two dimensions in Fig. 8.

F. Moment Generating Functions

Under the differential bias assumption, several simplifications in connection with the required moment generating functions occur. We first consider $\delta_c^{(k)}(r)$. By taking advantage of the independence among noise samples, we obtain

---

† This assumption was recently weakened to the requirement that

$$\sum_{i=1}^{k} |z_i - z_i^*| > k\delta$$

for all incorrect paths of length k where the summation extends over the incorrect portion of the path. The calculation of the moment generating functions under this weakened assumption is sketched in Appendix C. For Gaussian white noise, the differential bias assumption can be weakened to

$$\sum_{i=1}^{k} (z_i - z_i^*)^2 > k\delta^2$$

for all incorrect paths.

$$\gamma_c^{(k)}(r) = E\left(\exp\left\{r \sum_{j=1}^{k} [R + \ln p_n(y_j|z_j)]\right\}\right) \quad , \quad r \leqslant 0$$

$$= e^{rkR} \{E\,[p_n(n)^r]\}^k$$

$$= e^{rkR}\, \gamma_1^k(r) \tag{22}$$

where

$$\gamma_1(r) = E\,[p_n(n)^r] \quad . \tag{23a}$$

Thus it is sufficient to calculate $\gamma_1(r)$ which depends only on the probability density function for the noise.

In dealing with $\gamma_i^{(k)}(t)$ and $\gamma_i^{(n,\,k)}(r, t)$, we shall show that the corresponding true moment generating functions are upper bounded by generating functions calculated under the differential bias assumption alone. Thus, although these moment generating functions were defined by Eqs. (13), (20), and (21) along specific paths, they are upper bounded by moment generating functions independent of the particular incorrect path. In addition, dependencies along incorrect paths due to the internal constraints of the transducer are removed from consideration. This upper bound is made explicit by the following theorem.

Theorem.

If we define

$$\gamma_2(t) = \int p_n(z + n|z)\, p_n(z + n|z + \delta_o)^t\, dn \tag{23b}$$

and if $p_n(y/z)$ is a symmetric, monotone-decreasing function of $|y - z| = |n|$,

$$\gamma_2(t) > \int p_n(z + n|z)\, p_n(z + n|z + \delta)^t\, dn \tag{24}$$

if $\delta > \delta_o$ and $t > 0$.

Proof.

By assumptions described in the theorem, $p_n(y/z) = p_n(n)$ is a monotone-decreasing symmetric function of $|n|$. But a positive power of such a function is also of the same type. Hence by Lemma 2 in Appendix A, the theorem is proved.

Turning now to $\gamma_i^{(k)}(t)$, we again use the independence of the noise samples. From Eq. (13), we have

$$\gamma_i^{(k)}(t) = E\left(\exp\left\{t \sum_{j=1}^{k} [R + \ln p_n(z_j - z_j^* + n_j)]\right\}\right) \quad , \quad t \geqslant 0$$

$$= e^{tkR} \int \cdots \int \prod_{j=1}^{k} p_n(n_j) \exp\left[t \sum_{j=1}^{k} \ln p_n(z_j - z_j^* + n_j)\right] \quad dn_1 \cdots dn_k$$

$$\gamma_i^{(k)}(t) = e^{tkR} \int \cdots \int \prod_{j=1}^{k} p_n(n_j)\, p_n(z_j - z_j^* + n_j)^t \, dn_1 \cdots dn_k$$

$$= e^{tkR} \prod_{j=1}^{k} \int p_n(n_j)\, p_n(z_j - z_j^* + n_j)^t \, dn_j$$

$$\leqslant e^{tkR}\, \gamma_2^k(t) \tag{25}$$

where

$$\gamma_2(t) = \int p_n(n)\, p_n(n + \delta)^t \, dn \quad . \tag{26}$$

The inequality follows from the theorem expressed by Eq. (24). Thus $\gamma_i^{(k)}(t)$ is bounded by a function dependent only on the noise probability density function and on the constant δ, introduced by the differential bias assumption.

In the same way $\gamma_i^{(n,k)}(r,t)$ can be shown to be bounded by a function depending only on the probability density function of the noise and on the constant δ. From Eq. (20)

$$\gamma_i^{(n,k)}(r,t) = \int \cdots \int \prod_{j=1}^{k} p_n(n_j) \exp \left\{ r \sum_{j=1}^{n} [R + \ln p_n(n_j)] \right.$$

$$\left. + t \sum_{j=1}^{k} [R + \ln p_n(z_j - z_j^* + n_j)] \right\} dn_1 \cdots dn_k$$

$$= \exp\{nrR + ktR\} \int \cdots \int \prod_{j=1}^{n} p_n(n_j)^{1+r}\, p_n(z_j - z_j^* + n_j)^t \, dn_1 \cdots dn_n$$

$$\times \int \cdots \int \prod_{j=n+1}^{k} p_n(n_j)\, p_n(z_j - z_j^* + n_j)^t \, d_{k+1} \cdots dn_k$$

$$\leqslant \exp\{nrR + ktR\}\, \gamma_3^n(r,t)\, \gamma_2^{k-n}(t) \tag{27}$$

for $k \geqslant n$, $t \geqslant 0$, $r \leqslant 0$, where

$$\gamma_3(r,t) \triangleq \int p_n(n)^{1+r}\, p_n(n + \delta)^t \, dn \tag{28}$$

and $\gamma_2(t)$ is defined in Eq. (26). If $n \geqslant k$, Eq. (27) is replaced by

$$\gamma_i^{(n,k)}(r,t) \leqslant \exp\{nrR + ktR\}\, \gamma_3^k(r,t)\, \gamma_1^{n-k}(r) \tag{29}$$

where $\gamma_1(r)$ is defined in Eq. (23a).

The fact that a different bound obtains in the two cases will make later computations very laborious. However, a simple application of the Schwartz inequality[12] gives us an upper bound that is common to the two expressions above. This bound is derived in Appendix A as Lemma 1

and indicates that we can define two functions, each of which is simply related to the pertinent moment generating function in the following manner:

$$\gamma'_1(r) = [\gamma_1(2r)]^{1/2}$$

$$\gamma'_2(t) = [\gamma_2(2t)]^{1/2} \quad .$$

Then

$$\gamma_3(r, t) \leqslant \gamma'_1(r)\, \gamma'_2(t)$$

$$\gamma_1(r) \leqslant \gamma'_1(r)$$

$$\gamma_2(t) \leqslant \gamma'_2(t) \quad . \tag{30}$$

Applying these bounds, we obtain from Eqs. (27) and (30) the following bound to $\gamma_i^{(n, k)}(r, t)$ which holds for all values of n and k.

$$\gamma_i^{(n, k)}(r, t) \leqslant \exp\{nrR + ktR\}\, [\gamma'_1(r)]^n\, [\gamma'_2(t)]^k \tag{31a}$$

and $r \leqslant 0$ and $t \geqslant 0$.

Hence we can deal with $\gamma_1(r)$ and $\gamma_2(t)$ which depend only on the noise density function and the constant δ. It will be convenient to define

$$\mu_1(r) = \ln \gamma_1(r) = \ln E\, [p_n(n)^r] \quad , \quad r \leqslant 0$$

and

$$\mu_2(t) = \ln \gamma_2(t) = \ln E\, [p_n(n + \delta)^t] \quad , \quad t \geqslant 0 \tag{31b}$$

so that from Eqs. (31a) and (31b)

$$\gamma_i^{(n, k)}(r, t) \leqslant \exp\{n\, [rR + \tfrac{1}{2}\, \mu_1(2r)] + k\, [tR + \tfrac{1}{2}\, \mu_2(2t)]\} \tag{32}$$

for $r \leqslant 0$ and $t \geqslant 0$.

Now that we have discussed the moment generating functions and have introduced the differential bias assumption, we can return to the main objective, that of bounding $P(T)$, $\overline{N}(T^*)$, and $\overline{N}(T^* \mid T)$, the probability that the metric on the correct path falls below T for some depth, the average number of incorrect nodes along all incorrect paths for which the metric exceeds T^*, and the same quantity conditional on the correct path's falling below T. Since the probability of a union of events is less than or equal to the sum of the individual events, we can upper bound these quantities by the proper sums over n and k. Thus

$$P(T) \leqslant \sum_{n=1}^{\infty} P_n(T) \tag{33}$$

$$\overline{N}(T^*) \leqslant \sum_{k=1}^{\infty} \overline{N}_k(T^*) \tag{34}$$

$$\bar{N}(T^* \mid T) \leq \sum_{k=1}^{\infty} \sum_{n=1}^{\infty} \bar{N}_{k/n}(T^* \mid T)\, P_n(T) \tag{35}$$

where $P_n(T)$ is the probability that the correct path is below T at depth n, $\bar{N}_k(T^*)$ is the average number of nodes along incorrect paths at depth k which exceed T^*, and $\bar{N}_{k|n}(T^* \mid T)$ is the average number of nodes along incorrect paths at depth k which exceed T^* when the correct path falls below T at depth n, as discussed in Sec. III-D.

G. Performing the Sums

The contents of the previous sections can be summarized by indicating three summations to be performed. Combining Eqs. (3), (11), (22), (30), and (33), we obtain

$$\begin{aligned} \bar{N}_c &\leq 1 + \sum_{j=0}^{\infty} \sum_{n=1}^{\infty} \exp\{n\,[rR + \tfrac{1}{2}\,\mu_1(2r)] + jrT_o\} \\ &= 1 + \sum_{j=0}^{\infty} \sum_{n=1}^{\infty} \exp\{jrT_o + n\alpha(r)\} \quad , \quad r \leq 0 \quad . \end{aligned} \tag{36}$$

$$\alpha(r) = rR + \tfrac{1}{2}\,\mu_1(2r)$$

From Eqs. (5), (15), (25), (30), and (34), we get

$$\begin{aligned} \bar{N}_i^+ &\leq \sum_{j=-1}^{\infty} \sum_{k=1}^{\infty} (D-1)\,D^{k-1} \exp\{k\,[tR + \tfrac{1}{2}\,\mu_2(2t)] - jtT_o\} \\ &= \frac{D-1}{D} \sum_{j=-1}^{\infty} \sum_{k=1}^{\infty} \exp\{-jtT_o + k\,[tR + \tfrac{1}{2}\,\mu_2(2t) + \ln D]\} \\ &= \frac{D-1}{D} \sum_{j=-1}^{\infty} \sum_{k=1}^{\infty} \exp\{-jtT_o + k\beta(t)\} \quad , \quad t \geq 0 \end{aligned} \tag{37}$$

$$\beta(t) = tR + \tfrac{1}{2}\,\mu_2(2t) + \ln D \quad .$$

Finally by considering Eq. (7) and successively substituting Eqs. (18), (21), (32), and (35), we obtain

$$\begin{aligned} \bar{N}_i^- &\leq \sum_{j=0}^{\infty} \sum_{k=1}^{\infty} \sum_{n=1}^{\infty} (D-1)\,D^{k-1} \exp\{jrT_o + (j+2)\,tT_o + n\,[rR + \tfrac{1}{2}\,\mu_1(2r)]\} \\ &\quad \times \exp\{k\,[tR + \tfrac{1}{2}\,\mu_2(2t)]\} \\ &= \frac{D-1}{D} \sum_{j=0}^{\infty} \sum_{k=1}^{\infty} \exp\{(j+2)\,tT_o + k\,[tR + \tfrac{1}{2}\,\mu_2(2t) + \ln D]\} \\ &\quad \times \sum_{n=0}^{\infty} \exp\{jrT_o + n\,[rR + \tfrac{1}{2}\,\mu_1(2r)]\} \end{aligned}$$

$$\bar{N}_i = \frac{D-1}{D} \sum_{j=0}^{\infty} \sum_{k=1}^{\infty} \exp\{(j+2)\, tT_o + k\beta(t)\} \sum_{n=0}^{\infty} \exp\{jrT_o + n\alpha(r)\} \tag{38}$$

where

$$\beta(t) = tR + \frac{1}{2}\mu_2(2t) + \ln D \quad , \quad t \geqslant 0 \tag{39}$$

and

$$\alpha(r) = rR + \frac{1}{2}\mu_1(2r) \quad , \quad r \leqslant 0 \tag{40}$$

and $\mu_1(2r)$ and $\mu_2(2t)$ are given in Eq. (31b).

The parameters r and t appearing in these summations were introduced in the Chernoff bounds to terms that have been combined in the calculations. It is not necessary, nor is it desirable, that r and t be chosen the same for all these terms, but rather each of these parameters should be chosen to minimize the bound. Thus the optimum r and t are really functions of the summing indices j, k, and n.

Because of the arithmetic complications produced by complete optimization, it is desirable to pick only two values for r and two for t. Thus we choose

$$r = \begin{cases} r_o & n < n_1 \\ r_1 & n \geqslant n_1 \end{cases} \tag{41}$$

and

$$t = \begin{cases} t_o & k < k_1 \\ t_1 & k \geqslant k_1 \end{cases} \quad . \tag{42}$$

Since the exponent in Eq. (38) is dominated by the terms independent of n and k when n and k are small, we shall choose r_o and t_o such that the coefficients of n and k are each zero. Then, as n and k increase beyond n_1 and k_1, respectively, and this term becomes more important, we shall choose r_1 and t_1 to minimize the coefficient. More precisely, r_o, r_1, t_o, and t_1 are chosen to satisfy

$$\alpha(r_o) = 0 \tag{43}$$

$$\beta(t_o) = 0 \tag{44}$$

$$\alpha'(r_1) = 0 \tag{45}$$

$$\beta'(t_1) = 0 \quad . \tag{46}$$

In addition, n_1 and k_1 are chosen as those values of n and k for which the bounds obtained using r_o and t_o just exceed those obtained using r_1 and t_1.

That is, we choose n_1 such that the term corresponding to $n = n_1 - 1$ is smaller for $r = r_o$ than for $r = r_1$, whereas the term corresponding to $n = n_1$ is larger for $r = r_o$ than for $r = r_1$. Thus

$$jr_oT_o \leqslant (n_1 - 1)\,\alpha(r_1) + jr_1T_o \tag{47}$$

$$jr_o T_o > n_1 \alpha(r_1) + jr_1 T_o \quad . \tag{48}$$

That is, n_1 is defined as an integer satisfying

$$\frac{j(r_o - r_1)\, T_o}{\alpha(r_1)} \leqslant n_1 < \frac{j(r_o - r_1)\, T_o}{\alpha(r_1)} + 1 \tag{49}$$

for $jT_o > 0$ and $n_1 = 0$ for $jT_o = 0$. Similarly, we define k_1 as the integer satisfying

$$\frac{j(t_o - t_1)\, T_o}{\beta(t_1)} \leqslant k_1 < \frac{j(t_o - t_1)\, T_o}{\beta(t_1)} + 1 \tag{50}$$

for $jT_o > 0$ and $k_1 = 0$ for $jT_o = 0$. Therefore,

$$\exp[n_1 \alpha(r_1) + jr_1 T_o] \leqslant \exp[jr_o T_o] \tag{51}$$

and

$$\exp[k_1 \beta(t_1) + jt_1 T_o] \leqslant \exp[jt_o T_o] \quad . \tag{52}$$

We shall carry out the summations first, and then discuss the conditions under which solutions can be obtained.

$$\overline{N}_c \leqslant 1 + \sum_{j=0}^{\infty} \left\{ \sum_{n=1}^{n_1 - 1} \exp[jr_o T_o] + \sum_{n=n_1}^{\infty} \exp[jr_1 T_o + n\alpha(r_1)] \right\} \quad .$$

Using Eq. (49) and the relation $\Sigma\, x^i = 1/(1 - x)$,

$$\overline{N}_c \leqslant 1 + \sum_{j=0}^{\infty} \left(j \left[\frac{(r_o - r_1)\, T_o}{\alpha(r_1)} \right] \exp[jr_o T_o] + \left\{ \frac{1}{1 - \exp[\alpha(r_1)]} \right\} \exp[jr_o T_o] \right) \quad .$$

Next, using the relation $\Sigma\, ix^i = x/(1 - x)^2$,

$$\overline{N}_c \leqslant 1 + \frac{(r_o - r_1)\, T_o}{\alpha(r_1)} \frac{e^{r_o T_o}}{\left(1 - e^{r_o T_o}\right)^2} + \frac{1}{\left[1 - e^{\alpha(r_1)}\right]\left(1 - e^{r_o T_o}\right)} \quad . \tag{53}$$

In the sum for $\overline{N}_i^+$, we note that except for the first term, we are dealing with positive threshold values. Thus the bound describing the choice of k_1 is not valid and instead we use a single value of t, t_2, for all nonnegative values of j. The final bound can thus be optimized over this additional parameter. Thus, from Eqs. (37), (42), and (50),

$$\overline{N}_i^+ \leqslant \frac{D - 1}{D} \left(\exp[t_o T_o] \left\{ (k_1 - 1) + \exp[t_1 T_o + k_1 \beta(t_1)] \sum_{k=0}^{\infty} \exp[k\beta(t_1)] \right\} \right.$$

$$\left. + \sum_{j=-\infty}^{0} \exp[jt_2 T_o] \sum_{k=1}^{\infty} \exp[k\beta(t_2)] \right)$$

$$\bar{N}_i^+ = \frac{D-1}{D}\left(\exp[t_o T_o]\,\frac{(t_o - t_1)\,T_o}{\beta(t_1)} + \frac{\exp[t_o T_o]}{\{1-\exp[\beta(t_1)]\}}\right.$$

$$\left. + \frac{\exp[\beta(t_2)]}{\{1-\exp[-t_2 T_o]\}\,\{1-\exp[\beta(t_2)]\}}\right) . \tag{54}$$

Finally, from Eqs. (38), (41), (42), (49), and (50) as well as the relation $\Sigma\, i^2 x^i = x(1-x)/(1-x)^3$,

$$\bar{N}_i^- \le \frac{D-1}{D}\sum_{j=0}^{\infty}\left\{\sum_{k=1}^{k_1-1}\exp[(j+2)\,t_o T_o] + \sum_{k=k_1}^{\infty}\exp[(j+2)\,t_1 T_o + k\beta(t_1)]\right\}$$

$$\times\left\{\sum_{n=1}^{n_1-1}\exp[jr_o T_o] + \sum_{n=n_1}^{\infty}\exp[jr_1 T_o + n\alpha(r_1)]\right\}$$

$$= \frac{D-1}{D}\left[\exp[2t_o T_o]\,\frac{(r_o - r_1)\,(t_o - t_1)}{\alpha(r_1)\,\beta(t_1)}\,T_o^2\,\frac{\exp[(t_o + r_o)\,T_o]\,(1+\exp[(t_o + r_o)\,T_o])}{\{1-\exp[(t_o + r_o)\,T_o]\}^3}\right.$$

$$+\left(2\exp[2t_o T_o]\,\frac{(r_o - r_1)\,(t_o - t_1)}{\alpha(r_1)\,\beta(t_1)}\,T_o^2 + \frac{\exp[2t_o T_o]\,(t_o - t_1)\,T_o}{\{1-\exp[\alpha(r_1)]\}\,\beta(t_1)}\right.$$

$$\left.+\frac{(r_o - r_1)\,T_o}{\alpha(r_1)\,\{1-\exp[\beta(t_1)]\}}\right)\frac{\exp[(t_o + r_o)\,T_o]}{\{1-\exp[(t_o + r_o)\,T_o]\}^2} + \left(\frac{2\exp[2t_o T_o]\,(t_o - t_1)\,T_o}{\{1-\exp[\alpha(r_1)]\}\,\beta(t_1)}\right.$$

$$\left.\left.+\frac{1}{\{1-\exp[\alpha(r_1)]\}\,\{1-\exp[\beta(t_1)]\}}\right)\frac{1}{\{1-\exp[(t_o + r_o)\,T_o]\}}\right] \tag{55}$$

if $\alpha(r_1) < 0$, $\beta(t_1) < 0$, and $t_o + r_o < 0$.

We shall see that these conditions on r_1, t_1, r_o, and t_o place restrictions on the range of the ratio δ^2/σ^2 that permits convergence of the sums. If these conditions can be satisfied, we shall have shown that the number of computations for decoding one branch is bounded by a constant.

H. Existence Conditions

It remains to show that solutions to the equations

$$\alpha(r_o) = 0 \qquad r_o < 0$$

$$\beta(t_o) = 0 \qquad t_o > 0$$

$$\alpha'(r_1) = 0 \qquad r_1 < 0$$

$$\beta'(t_1) = 0 \qquad t_1 > 0$$

exist in such a manner that

$$r_o + t_o < 0 \quad .$$

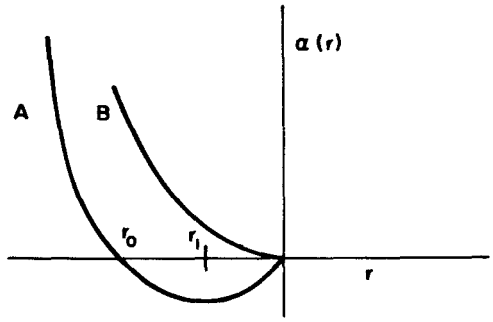

Fig. 9. Typical α(r) behavior.

We deal first with $\alpha(r)$. It must be shown that $\alpha(r)$ has the appearance of curve A of Fig. 9. That is, there is an $r_0 < 0$ and an $r_1 < 0$ such that

$$\alpha(r_0) = 0$$

and

$$\alpha'(r_1) = 0 \quad .$$

We shall show that $\alpha'(0)$ is positive for noise powers less than some critical value, that $\alpha(r)$ is convex upward, and that $\alpha(r)$ takes on a positive value for $r \geqslant -1/2$. These conditions provide the desired result.

Some of the properties of $\alpha(r)$ are easily calculated. From Eqs. (23a), (31b), and (40),

$$\alpha(r) = \frac{1}{2} \ln \int p_n(n)^{1+2r}\, dn + rR$$

$$\alpha(0) = 0$$

$$\alpha\left(-\frac{1}{2}\right) = \infty$$

unless $p_n(n) = 0$ for some interval of nonzero length. From an engineering standpoint, this is impossible since <u>some</u> noise will always be present and should be included in any realistic model.

Further,

$$\alpha'(r) = R + \frac{\int p(n)^{1+2r} \ln p(n)\, dn}{\int p(n)^{1+2r}\, dn}$$

$$\alpha'(0) = R + \int p(n) \ln p(n)\, dn = R - H(N) \quad .$$

If R exceeds H(N), the entropy of the noise, then $\alpha'(0)$ will be positive. $\alpha(r)$ is convex upward:

$$\alpha''(r) = \frac{2 \int p(n)^{1+2r} [\ln p(n)]^2\, dn \cdot \int p(n)^{1+2r}\, dn}{\left[\int p(n)^{1+2r}\, dn\right]^2} - 2\left[\frac{\int p(n)^{1+2r} \ln p(n)\, dn}{\int p(n)^{1+2r}\, dn}\right]^2 \quad .$$

Application of the Schwartz inequality to the numerator gives the desired result that $\alpha''(r) \geqslant 0$. Lemma 3 in Appendix A provides the proof that r_o and r_1 do exist.

Turning now to $\beta(t)$, we obtain several of its properties:

$$\beta(t) = tR + \frac{1}{2} \ln \int p(n)\, p(n+\delta)^{2t}\, dn + \ln D$$

$$\beta(0) = \ln D$$

$$\beta'(t) = R + \frac{\int p(n)\, p(n+\delta)^{2t} \ln p(n+\delta)\, dn}{\int p(n)\, p(n+\delta)^{2t}\, dn}$$

$$\beta''(t) = \frac{2 \int p(n)\, p(n+\delta)^{2t} [\ln p(n+\delta)]^2\, dn \cdot \int p(n)\, p(n+\delta)^{2t}\, dn}{[\int p(n)\, p(n+\delta)^{2t}\, dn]^2}$$

$$- 2 \left[\frac{\int p(n)\, p(n+\delta)^{2t} \ln p(n)\, dn}{\int p(n)\, p(n+\delta)^{2t}\, dn} \right]^2 .$$

Again applying the Schwartz inequality, we have the result that $\beta''(t) \geqslant 0$.

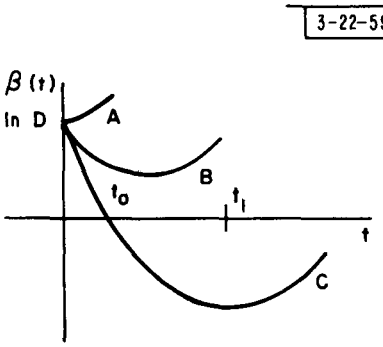

Fig. 10. Typical β(t) behavior.

These properties of $\beta(t)$ show that it has one of the three forms illustrated in Fig. 10. As this figure points out, only form C satisfies the conditions

$$\beta(t_o) = 0 \qquad t_o > 0$$

and

$$\beta'(t_1') = 0 \qquad t_1 > 0 \quad .$$

Unfortunately, the specific form of p(n) must be considered before it can be definitely established that $\beta(t)$ has form C. In addition, the requirement that $t_o + r_o < 0$ cannot be established. We therefore turn to a specific form for p(n), the Gaussian form, which will be studied in detail because of its practical interest.

I. Gaussian Noise

Since Gaussian white noise is that most commonly encountered in practice, we shall discuss it in detail. The noise vector has independent components each determined according to the probability density function

$$p_n(n) = (2\pi\sigma^2)^{-1/2} \exp[-n^2/2\sigma^2] \quad . \tag{56}$$

Using this density function, the various moment generating functions can be computed by simple integration. From Eqs. (23a) and (23b),

$$\gamma_1(r) = \int p(n)^{1+r}\, dn$$

$$= \int_{-\infty}^{\infty} (2\pi\sigma^2)^{-(1+r)/2} \exp[-n^2(1 + r)/2\sigma^2]\, dn$$

$$= [(2\pi\sigma^2)^r\ (1 + r)]^{-1/2} \tag{57}$$

$$\gamma_2(t) = \int p(n)\ p(n + \delta)^t\, dn$$

$$= \int_{-\infty}^{\infty} (2\pi\sigma^2)^{-(1+t)/2} \exp\{-[n^2 + t(n + \delta)^2]/2\sigma^2\}\, dn$$

$$= [(2\pi\sigma^2)^t\ (1 + t)]^{-1/2} \exp[-\delta^2 t/2\sigma^2(1 + t)] \quad . \tag{58}$$

Thus, using Eqs. (39) and (40),

$$\alpha(r) = r(R - \tfrac{1}{2} \ln 2\pi\sigma^2) - \tfrac{1}{4} \ln(1 + 2r) \tag{59}$$

and

$$\beta(t) = t(R - \tfrac{1}{2} \ln 2\pi\sigma^2) - \tfrac{1}{4} \ln(1 + 2t) - \frac{\delta^2 t}{2\sigma^2(1 + 2t)} + \ln D \quad . \tag{60}$$

Because of the transcendental nature of these equations, it is not possible to solve them explicitly for r_o and t_o. However, solutions can be found for r_1 and t_1.

$$r_1 = \frac{1 - 2C}{4C}$$

$$t_1 = -\tfrac{1}{2} + \left(\frac{1 \pm \sqrt{8CS + 1}}{8C}\right)$$

where

$$C = R - \tfrac{1}{2} \ln 2\pi\sigma^2$$

and

$$S = \frac{\delta^2}{\sigma^2} \quad .$$

Although it will not always do so, the positive term in the brackets is the only one which can lead to a positive t_1 for positive C and S.

It was not possible to obtain closed-form conditions under which $\beta(t_1)$ and $t_o + r_o$ are negative. In view of these difficulties, as well as the complexity of the bounds to $\bar{N}_c$, $\bar{N}_i^+$, and $\bar{N}_i^-$, we have plotted the bounds as a function of $R - \frac{1}{2} \ln 2\pi\sigma^2$, the value of the metric when the noise

sample is zero. The three bounds, as well as their sum $\overline{N}$, are plotted in Fig. 11(a-d), with the ratio δ^2/σ^2 as a parameter. In plotting these curves, D was set equal to 2 and T_o was chosen to be one-half the constant $R - \frac{1}{2} \ln 2\pi\sigma^2$. These curves will be discussed in the next section.

J. Summary

The results of this section can be summarized in the following theorem:

Theorem.

If D-level, sequentially involved parameters are decoded from data perturbed by additive noise with probability density given by $p(y|z)$, a monotone-decreasing symmetric function of $|y - z|$, and if each noise-free data point along an incorrect path differs from the corresponding noise-free point on the correct path by at least δ, the average number of computations to decode a branch is bounded by the sum of the three expressions for $\overline{N}_c$, $\overline{N}_i^+$, and $\overline{N}_i^-$ given in Sec. III-G.

The fact that this bound is a constant, independent of the depth of the reference node, indicates that as long as the conditions of the theorem hold, the average number of computations for decoding a branch is fixed for all depths.

To better understand the bounds calculated in this section, we discuss them in detail for Gaussian noise. We see in Fig. 11(a) that the number of computations for decoding correct branches that stem from the reference node is small whenever the bias constant, $R - \frac{1}{2} \ln 2\pi\sigma^2$, is large, and is very large whenever the constant is small. This is due to the fact that whenever the bias is too small, the correct path will always be negative and will therefore appear like an incorrect path to the decoder. Since considerations along the correct path do not involve points along incorrect paths, the distance of these paths from the correct one does not enter the bound.

The contribution to the average number of computations along incorrect paths, when the threshold is above $-T_o$, increases with the bias constant and does so more rapidly as δ^2/σ^2 increases. This is seen in Fig. 11(b). If the bias constant increases, more incorrect nodes will belong to this group and will appear correct to the decoder. If δ^2/σ^2 is small, the correct path will look very similar to the incorrect paths, and many branches will be traversed before conditions bring about a return to the correct path.

Finally, we consider the average number of computations along incorrect paths when the threshold is below $-T_o$. When the bias is small, most of the incorrect will belong to this group, and if it is very small the correct path will also be decreasing, thereby causing these incorrect paths to be investigated frequently. Thus there is a sharp increase in $\overline{N}_i^-$ for small bias, as can be seen in Fig. 11(c). If the bias constant is very large, an incorrect path in this category would be investigated only if a very large noise sample occurs. In the event that it does occur, very many computations would be needed to overcome it, especially if δ^2/σ^2 is too small.

In Fig. 11(d), the composite curves are plotted. The choice of the bias constant does not seem to be too critical, so long as δ^2/σ^2 is not too small. As this quantity decreases, the sensitivity of $\overline{N}$ to the bias constant increases.

IV. PROBABILITY OF ERROR

A. Introduction

In this section, we shall compute a bound to the probability of reaching an incorrect terminal node that is satisfactory to the decoder. We shall see that it decreases exponentially with W, the

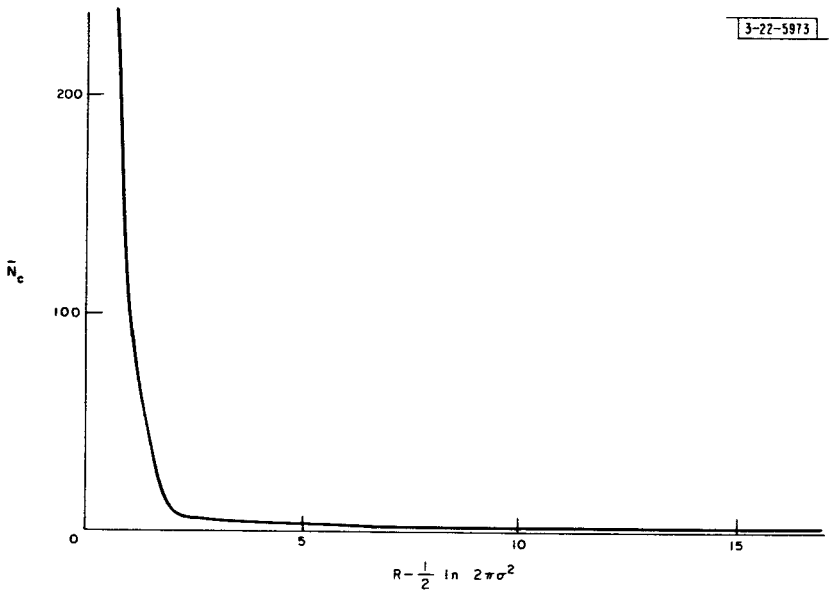

(a) $\bar{N}_c$ vs bias constant.

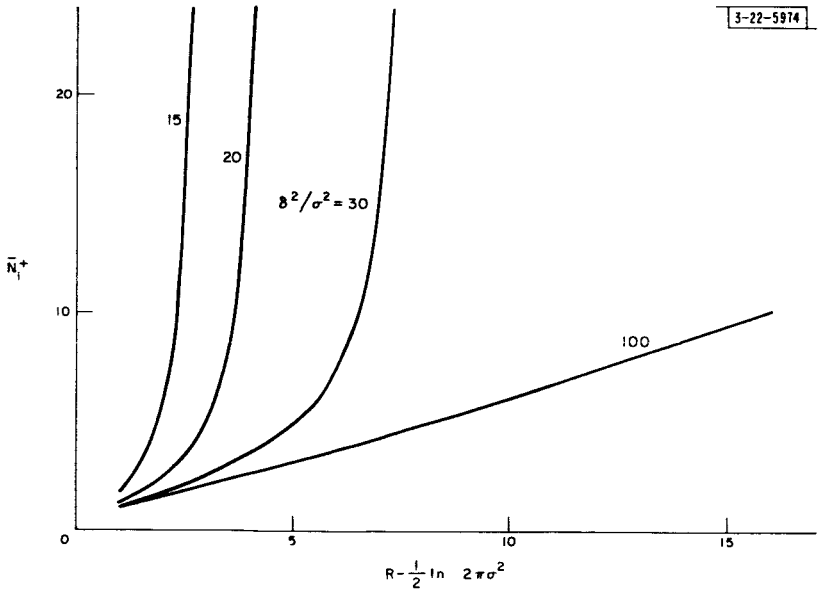

(b) $\bar{N}_i^+$ vs bias constant.

Fig. 11. Behavior of $\bar{N}$ and its components vs bias constant.

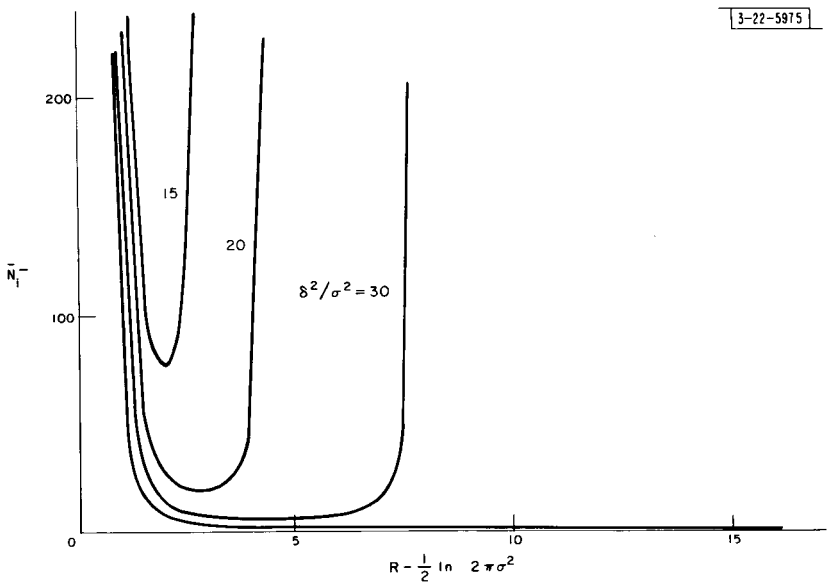

(c) $\bar{N}_i^-$ vs bias constant.

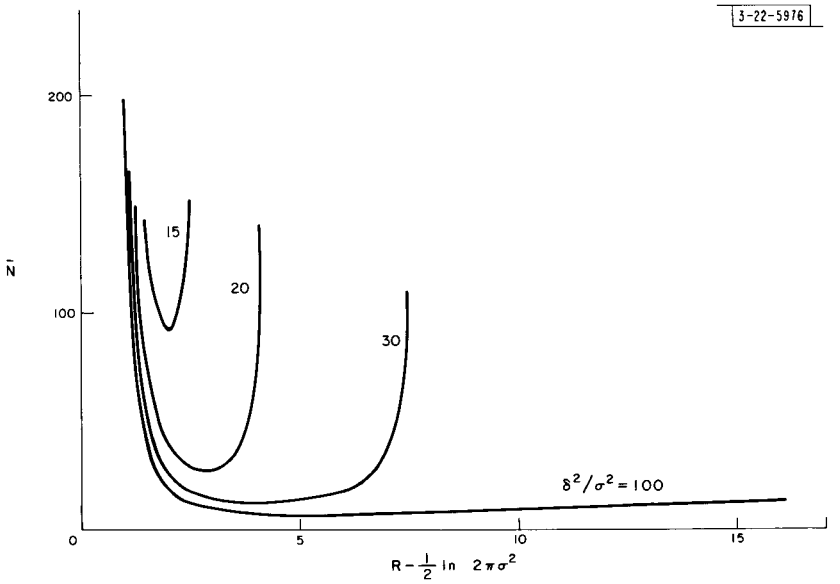

(d) $\bar{N}$ vs bias constant.

Fig. 11. Continued.

length of the tail, and that the exponent improves as the incremental bias δ increases for a fixed-probability density function. The error-probability bound is derived with the bias constant as a parameter, and the effects of varying it are considered by means of curves derived for Gaussian noise.

B. Events Leading to Errors

Recall that in Sec. III we introduced the notion of a reference node, and computed the average number of computations required to accept the correct branch stemming from it. The finite size of the tree was ignored, since the infinite size case provided an upper bound and was simpler to consider. However, the finite size of the tree could cause the decoder to complete the hypothesis vector along an incorrect path before the metric on the incorrect path has begun to fall. Consequently, the finite size of the tree plays a role in producing errors and must be considered when calculating the error probability.

In this consideration of the finite tree, the nodes along the correct path are no longer homogeneous. Therefore, each correct node must be considered separately, and the theorem on the probability of a union of events must be used to bound the total error probability. As before, we consider each node along the correct path as the reference node separately. Because of the inhomogeneity of the nodes along the correct path, we must define $T_1(\ell)$ as the highest threshold below the metric value at the reference node for depth ℓ. Since we are again considering only changes in the metric, we may arbitrarily choose its reference. For convenience, we choose the metric to be zero at the reference node. Thus $-T_o < T_1(\ell) \leq 0$.

There are two situations from which errors can arise. Suppose, first, that there is an incorrect path leaving the correct path at depth ℓ with a metric which remains above $T_1(\ell)$ for the entire tree duration after depth ℓ, and that this path is tested by the decoder before the correct one. It is clear that this path will appear satisfactory to the decoder regardless of the behavior of the metric on the correct path. Unless the metric on a path under test falls below $T_1(\ell)$, the decoder will never return to the node to change its incorrect decision.

Let Q_ℓ^+ be the probability that there is an incorrect path remaining above $T_1(\ell)$ for all depths greater than ℓ. Let Q^+ be the total contribution to the error probability by situations of this type. Since the probability of a union of events is bounded by the sum of the probabilities of the individual events, we have

$$Q^+ \leq \sum_{\ell=1}^{L} Q_\ell^+ \quad . \tag{61}$$

The other situation resulting in error takes place if the metric on the correct path at some node beyond ℓ falls below a threshold value $T \leq T_1(\ell)$. If the correct path falls below T and there should be an incorrect path leaving the correct path at node ℓ and remaining above $T - T_o$ until the end of the tree, difficulty might arise. For when the metric on the correct path falls below some T, other paths will be tried until one is found which is above $T - T_o$. Such a path will be followed until it falls below $T - T_o$. If it does not, an error will occur.

Define, therefore, Q_ℓ^- as the probability that the metric on the correct path starting at depth ℓ falls below some threshold value $T \leq T_1(\ell)$ and that there is an incorrect path leaving the correct path at depth ℓ with metric remaining above $T - T_o$. Then, using the theorem on the probability of a union of events, we bound the total contribution to the error probability from this second error situation Q^- by the sum

$$Q^- \leq \sum_{\ell=1}^{L} Q_\ell^- \quad . \tag{62}$$

Finally, the total error probability is bounded by the sum of the two contributions so that

$$P_e \leq Q^+ + Q^- \quad . \tag{63}$$

C. Chernoff Bounds

First, we shall compute a bound to Q_ℓ^+, the probability that there is some incorrect path with a metric remaining above $T_1(\ell)$ for the entire tree duration. We consider the probability that a particular incorrect path remains above $T_1(\ell)$, using for the computation that path most likely to remain above $T_1(\ell)$. We can then multiply by the number of paths to obtain a bound on the desired probability for some path. This is the same procedure used in the calculation of $\bar{N}$.

For the particular path used in the computation, we desire the probability that its metric remains above $T_1(\ell)$ at depths ℓ, $\ell + 1, \ldots, L$. This is the intersection of the events that the metric is above $T_1(\ell)$ at each depth individually. However, the probability of an intersection of events is upper bounded by the probability of any one of the composite events. Since the probability that an incorrect path is above T^* at depth k decreases with increasing k, we choose as the event in this bound the one corresponding to depth $L + W$, where L is the depth of the tree and W is the number of observations remaining after the last node has been reached. Consequently,

$$Q_\ell^+ \leq P^*_{W+L-\ell}\,[T_1(\ell)] \cdot (D-1)\,D^{L-\ell-1} \tag{64a}$$

where $P^*_{W+L-\ell}\,[T_1(\ell)]$ is the probability that a particular path, composed of $W + L - \ell$ incorrect noise-free data points differing from the correct noise-free data points by δ, remains above $T_1(\ell)$. If we recall that $P^*_{W+L-\ell}(T)$ increases with decreasing T, we can eliminate $T_1(\ell)$ by the inequality

$$P^*_{W+L-\ell}\,[T_1(\ell)] \leq P^*_{W+L-\ell}(-T_o) \quad . \tag{64b}$$

But we have bounded $P^*_{W+L-\ell}(T)$ in Sec. III-D. Thus, from Eqs. (14), (25), and (64b)

$$\begin{aligned} P^*_{W+L-\ell}[T_1(\ell)] &\leq \gamma_i^{(W+L-\ell)}(t)\,\exp[tT_o] \\ &\leq \gamma_2^{W+L-\ell}(t)\,\exp\{t\,[(W+L-\ell)\,R + T_o]\} \quad . \end{aligned} \tag{65}$$

We now turn to Q_ℓ^-, the probability that the correct path falls below T_1 and that some incorrect path starting at depth ℓ falls at most T_o below the smallest value to which the correct path falls. This quantity is bounded by the sum over T of the conditional probability $Q_\ell^-(T)$ that the correct path falls below T while some incorrect path remains above $T - T_o$, that is

$$Q_\ell^- \leq \sum_{j=0}^{\infty} Q_\ell^-(T_1 - jT_o) \quad . \tag{66}$$

Again we consider there are $(D-1)\,D^{L-\ell-1}$ incorrect paths with lower probabilities than those on a particular incorrect path, and again we assume that the noise-free data points on this

particular path differ from those on the correct path by δ at all time intervals. By the same reasons used earlier,

$$Q_\ell^-(T) \leqslant (D-1)\, D^{L-\ell-1} \sum_{k=1}^{L+W-\ell} P_r(M_k < T \quad , \quad M^*_{L+W-\ell} \geqslant T - T_o) \tag{67}$$

where the summation is a bound to the probability that the correct path falls below T for some depth beyond ℓ and the particular incorrect path remains above $T - T_o$ for all depths beyond ℓ.

Finally, we can employ the Chernoff bound to the summand obtained in Sec. III-D. From Eqs. (67), (21), and (27),

$$\begin{aligned} Q_\ell^-(T) &\leqslant (D-1)\, D^{L-\ell-1} \sum_{k=1}^{L+W-\ell} \gamma_i^{(k,\, L+W-\ell)}(r,t) \exp[-rT - t(T-T_o)] \\ &\leqslant (D-1)\, D^{L-\ell-1} \sum_{k=1}^{L+W-\ell} \gamma_3^k(r,t)\, \gamma_2^{L+W-\ell-k}(t) \\ &\quad \times \exp\{r(kR-T) + t[(L+W-\ell-k)R - T + T_o]\} \quad . \end{aligned} \tag{68}$$

In the next section, we consider these sums.

D. Carrying Out the Sums

The results of this section can be summarized by the two inequalities. From Eqs. (61), (64), and (65), we obtain

$$Q^+ \leqslant \sum_{\ell=1}^{L} (D-1)\, D^{L-\ell-1}\, \gamma_2^{W+L-\ell}(t) \exp\{t[(W+L-\ell)R + T_o]\} \quad , \quad t \geqslant 0 \tag{69}$$

and, from Eqs. (62), (66), and (68), we conclude that

$$\begin{aligned} Q^- \leqslant \sum_{\ell=1}^{L} \sum_{j=0}^{\infty} (D-1)\, D^{L-\ell-1} \sum_{k=1}^{L+W-\ell} \gamma_3^k(r,t)\, \gamma_2^{W+L-\ell-k}(t) \\ \times \exp\{r(kR + jT_o) + t[(W+L-\ell-k)R + (j+2)T_o]\} \quad , \quad t \geqslant 0,\ r \leqslant 0 \end{aligned} \tag{70}$$

where we have eliminated T_1 by using instead 0 or $-T_o$, whichever provided an upper bound. Amending these results with one expressed in Eq. (30), we obtain

$$Q^+ \leqslant \sum_{\ell=1}^{L} (D-1)\, D^{L-\ell-1} \exp\{(W+L-\ell)[\tfrac{1}{2}\mu_2(2t) + tR] + tT_o\} \quad , \quad t \geqslant 0 \tag{71}$$

$$\begin{aligned} Q^- \leqslant \sum_{\ell=1}^{L} \sum_{j=0}^{\infty} \sum_{k=1}^{L+W-\ell} (D-1)\, D^{L-\ell-1} \exp\{k[\tfrac{1}{2}\mu_1(2r) + rR] + k[\tfrac{1}{2}\mu_2(2t) + tR]\} \\ \times \exp\{(W+L-\ell-k)[\tfrac{1}{2}\mu_2(2t) + tR] + jrT_o \\ + (j+2)tT_o\} \quad , \quad t \geqslant 0,\ r \leqslant 0 \quad . \end{aligned} \tag{72}$$

These sums may be carried out with a single value for r and t, but a better result is achieved if an attempt is made to choose values closer to the optimum values for each term in the same manner as in Sec. III.

We consider Q^+ first. Recalling that

$$\beta(t) = \frac{1}{2}\,\mu_2(2t) + tR + \ln D \qquad \text{[Eq. (39)]}$$

and letting $m = W + L - \ell$, Eq. (71) can be rewritten

$$Q^+ \leqslant \frac{(D-1)}{D^{W+1}} \sum_{m=W}^{W+L-1} \exp[m\beta(t) + tT_o] \quad , \quad t \geqslant 0 \quad . \tag{73}$$

The variable t is a function of m and should be chosen according to

$$\beta'(t) = -\frac{T_o}{m} \tag{74}$$

for each value of the index. However, such a procedure would complicate the summations unnecessarily. Instead, we note that for large W, and we are chiefly interested in the exponential behavior with W, T_o/m in Eq. (74) approaches zero. Hence t becomes essentially constant and equal to t_1. Thus the sum can be carried out for $t = t_1$ to obtain

$$Q^+ \leqslant \frac{D-1}{D} \left\{ \frac{1 - \exp[L\beta(t_1)]}{1 - \exp[\beta(t_1)]} \right\} e^{t_1 T_o} \exp\{-W\,[\ln D - \beta(t_1)]\} \quad . \tag{75}$$

Turning now to Q^-, we apply a fairly loose bounding technique for the sake of simplicity. We remark, however, that the two-value method used in all previous calculations could be applied instead, but owing to the triple sum to be performed and the fact that the index at which the approximation changes can fall outside the summation limits as well as inside, the result rapidly becomes cumbersome.

Recalling that

$$\alpha(r) = \frac{1}{2}\,\mu_1(2r) + rR \qquad \text{[Eq. (40)]}$$

and

$$\beta(t) = \frac{1}{2}\,\mu_2(2t) + tR + \ln D \qquad \text{[Eq. (39)]}$$

and letting $m = L - \ell$, we rewrite the bound to Q^- of Eq. (72),

$$Q^- \leqslant \frac{D-1}{D^{W+1}} \sum_{j=0}^{\infty} \sum_{m=0}^{L-1} \sum_{k=1}^{W+m} \exp[k\alpha(r) + jrT_o + (W+m)\,\beta(t) + (j+2)\,tT_o] \tag{76}$$

for $t \geqslant 0$ and $r \leqslant 0$.

Noting first that the choice of r depends only on k and j while the choice of t depends on m and j, we consider choosing both these parameters for a fixed j. The optimum value of r could be chosen for each value of k and j according to

$$\alpha'(r) = -j\,\frac{T_o}{k} \quad . \tag{77a}$$

However, this would make the analysis very complex. Instead, we choose a single value of r and optimize the result over this parameter. Similarly, a different t could be chosen for each value of m and j according to

$$\beta'(t) = \frac{-(j+2)\,T_o}{W+m} \quad . \tag{77b}$$

Again this leads to unmanageable detail. We note that the exponent proportional to t in Eq. (76) grows without bound as the sum on j proceeds. Therefore, we choose one value of t in terms with a small value of j and set t = 0 for the remaining terms.

We now note that when $\alpha(r)$ is negative, the dominant term in the sum on k is that corresponding to k = 1 and that the dominant term in the sum on m is that corresponding to m = 0. Thus Eq. (76) can be bounded to obtain

$$Q^- \leqslant \frac{D-1}{D^{W+1}} \sum_{j=0}^{\infty} \sum_{m=0}^{L-1} (W+m) \exp[\alpha(r) + jrT_o + W\beta(t) + (j+2)\,tT_o]$$

$$= \frac{L(2W+L-1)\,(D-1)}{2D^{W+1}} \sum_{j=0}^{\infty} \exp[\alpha(r) + jrT_o + W\beta(t) + (j+2)\,tT_o] \quad . \tag{78a}$$

Thus the exponential behavior with respect to the tail length W is controlled by $\beta(t)$ alone. Since $\beta(t)$ is a minimum for $t = t_1$, we choose t according to

$$t = \begin{cases} t_1 & j < j_o \\ 0 & j \geqslant j_o \end{cases} \quad . \tag{78b}$$

Therefore, from Eqs. (78a) and (78b),

$$Q^- \leqslant \frac{L\,(2W+L-1)\,(D-1)}{2D^{W+1}} \left\{ \sum_{j=0}^{j_o-1} \exp[\alpha(r) + jrT_o + W\beta(t_1) + (j+2)\,t_1T_o] \right.$$

$$\left. + \sum_{j=j_o}^{\infty} \exp[\alpha(r) + jrT_o + W \ln D] \right\} \quad . \tag{79}$$

We change from $t = t_1$ to t = 0 at the term for which the second value of t gives a smaller value than the first. This occurs for

$$\frac{W\,[\ln D - \beta(t_1)]}{t_1T_o} - 2 < j_o \leqslant \frac{W\,[\ln D - \beta(t_1)]}{t_1T_o} - 1 \quad . \tag{80}$$

The first summation in the braces of Eq. (79) can be bounded by the product of the number of terms and the largest term. If this bound is employed, the sign of the sum $r + t_1$ delineates two cases which must be considered separately. Thus, from Eq. (79) and the relationship

$$\sum_{j=j_o}^{\infty} x^j = \frac{x^{j_o}}{1-x} \quad ,$$

we obtain for $r + t_1 > 0$

$$Q^- \leqslant \frac{L(2W + L - 1)(D - 1)}{2D^{W+1}} \left\{ j_o \exp[\alpha(r) + W\beta(t_1) + 2t_1 T_o + j_o(r + t_1) T_o] + \frac{\exp[\alpha(r) + W \ln D + j_o r T_o]}{1 - e^{rT_o}} \right\}$$

$$\leqslant \frac{L(2W + L - 1)(D - 1)}{2D} \left(j_o \exp\left\{\alpha(r) + t_1 T_o - rT_o + \frac{Wr}{t_1} [\ln D - \beta(t_1)]\right\} + \frac{\exp\left\{\alpha(r) - 2rT_o + \frac{Wr}{t_1} [\ln D - \beta(t_1)]\right\}}{1 - e^{rT_o}} \right) \tag{81}$$

for any $r \leqslant 0$, and if $r + t_1 \leqslant 0$

$$Q^- \leqslant \frac{L(2W + L - 1)(D - 1)}{2D} \left(j_o \exp\{\alpha(r) + 2t_1 T_o - W [\ln D - \beta(t_1)]\} + \frac{\exp\left\{\alpha(r) - 2rT_o + \frac{Wr}{t_1} [\ln D - \beta(t_1)]\right\}}{1 - e^{rT_o}} \right) \tag{82}$$

for any $r \leqslant 0$.

In the bound to Q^-, the chief interest is the part of the exponent proportional to W, the length of the tail. When $r + t_1 > 0$, the coefficient of W is given by

$$\frac{r}{t_1} [\ln D - \beta(t_1)]$$

but when $r + t_1 < 0$, the bound has two terms each with a different coefficient. In this case, however, $r/t_1 < -1$ so that the coefficient

$$[\ln D - \beta(t_1)]$$

is the dominant one.

The choice of r must now be made. Since we required $\alpha(r)$ to be nonpositive in the bounding process, and since the best exponent is obtained when r is as negative as possible, we choose $r = r_o$. With these bounds on Q^+ and Q^-, we can proceed to the final step.

The bounds to Q^+ and Q^-, when summed, give a bound to P_e, the probability of reaching the end of the tree on a path other than the correct one. Because of the complexity of the expressions, we cannot discuss them in general. For Gaussian noise, however, we can plot the exponent as a function of the various parameters, and then discuss its behavior for this important case.

E. Gaussian Noise

Using the moment generating functions found under the differential bias assumption in Sec. III, we can consider in detail the error probability for Gaussian noise. If the expressions are examined, it becomes clear that P_e decreases exponentially with W, the length of the tail beyond the last node of the tree. This is due to the fact that at earlier depths, the number of

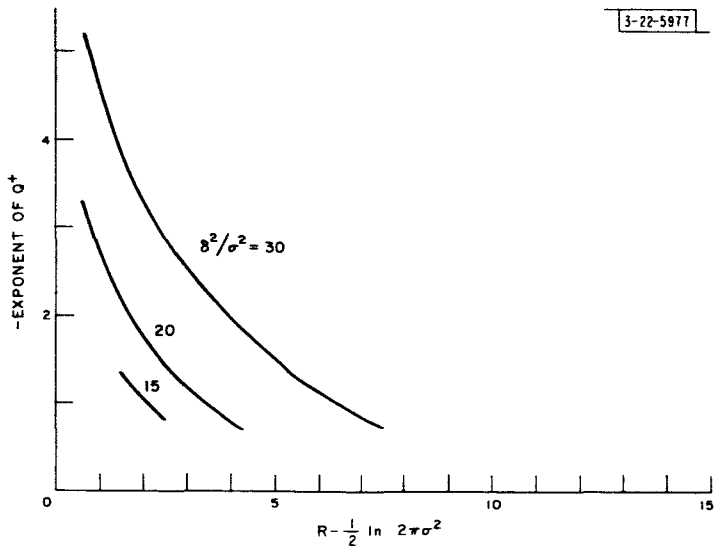

Fig. 12. Exponent of Q^+ vs bias constant.

alternatives is growing exponentially. Thus the additional data points which become available as the process continues do not contribute to lowering the error probability.

Since P_e can be made as small as desired by increasing W, we plot the coefficient of W as a function of the bias constant for various values of the ratio δ^2/σ^2. The part of P_e due to the first type of error is plotted in Fig. 12. For a fixed value of δ^2/σ^2, the exponent becomes more negative as the bias constant decreases. This is due to the fact that for a larger value of the bias constant, it is more likely that the metric on an incorrect path will remain above the reference metric value for the entire tree duration. As δ^2/σ^2 increases, the whole curve shifts to more negative values.

The remaining portion of P_e due to errors of the second kind has a peaked behavior and is plotted in Fig. 13. In the events leading to errors of the second kind, the joint behavior of the metric on the correct path and on incorrect paths is involved. Since the probability that an incorrect path remains above a particular threshold increases with increasing bias constant and the probability that the correct path falls below the threshold decreases with increasing bias constant, there are regions in which each situation dominates. Thus there is a best error exponent for the second type of error at an intermediate value of the bias constant. We note that the exponent for large bias constant is the same for errors of the first kind as for the second kind, and that for small bias constant, errors of the second kind predominate. Hence the curves of Fig. 13 also display the behavior of the total error exponent.

Finally, the exponent for the optimum value of the bias constant is plotted in Fig. 14. It is seen to have the usual behavior for exponents of this type.

F. Probability of First Error

Of alternate interest in many measurement problems is the probability of making a first error, rather than the probability of making any error at all. However, it is clear from Sec. IV-B that the probability of making an error at depth ℓ, P_ℓ is upper bounded according to

$$P_\ell \leq Q_\ell^+ + Q_\ell^-$$

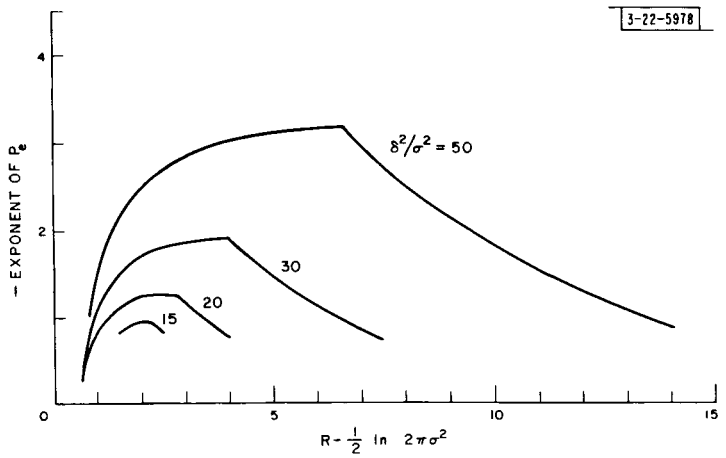

Fig. 13. Exponent of Q^- and P_e vs bias constant.

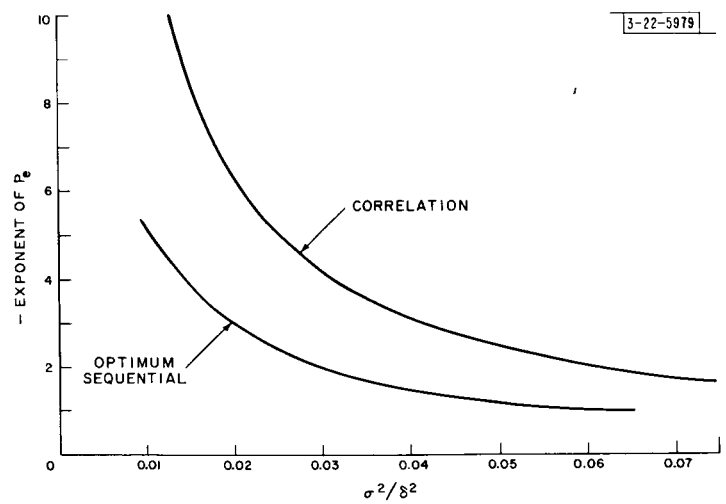

Fig. 14. Optimum exponent of P_e vs σ^2/δ^2.

where Q_ℓ^+ and Q_ℓ^- are given by Eqs. (64) and (66). Thus the summand of Eq. (71) and the sum on j and k in Eq. (72) provide the desired bound to Q_ℓ^+ and Q_ℓ^-, respectively.

Thus, after a rearranging of terms and setting $t = t_1$,

$$Q_\ell^+ \leqslant \frac{D-1}{D}\, e^{tT_o} \exp[-W\{\ln D - \beta(t_1)] + \frac{L-\ell}{W}\,\beta(t_1)\}] \quad . \tag{83}$$

Since $\beta(t_1)$ is negative, we see that the exponent is better if we consider the location of the first error closer to the origin of the tree.

Similarly, we consider Q_ℓ^-. From Eq. (76),

$$Q_\ell^- \leqslant \frac{D-1}{D}\, D^{-W} \sum_{j=0}^{\infty} \sum_{k=1}^{W+L-\ell} \exp[k\alpha(r) + jrT_o + (W+L-\ell)\,\beta(t) + (j+2)\,tT_o] \quad . \tag{84}$$

Again we note that for $\alpha(r) \leqslant 0$, the dominant term in the sum on k is that corresponding to k = 1. Hence

$$Q_\ell^- \leqslant \frac{D-1}{D}\, D^{-W} \sum_{j=0}^{\infty} (W+L-\ell) \exp[\alpha(r) + jrT_o + (W+L-\ell)\,\beta(t) + (j+2)\,tT_o] \quad . \tag{85}$$

Since the exponential behavior is again controlled by $\beta(t)$, we can use the same rationale for choosing t. Thus let

$$t = \begin{cases} t_1 & j < j_o \\ 0 & j \geqslant j_o \end{cases} \quad . \qquad \text{[Eq. (78b)]}$$

Thus, from Eqs. (85) and (78b),

$$Q_\ell^- \leqslant \frac{(D-1)\,(W+L-\ell)}{D^{W+1}}\, e^{\alpha(r)} \left\{ \sum_{j=0}^{j_o-1} \exp[jrT_o + (W+L-\ell)\,\beta(t_1) + (j+2)\,t_1T_o] + \sum_{j=j_o}^{\infty} \exp[jrT_o + (W+L-\ell)\ln D] \right\} \quad . \tag{86}$$

We choose j_o according to

$$\frac{(W+L-\ell)\,[\ln D - \beta(t_1)]}{t_1T_o} - 2 < j_o \leqslant \frac{(W+L-\ell)\,[\ln D - \beta(t_1)]}{t_1T_o} - 1 \quad . \tag{87}$$

Consequently for $r + t_1 > 0$, we obtain from Eqs. (86) and (87),

$$Q_\ell^- \leqslant \frac{(D-1)\,(W+L-\ell)}{D^{W+1}}\, e^{\alpha(r)} \left\{ j_o \exp[(W+L-\ell)\,\beta(t_1) + 2t_1T_o + (j_o-1)\,(r+t_1)\,T_o] + \frac{\exp[(W+L-\ell)\ln D + j_o rT_o]}{1 - e^{rT_o}} \right\}$$

$$Q_\ell^- \leq \frac{D-1}{D}\,(W+L-\ell)\,e^{\alpha(r)}\left[j_o \exp\left(2t_1T_o + \frac{Wr}{t_1}\left\{\ln D - \beta(t_1)\right.\right.\right.$$
$$\left.\left. + \frac{L-\ell}{W}\left[\left(1+\frac{t_1}{r}\right)\ln D - \beta(t_1)\right]\right\}\right) + \exp\left(-2rT_o + \frac{Wr}{t_1}\left\{\ln D - \beta(t_1)\right.\right.$$
$$\left.\left.\left. + \frac{L-\ell}{W}\left[\left(1+\frac{t_1}{r}\right)\ln D - \beta(t_1)\right]\right\}\right)\right] \tag{88}$$

for any $r < 0$.

If, on the other hand, $r + t_1 \leq 0$, we obtain

$$Q_\ell^- \leq \frac{(D-1)\,(W+L-\ell)}{D^{W+1}}\,e^{\alpha(r)}\left\{j_o \exp[(W+L-\ell)\,\beta(t_1) + 2t_1T_o]\right.$$
$$\left. + \frac{\exp[(W+L-\ell)\ln D + j_o rT_o]}{1-e^{rT_o}}\right\}$$
$$\leq \frac{D-1}{D}\,(W+L-\ell)\,e^{\alpha(r)}\left[j_o \exp\{-W\,[\ln D - \beta(t_1) - \frac{(L-\ell)}{W}\,\beta(t_1)]\}\right.$$
$$\left. + \frac{\exp\left(-2rT_o + \frac{Wr}{t_1}\left\{\ln D - \beta(t_1) + \frac{L-\ell}{W}\left[\left(1+\frac{t_1}{r}\right)\ln D - \beta(t_1)\right]\right\}\right)}{1-e^{rT_o}}\right] \quad . \tag{89}$$

The exponent in these expressions can now be examined. When $r + t_1 > 0$, the coefficient of W is identical in the two terms and is given by

$$\frac{r}{t_1}\left\{\ln D - \beta(t_1) + \frac{L-\ell}{W}\left[\left(1+\frac{t_1}{r}\right)\ln D - \beta(t_1)\right]\right\} \quad .$$

When $r + t_1 \leq 0$, there are two different exponents but it is clear that the more positive, and consequently the dominant, one is

$$-[\ln D - \beta(t_1) - \frac{L-\ell}{W}\,\beta(t_1)] \quad .$$

The choice of r can be made as in Sec. IV-D, $r = r_o$.

Turning at last to $P_\ell \leq Q_\ell^+ + Q_\ell^-$, we note that for some cases the dominant exponent is given by the bound to Q_ℓ^- and that in others it is the same for Q_ℓ^+ and Q_ℓ^-. Thus we need consider only the exponent in the bound for Q_ℓ^-.

In these bounds, the main interest lies in the coefficient of W. By comparing Eqs. (88) and (89) with (81) and (82), it is clear that this coefficient in the expression for the probability of first error is better than that for the probability of any error by a term that grows linearly with the distance of the error point from the end of the tree. Thus the probability of an error at a particular point depends not only on the length of the tail, but also on the number of output samples available beyond this point.

G. Summary

The error probability for the sequential measurement technique on a finite tree is bounded by a quantity that decreases exponentially with W. The exponent is calculated in detail for Gaussian noise. This exponent is plotted in Fig. 14 along with a similar bound for a correlation technique discussed in Appendix B. As is evident from the curves, there is a degradation in error probability exponent due to the sequential procedure† but in the cases considered here, the number of computations is the critical issue and for reasonable values of δ^2/σ^2, the sequential procedure is more attractive from this viewpoint.

V. SIMULATION

A. Introduction

In the preceding two sections, we analyzed the sequential algorithm as applied to measurement problems which satisfy two requirements. First, we required that a tree structure exist and second, we imposed a somewhat abstract assumption describing the relations among the hypotheses in the output space. This assumption was referred to as the differential bias assumption. Under these assumptions, we demonstrated that the sequential algorithm could be used to perform the measurement with a limited number of computations and with an error probability that decreases exponentially with the number of observations not dependent on undetermined parameters.

However, analysis is only to suggest the operational characteristics of a system; in order to test the model, to verify the hypotheses, and to suggest avenues for further analysis, experiments should be conducted. With this view in mind, an experimental "apparatus" in the form of a simulation program was designed and assembled. A number of experiments were performed and the resultant data indicated that the mathematical model was a satisfactory representation of the experimental model. In this section, we describe in detail the experiments and the results.

B. Simulation Objectives

There were several specific reasons for the simulation. In the first place, the sequential algorithm itself is fairly complex and tracing through the flow chart of Fig. 5 manually is, at best, tedious. A simulation that would graphically indicate the dynamics of the algorithm would do much to aid in its understanding and perhaps to suggest methods of improvement.

A second reason for the simulation was to test the various assumptions used in the analysis. Although the differential bias assumption specifies conditions under which the sequential measurement technique will function satisfactorily, it is difficult to assess, in most situations of practical interest, whether or not it is satisfied. Of course, an exhaustive computational analysis could be employed for a specific measurement situation, but this would produce little understanding of the general class of problems to which it applies.

In addition, although the differential bias assumption is sufficient to prove that the sequential method can be used in measurement problems, it may not be necessary. That is, weaker requirements on the differences between output vectors may still allow the sequential method to be employed. For this reason, and for the previous one, the simulation became desirable. By using the simulation, we could ascertain whether or not the sequential method could be applied to a particular measurement problem.

---

† The error probability for sequential measurement is lower bounded by the correlation error probability for the last decision.

Finally, we recall the coarseness of the bounds used to obtain the theoretical results. A compilation of data on typical problems would indicate whether these approximations left the essential characteristics of the bounded quantities intact.

In the bulk of the simulations work, the measurement problem considered was that of geophysical exploration. This problem was chosen for simulation because of a need for improved data-processing methods in that area. In addition, the geophysical exploration problem seemed typical of the many measurement situations in which it is difficult to assess the applicability of the algorithm. The model described in Sec. II was used, since it displayed the essential characteristics of the real problem without introducing excessive computational difficulties.

C. Simulation Program

The author was fortunate to have the opportunity to carry out the simulation on a time-shared IBM 7094 computer.[13] These facilities were available at Project MAC, an M.I.T. research group directed toward improved man-machine communication. Through on-line interaction with the computer, it was possible to observe directly and immediately how the simulator was operating, and to modify it at once whenever a change was necessary. More important, however, the dynamics of the decoder became readily available, thus leading to a significantly improved understanding of the decoder's operation. The availability of a graphic display unit made the dynamics very clear. Examples of the display were presented in Sec. II in connection with the description of the Fano sequential decoding algorithm. By varying the decoder's characteristic constants (R, T_o) and the noise variance, one could observe directly the effects of these variations on the over-all decoding process. Then one could plan intelligently the bulk of the off-line experimental work.

The simulation program is divided into several parts as indicated in Fig. 15, according to the various tasks that must be performed. First, all parameters are set to their initial values. These include various counters to tally the number of computations, the location variable which indicates the current location of the decoder, the choice vector i(n) which indicates the alternative chosen by the decoder at each node, the threshold value, and the metric. In addition, the

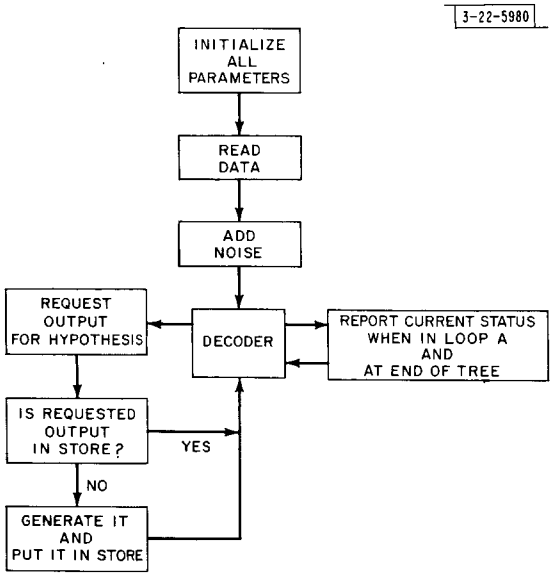

Fig. 15. Main sections of simulation program.

noise-free data store is emptied. Then the program is set up to read data for the next run. The following quantities are read as inputs:

The true values for the unknown parameters.

The probe signal.

The true noise-free data sequence resulting from the true parameters and probe signal. Reading this in saves recomputation when the same noise-free data are to be retested.

A set of independent Gaussian noise samples of zero mean and unit variance.

The set of quantization levels.

The noise variance.

The bias constant.

The metric increment.

A series of parameters governing the frequency of output.

After these parameters are read in, the noise is scaled according to the variance. It is then added to the true noise-free data sequence to provide noisy data to the decoder. The decoder is then entered.

The decoder operates according to the algorithm of the flow chart discussed in Sec. II. At each stage, it computes an increment to the metric according to

$$d_i = \sum_{j=i\nu}^{(i+1)\nu-1} [C - (y_j - z_j)^2] \tag{90}$$

where C is a constant, ν is the number of intervals along a tree branch, y_j is the received noisy data at time j and z_j is the noise-free output consistent with the current hypothesis and the probe signal. The sum is over all those intervals depending on the i^{th} hypothesis, but not on the $(i + 1)^{th}$.

We note that this metric is of the form

$$\sum_j [R + \ln p_n(y_j | z_j)]$$

for Gaussian noise. For in that case

$$R + \ln p_n(y_j | z_j) = R + \ln \left\{ \frac{1}{\sqrt{2\pi}\,\sigma} \exp[-(y_j - z_j)^2/2\sigma^2] \right\}$$

$$= \frac{1}{2\sigma^2} [2\sigma^2 R - \sigma^2 \ln 2\pi\sigma^2 - (y_j - z_j)^2] \quad . \tag{91}$$

Thus Eqs. (90) and (91) are proportional if

$$C = \sigma^2(2R - \ln 2\pi\sigma^2) \quad . \tag{92}$$

Consequently, the requirement that R be greater than the noise entropy introduced in Sec. III-H

$$R > H(N)$$

or

$$R > \frac{1}{2} \ln (2\pi e\sigma^2)$$

$$= \frac{1}{2} \ln e + \frac{1}{2} \ln 2\pi\sigma^2$$

$$= \frac{1}{2} + \frac{1}{2} \ln 2\pi\sigma^2$$

reduces to

$$C > \sigma^2 \quad . \tag{93}$$

This is to be expected since $C - \sigma^2$ is the expected value of the metric on the correct path and the operation of the decoder presupposes this to be positive.

The hypothesized noise-free output values $\{y_j\}$ are computed according to a subprogram which is changed with the measurement problem. Usually the $\{y_j\}$ are time consuming to compute. It is therefore desirable to store them until it no longer appears that they will be needed. Then they can be discarded. In the simulation program discussed here, a list structure technique is used to store the $\{y_j\}$ in a manner that makes their recall time short but does not require rearrangement of data in the store when items are to be discarded. This technique is discussed in detail in Sec. V-D.

Finally, provision is made to output the decoder's conditions at a selected frequency of passage through loop A. This output is in either a printed form giving the current hypothesis or in an oscillographic form displaying the metric values along those branches investigated by the decoder. Photographs of this display were presented in Fig. 6 to illustrate the operation of the algorithm.

D. Hypothesis Storage

Because of the computation time necessary in many measurement problems to compute the noise-free output resulting from a particular hypothesis and probe signal, it is worthwhile to consider techniques of storing these quantities. A satisfactory method must permit rapid access and small bookkeeping cost with respect to time and storage.

Several obvious techniques present themselves. First, a storage location could be provided for each possible composite hypothesis. The multidimensional aspect of the hypothesis vector makes this procedure absurd because of the huge storage required.

Second, a storage location could be provided for all hypotheses having a common first part, but differing in the tail. This method would require D^t locations if the tail is of length t. Thus the number of required locations remains fixed, as the decoder advances further into the tree. However, care must be taken in the design of the storage to permit rapid access to the information and to avoid excessive time spent in moving the data within the store as the decoder advances.

The method chosen for the simulation is of this type, but once the method is described, a third method can be suggested which permits the length of the tail to vary in a desirable manner. Before continuing, it is necessary to say a few words about list structures.

A list in a computer is a group of storage locations which are tied together by means of secondary locations we shall refer to as links. These links contain the machine addresses of other members of the list. Table I is an example of a three-element list. Link A contains the address of link B, and link B contains that of link C, etc. N_A, N_B, and N_C, entries on the list, are thus tied together by the links. If link A is tagged in some way to be the designated first

TABLE I

A SIMPLE ORDERED LIST

Machine Address	Symbolic Name	Contents
.		
.		
.		
4714	Link C	000
4715	List element C	N_C
.		
.		
.		
6102	Link A	7452
6103	List element A	N_A
.		
.		
.		
7452	Link B	4714
7453	List element B	N_B

element of the list, we can consider the list in the table as an ordered list, with the links detailing the order A, B, C.

A list structure develops if one of the members of a list is the name of a second list, known as a sublist of the first. The process may, of course, continue indefinitely, with sublists on sublists of other lists, etc.

With these preliminary definitions, we can describe the storage technique used in the simulation program. Each node which the decoder considers is stored as a separate ordered list. When the node list is first created, it contains 2D list elements, but an additional element is added whenever one of the branches leaving this node is tried by the decoder. Of the original list elements, the odd-numbered ones contain the hypothesized parameter values for the node and the even-numbered ones contain the noise-free output values. Exactly which noise-free output values are contained in the original even-numbered list elements will become apparent when the list structure is indicated. The parameter values of the list are ordered according to their likelihood on the basis of the data.

Once the decoder chooses a parameter at a node, it moves to the next node in the tree and creates a new list for it. The name of this list is entered on the list corresponding to the previous node, two entries below the chosen parameter value. Thus the main list has a tree structure of sublists, each corresponding to a node in the tree. For the sublist corresponding to a particular node to be reached, one must start at the main list and then proceed further to those

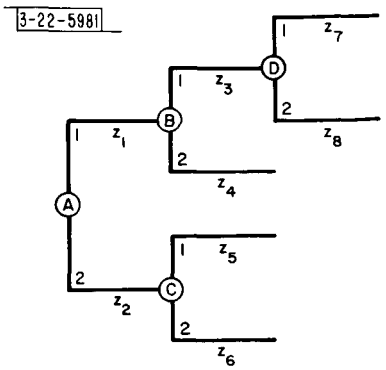

(a) Tree structure.

A	B	C	D
h_1	h_2	h_1	h_2
z_1	z_4	z_5	z_8
B	h_1	h_2	h_1
h_2	z_3	z_6	z_7
z_2	D		
C			

(b) Corresponding list structure.

Notes: (1) z_4 is the noise-free output resulting from alternative 1 for the first parameter and alternative 2 for the second parameter.
(2) At node D, the second alternative is more likely than the first.

Fig. 16. List structure.

successive sublists designated by the list names in the list structure. The structure is illustrated in Fig. 16.

To recover a noise-free output value from the list structure, one proceeds through the structure choosing successive lists to visit on the basis of the list names that follow the hypothesized parameters on each sublist. The list element below the hypothesized parameter on the list corresponding to the node of interest is the desired output value. Although the list structure method of storage sounds complex, it is only conceptually more involved than the usual methods. The important feature is that a storage word containing the machine address of the link belonging to the current hypothesis needs to be interrogated in order to determine the current decoder position and the data relevant to it. This storage word is then modified according to the information stored in the links as the decoder progresses. Because of the tree-like nature of the list structure, only a few links need be taken to reach any list that corresponds to a node of interest to the decoder.

When one decides to remove a node from the store, one must delete only the corresponding list name from lists on which it appears and then inform the bookkeeper that the extra list elements used in the list's formation are now available for other lists yet to be generated.

The removal of an entry in the list structure is governed, in the simulation program, by a simple but not optimum technique. Once the decoder reaches a fixed depth, say t, beyond a

node, all superfluous nodes prior to t nodes from the end of the tree are removed from the structure. Hence the required storage remains constant.

We note, however, that only a few of the D^t hypotheses in the tail will be tried; therefore, keeping D^t locations available in storage is wasteful of space. A better technique would consist of keeping the storage size fixed at some convenient level, and then removing early nodes from the store when, and only when, an overflow occurs. Hence a storage size of D^t would permit storage of nodes at depths earlier than t before the end of the tree

Coding the list manipulations was greatly simplified by the use of the Symmetric List Processor language.[14] This consists of a set of FORTRAN subroutines which automatically establish the links and extract information from the list structure as well as performing many other bookkeeping tasks. The reader is referred to Ref. 14 for further information on the system.

With these comments on the simulation program, we proceed to a discussion of the simulation itself.

E. Simulation Experiments

As discussed in Sec. II-E, a simplified model of the geophysical exploration problem was chosen to provide a measurement situation for testing the theoretical results by simulation. This model is described in that section.

In the simulation itself, the true impedance levels were chosen randomly in such a manner as to represent layers of various thicknesses. That is, a layer four units thick would be modeled by four equal, consecutive impedance values. Thus a fairly realistic fit could be made to many geological situations that involved only two materials.

The input signal was chosen, at first, to be a random sequence of pulses, but it soon became apparent that the largest possible signal-to-noise ratio should be provided to make the first estimate of an impedance value and thus a single pulse of maximum available energy is preferable. Only if there is a peak power limitation should an extended input be used.

For the given true parameter set and the input signal, it is possible to compute the true-observed noise-free data. This was done and noise was added from a set of Gaussian-distributed independent random samples. The noise level was varied by scaling a set of unit variance samples by the standard deviation. Once this addition was performed, a set of observed samples was available upon which the decoder could operate.

The program was organized to perform a number of sequential measurements on the same set of impedance values by varying for each the noise variance σ^2, the bias constant C, and the threshold increment T_o. In addition, the number of times the decoder passed through loop A in the flow chart of Fig. 5 was tallied to permit a progress report at any specified frequency. Provision was made to halt the measurement after a fixed number of passages through loop A. As we shall see in the next section, this possibility for termination will enter into the results of the simulation study.

To be definite, we shall define an experiment by using the simulator as an attempt to decode all unknown impedance values in a geophysical model that has a particular set of true quantized impedance values, a particular probe signal, a particular set of noise samples of variance σ^2, and particular values for the parameters C and T_o. A great many experiments of this type were conducted, but the total number was, of course, a minute fraction of those possible. The choice of which experiments to perform was governed to a great degree by experience gained during the

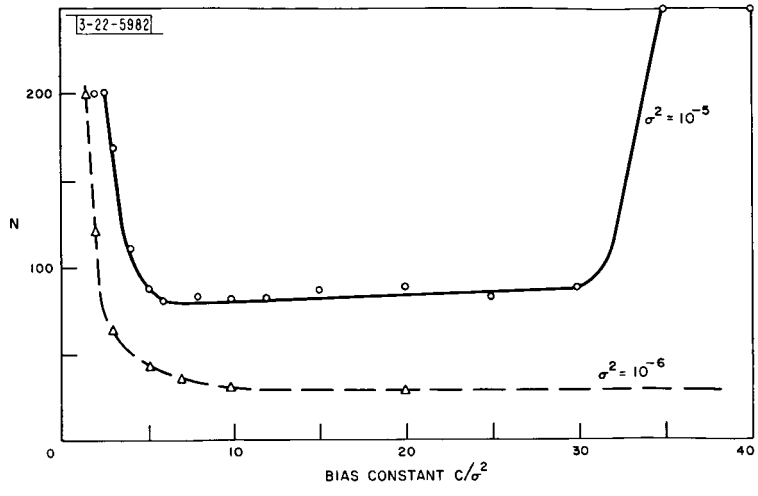

(a) First parameter set.

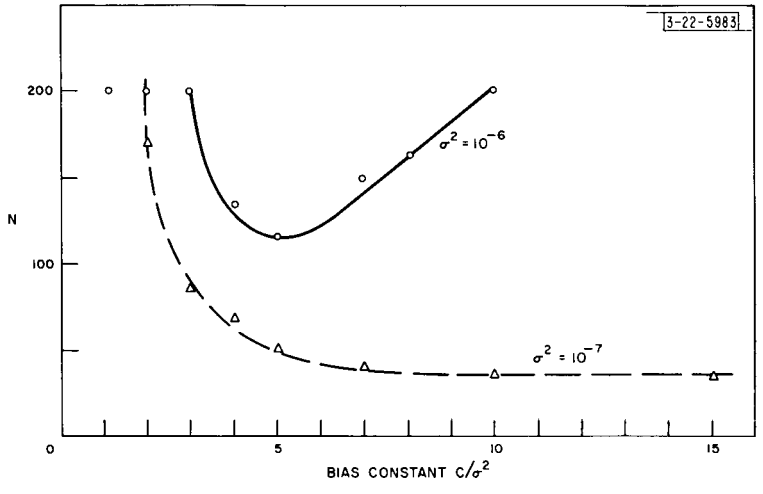

(b) Second parameter set.

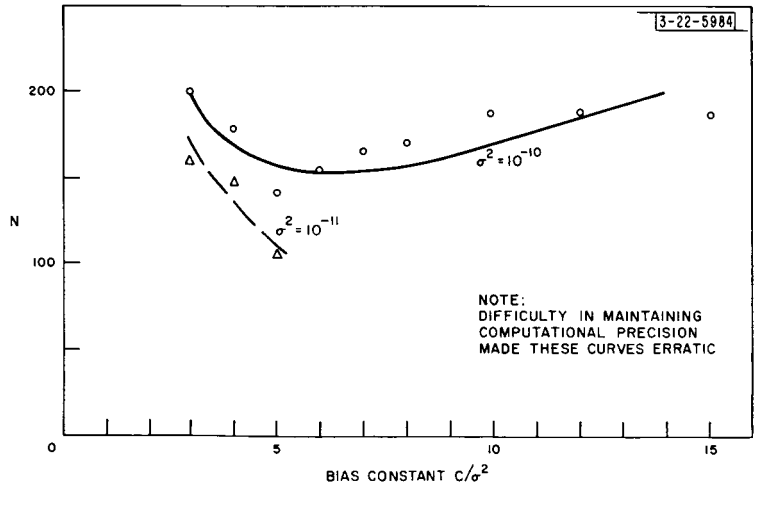

(c) Third parameter set.

Fig. 17. Number of computations vs bias (simulated).

on-line portion of the experimentation during which few actual data were obtained. On the basis of this experience, it was possible to choose a set of experiments that would be reasonable in number yet meaningful in result.

As mentioned earlier, the true impedance values were chosen to suggest a layered structure. Three different sets of 32 values were employed in the experimentation, each displaying a different degree of randomness. However, in choosing the values themselves, no conscious pattern was used. The intent was to represent typical geological environments. The characteristics of each of these sets will be discussed in more detail later.

The probe signal was a single pulse of amplitude 5.567. This particular value arose from a desire to compare the single-pulse results with those obtained for a sequence of 31 unit pulses with good autocorrelation function. Although no complete data were taken, the improvement obtained by using the single pulse was immediately apparent.

The noise samples were obtained from a Gaussian pseudo-noise generator available in the IBM 7094 library.[15] Only a few sequences of noise samples were used in the tests, and the noise level was varied by scaling the samples according to the standard deviation. This procedure permitted an evaluation of the effect of changing a parameter of the decoding process without concern for variation in the noise sequences, and without using the alternative of Monte Carlo operation to average the noise effects. In general, the change to a different basic sequence of noise samples did not affect the data significantly.

The noise variance σ^2 was varied a great deal in the experiments. It is important to note that its value was measured with respect to an input pulse amplitude. Thus, when one considers to what degree the noise obstructs the observations, a direct comparison of the noise variance with the effect under scrutiny is necessary. For example, if one is trying to measure an effect that appears in the fourth decimal place, it would be difficult to observe if the noise had a variance of 10^{-8} and a standard deviation of 10^{-4}.

The threshold increment T_o was varied along with C, the bias constant, and was always set equal to C/2. From the on-line experimentation, it was evident that T_o variations did not affect the results significantly, unless it was chosen too small. We shall see some data in support of this view later.

Finally, the bias constant C was varied considerably. Since the ratio C/σ^2 must exceed unity for the average metric value along the correct path to be positive, it was varied from that level by two orders of magnitude. We shall see that its choice was important in determining the outcome of an experiment.

Thus the main variations in the experimentation were of the noise variance σ^2 and the bias constant C. The results of the experiments could then be presented as a set of experimental curves of the same form as those derived theoretically in Sec. III.

F. Simulation Results

Figure 17(a-c) presents the results of the simulated measurement. Each point on these curves indicates the number of computations required to estimate a complete set of 32 parameters with a specified noise variance σ^2, threshold increment T_o, and bias constant C. All points thus plotted in each curve are for the particular set of 32 quantized impedance values listed in Table II. As becomes clear from an examination of the figures, the simulated curves are similar in form to those derived theoretically, but vary distinctly among themselves in the

TABLE II

PARAMETER VALUES FOR SIMULATION

Depth	Parameter Set For		
	Fig. 17(a)	Fig. 17(b)	Fig. 17(c)
1	1.0	1.0	1.0
2	1.0	1.0	0.1
3	1.0	0.1	1.0
4	0.1	0.1	1.0
5	0.1	0.1	1.0
6	0.1	0.1	1.0
7	1.0	1.0	0.1
8	1.0	0.1	0.1
9	1.0	0.1	1.0
10	0.1	0.1	1.0
11	0.1	1.0	0.1
12	0.1	1.0	1.0
13	0.1	1.0	0.1
14	0.1	1.0	0.1
15	0.1	1.0	1.0
16	0.1	1.0	0.1
17	0.1	0.1	0.1
18	1.0	0.1	1.0
19	1.0	1.0	1.0
20	1.0	1.0	1.0
21	1.0	1.0	0.1
22	1.0	1.0	0.1
23	0.1	1.0	1.0
24	0.1	0.1	0.1
25	0.1	0.1	0.1
26	1.0	1.0	1.0
27	1.0	1.0	0.1
28	1.0	0.1	1.0
29	1.0	0.1	0.1
30	1.0	0.1	0.1
31	1.0	0.1	0.1
32	1.0	1.0	1.0

noise variance value used to produce each separate curve. We shall see that this is due to the fact that a distinctly different differential bias parameter δ obtains for each set of parameter values.

We note that there are four types of points on these curves. First, there are those corresponding to a correct estimate of the complete parameter set; these are plotted along the curves. Second, there are those corresponding to an incorrect estimate of one or more parameters; these are plotted at the top of the graph. The third and fourth types arise because of the limit placed on the number of computations. If the decoder performs this maximum number of computations and tries the correct set of parameters, and this set has the maximum metric, the decoder has in effect been successful, although it did not satisfy its internal constraints. Such a point is plotted at $\overline{N} = 200$, the maximum number of computations permitted. If the decoder does not try the correct set before reaching the computational limit, an error is made. Such a point is also plotted at the top of the graph. It is possible to have a fifth type of point, although this did not occur in the simulation. If the decoder tries the correct parameter set as well as some others and one of these incorrect sets has the highest metric, the decoder will err. However, we note that any unbiased estimation procedure will also err, since the received signal vector is no longer closest to the correct noise-free vector in the output space.

This limitation on the number of computations was not the only special condition of the simulation. In all our previous discussions, we assumed that the decoder operated with perfect precision. Since this did not hold true in practice, there were several instances in which this effect became apparent. Generally speaking, they occurred when the additive noise level was low and the bias constant was also set at a low level. In this event, the metric increments on an incorrect branch would be several orders of magnitude larger than the total metric value. Thus, when an incorrect branch was tested, the threshold would be violated. When the decoder tried to retrace its steps to return to the correct path, all precision in the metric would have been lost.

This difficulty with the computer's precision arose also when internally calculated values were compared with the same values that have been transferred through the computer's input-output facility. Round-off errors brought about a second noise source that proved to be larger than the additive noise on several occasions.

As stated earlier, the data resulting from the simulation are presented in Fig. 17(a-c). Some general comments can be made about them. In the first place, they are seen to have the same over-all shape as the theoretical curves. For small bias constant, the number of computations is large because the correct path will tend to have negative metric increments as well as the incorrect paths. Thus the decoder may never leave the correct path, but it will repeatedly be forced back to the origin of the tree by increasingly negative metric values. For large bias constant, the incorrect paths will appear correct for several branches before a sufficient number of incorrect branches has been traversed to make the incorrect path have a very negative metric increment. Since the decoder will have to modify several hypotheses before returning to the correct path, the number of computations to rectify the error will be large.

An examination of the variance values on each curve indicates that the number of computations decreases as the noise level decreases. Indeed, it would be surprising if it were otherwise. However, we note that the particular noise variance on each curve is different for each set of true impedance values. In the next section, we shall see that this is due to a marked difference in the degree of dissimilarity between the correct output vector and the set of incorrect output vectors.

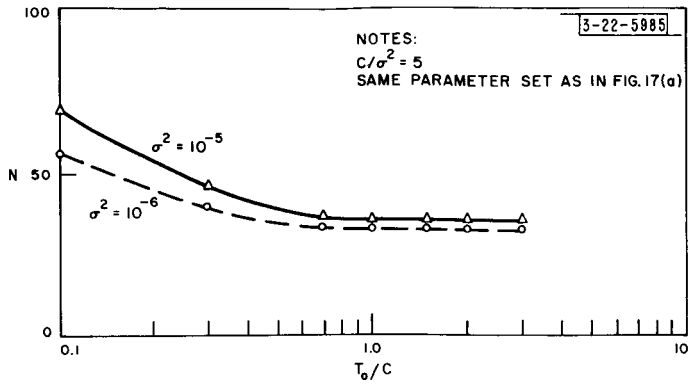

Fig. 18. Number of computations vs ratio of threshold increment to bias constant.

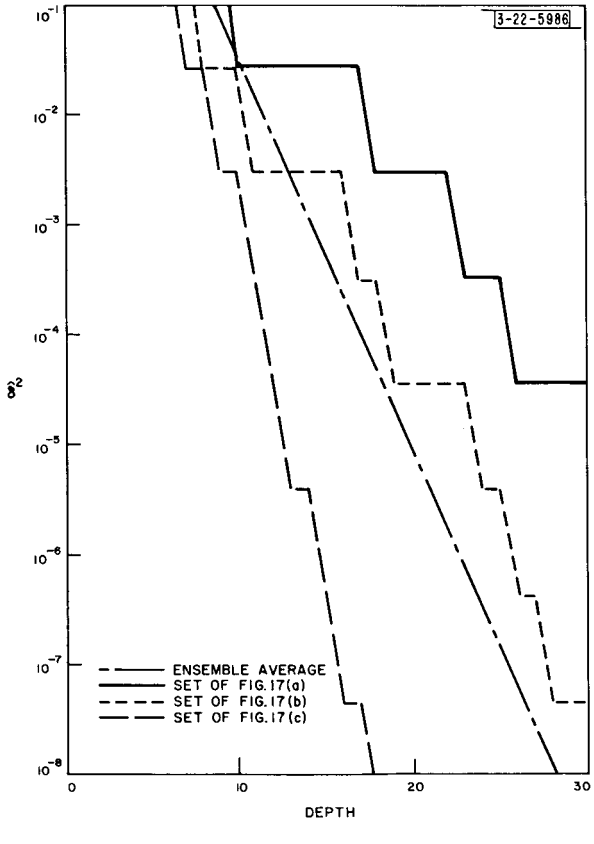

Fig. 19. Estimated δ^2 vs depth.

A few less formal results were obtained from the simulation. Although an attempt was made to analyze the microscopic behavior of the decoder, it did not seem useful to make any quantitative analyses; however, a few qualitative remarks are in order. Generally, the performance was as expected. As the bias constant was increased for a particular noise level, the number of computations required to correct a given error grew. This was due to the tendency of the metric on incorrect paths to increase when the bias is large. However, the number required to terminate the estimation after the correct hypothesis was tried for the first time decreased as the bias constant was increased. This was due to the fact that the tail includes many noise samples and this tends to produce a negative metric even on the correct path. As the bias constant becomes large, this tendency lessens. Finally as the noise level increases, the decoder makes its first error at an earlier depth in the tree.

Setting the threshold increment T_o at the value $C/2$ was done on the basis of evidence obtained from preliminary simulation work. Clearly, it should not be chosen too small or else many computations would be necessary to lower the threshold a fixed amount. If it is too large, the metric values on incorrect paths, although they decrease, will not fall below the threshold soon enough, causing incorrect paths to be searched unnecessarily. To check this choice of T_o, a series of runs was performed for different values of the ratio T_o/C. The results are presented in Fig. 18. It is clear that the choice of T_o/C is not critical.

G. Discussion of Results

Unfortunately, it is not possible to make a direct quantitative comparison of the theoretical and experimental results. This cannot be expected since, in the theoretical work, it was assumed that the bias introduced by following the incorrect path was independent of depth, whereas in the simulated geophysical problem this bias decreases exponentially with depth owing to the multiplicative coupling between layers. Nevertheless, some qualitative comparisons can be made.

We have already noted that the form of the curves obtained by simulation are similar to those obtained theoretically. We also remarked on the differences in variance required to produce a set of curves due to the dissimilarities in true impedance values. This dissimilarity would be reflected in the value of the differential bias parameter δ, if it could be computed. However, as noted earlier, computation of δ would require exhaustive effort.

Fortunately, a simply calculated quantity $\hat{\delta}$ indicates the magnitude of the effect one is using to originally hypothesize a value for a parameter. This quantity is the value obtained by calculating the noise-free output for each alternative at the nodes along the correct path, and then taking the difference between the output for the correct alternative and that for the incorrect one. For the particular parameter sets used in the simulation, this calculation was performed. The result as a function of depth is plotted for each parameter set in Fig. 19.

We can now compare the curves obtained by the simulation with those obtained theoretically. From Fig. 19, we observe that the parameter sets used to derive the curves of Fig. 17(a) has a lower $\hat{\delta}$ than those used to derive the curves of Fig. 17(b), and therefore should be less difficult to estimate. Indeed, that was the case. In the same way, the parameter set used for Fig. 17(c) is predicted to be more difficult to estimate than either of the other sets. Again, we note the agreement.

An estimate of the degree to which the particular parameter sets used in the simulation are typical can be obtained by computing the average value of $\hat{\delta}$ over the ensemble of parameter sets

with two impedance values being equally likely. This computation is given in Appendix D and the result for $Z_A/Z_B = 10$ is plotted in Fig. 19, along with the result for the specific curves. We see that the sets used were both better and worse than the average.

The curves describing the results of the simulation only indicate the experiments that were performed with a small enough noise variance so that the decoder would be successful in correctly estimating all 32 unknown impedances for some value of the bias constant. Other experiments were also carried out at higher noise levels at which the decoder could not successfully hypothesize the 32 values within the 200 computations allowed. In fact, as the noise level increased, the number of required computations grew more and more rapidly. Thus we see experimental evidence of the existence of a quantity analogous to R_{comp}, a rate at which the number of computations in communications grows without bound. This quantity is particularly important in connection with quantization effects, and therefore will be discussed further in Sec. VI.

In addition to the results obtained on the decoder's performance, both quantitatively and qualitatively, some insight into the geophysical problem was obtained. We shall discuss this understanding, as well as the effects of using the sequential algorithm on a nonquantized problem, in the next section.

H. Summary

The results of the simulation have borne out the theoretical results insofar as the general behavior of the number of computations vs the bias constant is concerned. A direct comparison of results is difficult because the decreasing amplitude of the effect depends on the unknown parameters in the simulated case. In view of the over-all character, however, it seems safe to say that the assumptions were reasonable and that the sequential measurement procedure is satisfactory on this simplified model of the geophysical layering problem.

VI. QUANTIZATION EFFECTS

A. Introduction

In this section, we consider briefly the problems arising from the quantization of the unknown parameters. We shall see that there is an upper limit to the precision obtainable with the sequential technique which may be below that obtainable with some other method. In addition, a masking noise arises which must be considered along with the additive noise in determining the total noise level.

B. Computational Cutoff

In the hypothesis testing done by the sequential algorithm, the differential bias parameter δ specified to what degree the various alternatives at a node affected the noise-free output vector. If these alternatives represent a set of quantization steps for a continuous parameter, the magnitude of δ is a measure of the effect produced at the output by a change of one quantization step.

The magnitude of δ is determined partly by the signal energy, partly by the transformation introduced by the transducer being measured, and partly by the size of the quantization steps. For a fixed available energy, the only one of these items which can be varied by the observer is the size of the quantization steps.

It is important to note that the ratio of the available energy to the receiver noise level is not sufficient to determine the precision. In particular, one must account for distortions which the

signal must undergo in the transducer after it "picks up" information about the unknown parameter, but before it can be observed. If, for example, this distortion were a saturation effect, a large change in the unknown parameter would be necessary to effect a small change in the transducer output. Thus, even though both the input and output energies, relative to the noise level, were large, those details in the output needed to determine precisely the unknown parameter would be lost in the compression. Consequently, one must consider transducer effects, as well as energy and noise level, in determining the precision that is possible.

We saw in both the theoretical and simulation work that when δ was too small relative to the noise, the decoder no longer efficiently chose the correct hypothesis set. Instead, it effectively began an exhaustive search of all possible hypotheses. Thus there was a critical value of the ratio δ/σ below which the decoder was ineffective. For fixed available energy, noise level, and transducer, this implies that there is a critical quantization step size below which the sequential method cannot be used. Since the size of the quantization steps indicates the precision of the measured parameter, the noise level, the available energy and the transducer all contribute to a maximum degree of precision that can be obtained.

It is informative to compare this limit with the corresponding limit in the communications case. Sequential decoding was found to be an effective and efficient decoding technique, as long as a particular rate R_{comp} was not exceeded. If communication at a higher rate was tried, the frequency of lengthy searches became so high that the average number of computations began to grow rapidly with constraint length.

If we now note that the precision of a parameter is the amount of information needed to specify it, we see that the precision obtained from a measurement is analogous to the rate of transmission in communications. Thus the critical size of the quantization steps in measurements and R_{comp} are analogous quantities. In addition, we note that it may be possible, by using an exhaustive nonsequential search procedure, to measure the unknown parameters to a higher degree of precision than is possible with a sequential method. This only means that the critical "rate" is below the maximum rate or channel capacity imposed by the available energy, the noise level, and the tranducer characteristics.

C. Masking Noise

In the preceding section, we observed that the available energy, the noise level, and the transducer set an upper limit to the degree of precision that can be obtained. The resultant imperfect precision leads to an effect which we shall refer to as masking noise.

When the sequential measurement technique is used, the k^{th} hypothesis is made on the basis of a quantity which was derived from the observed data vector and the set of $k-1$ hypotheses that has already been made. Define this quantity as the reduced data point for the k^{th} hypothesis. Because of the lack of precision in estimating the first $k-1$ unknown parameters, it will not be possible to compute exactly the reduced data point for the k^{th} hypothesis. The imprecision that results will be defined as the masking noise and must be considered with the additive noise when evaluating the noise level. If the precision is sufficiently high in estimating the first $k-1$ parameters, the masking noise will be small and will be dominated by the additive noise. If the precision is low, the masking noise will be the dominant problem. Thus the precision with which early estimates are made affects the error probability and number of computations for later estimates through the masking noise level.

We note that the masking noise is highly structured, since many dependencies exist among samples. Thus it cannot be considered simply as an increase in the additive noise level.

D. Precision in Geophysical Problem

We have noted in the preceding section how the precision at one depth in the decoding tree will affect the decoder in making estimates at later depths. We also noted in Sec. V that the output effect of varying an unknown parameter is an exponentially decreasing function of the number of previous discontinuities. In this section, we discuss the results of these effects in connection with the geophysical problem considered by simulation in Sec. V.

The limitation in precision discussed in Sec. VI-B led to the definition of a minimum value of the ratio δ/σ for which the sequential procedure could be used. Since this ratio decreases exponentially with depth in the geophysical layering problem, the precision which can be obtained (at a fixed noise level) decreases with depth as well. Thus the number of quantization levels should be reduced as one proceeds to deeper levels in the tree.

The decreasing precision with which the impedance value of an increasingly deep layer can be measured depends not only on the decreasing δ/σ ratio, but also on the increasing masking noise level that arises. As indicated in the preceding section, the masking noise level increases as one measures more and more parameters. Thus the masking noise level increases with depth in the geophysical layering problem. For this reason, one should quantize to as many levels as the δ/σ ratio permits. Then the masking noise will be reduced as much as possible for later hypotheses.

Consequently, because of the decreasing δ/σ ratio and the increasing masking noise, we see that the number of quantization levels should be decreased with depth, choosing the number at each depth as small as the δ/σ ratio permits. Thus we will determine the unknown parameters with a degree of precision that decreases with increasing depth.

VII. SUMMARY AND RECOMMENDATIONS

A. Summary

In this report, the applicability of a sequential measurement technique to a fairly broad class of problems was considered and was analyzed both theoretically and experimentally by computer simulation. Necessary conditions were determined under which the sequential procedure could be successfully operated with a limited number of computations, and with an error probability that decreased exponentially with the number of observations that can be made after the last hypothesis. A parameter was defined which could be used to characterize a particular measurement problem and in terms of which the performance could be estimated. In Secs. III and IV, curves were derived to indicate upper bounds to the level of this performance.

Since the value of the performance parameters is frequently difficult to determine and since many approximations were used in obtaining the theoretical results, it seemed desirable to simulate the sequential measurement algorithm that operates on a measurement problem of practical interest. Such a simulation was performed on a geophysical exploration model. From the simulation, it was possible to obtain curves of the same variables that were obtained theoretically, and thereby to compare the simulated results with those calculated. The comparison seemed to be a favorable one. The curves obtained by experiment were of the same general form as those obtained from the theory and by estimating the performance-dictating parameter mentioned

above, it was possible to make a slightly more specific comparison. Again, there seems to be good agreement between experiment and theory.

The shortcomings of this study seem to lie mainly in the reality of the model. We require a situation in which the successive data points are a function of an increasing number of unknown parameters and one in which the separation between possible parameter values, as viewed from the output, is clear. However, a preliminary investigation of the geophysical exploration problem through computation and simulation indicates that it satisfies these conditions. Thus the set of problems amenable to solution by the sequential measurement algorithm considered in this report seems to have at least one member. A detailed study of other measurement problems in order to formulate them into tree-like representation would be necessary for additional applications.

B. Suggestions for Further Research

Four research problems seem to follow as natural consequences of this work. In the first place, the applicability of the model introduced here for the geophysical exploration problem must be considered in greater detail. Such consideration would undoubtedly involve simulation with actual seismic data as recorded under field conditions, instead of the highly idealized data used in the simulation discussed above. Indeed, the simulator would require additional sophistication to account for the many seismic records obtained from the usual array of geophones and to include a priori information about the geological structure obtained from scattered drillings. Only when a complete simulation of this type is attempted would the applicability of the sequential method be ascertained.

The second area for further work lies in increasing the number of problems to which the algorithm applies. Indeed, there are many multidimensional parameter estimation problems of large proportions that are unassailable with the currently used hill-climbing techniques. If such a problem could be stated so that a tree structure becomes evident, it may well be possible that the sequential technique would be applicable.

Third, the possibility of a form of feedback can be noted. When the sequential algorithm is having difficulty, the difficulty is readily apparent. Thus the observer could stop the processing and rerun the experiment with new data or he could vary the parameters of the algorithm. Unlike the communication problem, there is no continual data stream being received. Thus no storage problem exists and the processing could be performed in nonreal time. Under such conditions, flexibility in modifying the algorithm as it operates is available and this freedom could be used to advantage.

Finally, it appears that a modification to the algorithm discussed here should be possible to permit specific consideration of parameters with continuous a priori distributions. If this distribution is known, and the noise distribution is also known, it is possible to measure the degree to which a set of estimates, as a whole, agrees with the data. Thus, if one incrementally picks the optimum value for a parameter in a sequential procedure, he may not be selecting the same value he would obtain by a joint estimation procedure. This notion suggests a coarse estimate with the incremental, sequential method, followed by a variational correction at a later stage, if the coarse estimate appears correct. An explicit technique for such a procedure, as well as its analysis, is outside the scope of this research. However, intuition gained from dealing with the sequential techniques suggests that a modification of this type would be possible

and that its implementation would substantially extend the scope of the problems amenable to a sequential measurement algorithm.

C. Conclusions

We have introduced a measurement technique that was suggested by the sequential decoding procedure for convolutionally encoded messages. This method was analyzed and found to be satisfactory, if several conditions of a fairly general nature were met. One specific, but complex, measurement problem was considered in detail and it satisfied these conditions. It is hoped that further research on this technique will show that it has applicability in other areas where multidimensional parameter sets are to be measured.

APPENDIX A
LEMMAS

Lemma 1.

If $\mu(r)$ is the log moment generating function of a random variable m, $\mu^*(t)$ is that of the random variable m*, and $\mu(r,t)$ is their joint log moment generating function, then

$$\mu(r,t) \leq \mu_o(r) + \mu_o^*(t)$$

$$\mu(r) \leq \mu_o(r)$$

$$\mu^*(t) \leq \mu_o^*(t)$$

where $\mu_o(r) = 1/2\ \mu(2r)$ and $\mu_o^*(t) = 1/2\ \mu^*(2t)$.

Proof.

Schwartz inequality, in its most general form, states that

$$E^2\ [f(x)\ g(x)] \leq E\ [f^2(x)]\ E\ [g^2(x)]$$

thus

$$\gamma^2(r,t) = E^2\ [e^{rm}\ e^{tm^*}] \leq E\ [e^{2rm}]\ E\ [e^{2tm^*}]$$

$$\gamma(r,t) \leq [\gamma(2r)\ \gamma^*(2t)]^{1/2}$$

$$\mu(r,t) \leq \frac{1}{2} \ln \gamma(2r) + \frac{1}{2} \ln \gamma^*(2t)$$

$$= \frac{1}{2}\ \mu(2r) + \frac{1}{2}\ \mu^*(2t)$$

$$= \mu_o(r) + \mu_o^*(t) \quad .$$

Also,

$$\gamma^2(r) = E^2\ [e^{rm}] \leq E\ [e^{2rm}]$$

$$\gamma(r) \leq [\gamma(2r)]^{1/2}$$

$$\mu(r) \leq \frac{1}{2} \ln \gamma(2r)$$

$$= \frac{1}{2}\ \mu(2r)$$

$$= \mu_o(r) \quad .$$

Similarly,

$$\mu^*(t) \leq \frac{1}{2} \ln \gamma^*(2t)$$

$$= \mu_o^*(t) \quad .$$

Lemma 2.

Let g(n) be a positive symmetric function of n, a random variable with symmetric probability element p(n) dn. Let g(n) be monotone decreasing as a function of $|n|$. Then, if $|\delta_2| \geq |\delta_1|$,

$$E\,[g(n-\delta_1)] > E\,[g(n-\delta_2)] \quad .$$

Proof.

Let $G(n) = g(n-\delta_1) - g(n-\delta_2)$. By Lemma 2a, G(n) is asymmetric about $(\delta_1+\delta_2)/2 \triangleq \delta_o$. If $\delta_2 < -|\delta_1|$, $\delta_o < 0$, and when $n < \delta_o$, $|n-\delta_2| = |n-\delta_1+(\delta_1-\delta_2)| < |n-\delta_1|$. Thus, by the monotone-decreasing assumption for g(n), $G(n) < 0$ for $n < \delta_o$ and $G(n) > 0$ for $n > \delta_o$. Similarly, if $\delta_2 > |\delta_1|$, $G(n) > 0$ for $n < \delta_o$, and $G(n) < 0$ for $n > \delta_o$. There are four cases:

(1) $\delta_2 \geq |\delta_1| \qquad \delta_1 \geq 0$

(2) $\delta_2 \geq |\delta_1| \qquad \delta_1 < 0$

(3) $\delta_2 \leq -|\delta_1| \qquad \delta_1 \geq 0$

(4) $\delta_2 \leq -|\delta_1| \qquad \delta_1 < 0$.

We consider in detail case (1); the others follow in a similar manner.

$$\int_{-\infty}^{\infty} p(n)\,G(n)\,dn = \int_{-\infty}^{(\delta_1+\delta_2)/2} p(n)\,G(n)\,dn + \int_{(\delta_1+\delta_2)/2}^{\infty} p(n)\,G(n)\,dn$$

$$= \int_{-\infty}^{(\delta_1+\delta_2)/2} p(n)\,G(n)\,dn + \int_{-\infty}^{(\delta_1+\delta_2)/2} p(\delta_1+\delta_2-n)\,G(\delta_1+\delta_2-n)\,dn$$

$$= \int_{-\infty}^{(\delta_1+\delta_2)/2} p(n)\,G(n)\,dn - \int_{-\infty}^{(\delta_1+\delta_2)/2} p(\delta_1+\delta_2-n)\,G(n)\,dn$$

$$= \int_{-\infty}^{(\delta_1+\delta_2)/2} G(n)\,[p(n) - p(n-\delta_1-\delta_2)]\,dn$$

$$\geq 0 \quad .$$

The inequality follows from the fact that $p(n) > p(n-\delta_1-\delta_2)$ for $n < (\delta_1+\delta_2)/2$ and the other manipulations are possible because of the symmetry assumption.

Lemma 2a.

If f(x) is a symmetric function of x, $f(x) - f(x-\delta)$ is asymmetric about $\delta/2$.

Proof.

By the definition of asymmetry,

$$g(x+\delta_o) = -\,g(-x+\delta_o)$$

then

$$f(x + \delta/2) - f(x + \delta/2 - \delta) = f(x + \delta/2) - f(x - \delta/2)$$

$$= f(-x - \delta/2) - f(\delta/2 - x)$$

$$= -[f(-x + \delta/2) - f(-x - \delta/2)]$$

$$= -[f(-x + \delta/2) - f(-x + \delta/2 - \delta)] ,$$

Q. E. D.

Lemma 3.

If f is a continuous function and has a continuous derivative on (a, b) and if f(b) = 0, f'(b) > 0, and f(a) > 0, then there exists an $x \in (a, b)$ such that f(x) = 0. In addition, there exists a $y \in (a, b)$ such that f'(y) = 0.

Proof.

Under the above conditions, there exists an $\delta_o > 0$ such that $f'(b - \delta) > 0$ for all δ, $0 \leqslant \delta \leqslant \delta_o$. Hence f is monotone increasing on $(b - \delta_o, b)$. Thus there exists a $w < b$, such that f(w) < 0. Since f is continuous, there exists an $x \in (a, b)$ such that f(x) = 0.

Rolle's theorem provides the second part. Since f(x) = f(b) there exists a $y \in (x, b)$ such that f'(y) = 0.

APPENDIX B
LINEAR REGRESSION ANALYSIS

If the equations expressing the relationship between the undisturbed filter output and the filter components are examined, it becomes clear that the problem can be formulated in terms of linear regression theory and that its techniques can be applied directly.[7] Now $y_1, \ldots, y_{2N-1}$ are $2N-1$ independent random variables, all having variances σ^2 and with means given by the so-called regression function

$$E[y_i] = z_i = \sum_{j=1}^{N} a_{ij} h_j \qquad i = 1, \ldots, 2N-1 \tag{B-1}$$

where the $(a_{i1}, \ldots, a_{iN})$, $i = 1, \ldots, 2N-1$ are known vectors constructed from the N input components $s_i, \ldots, s_N$. If we use normal linear regression analysis techniques, the parameters $h_1, \ldots, h_N$ can be estimated by considering them as regression coefficients to be determined.

Let ξ_i be an arbitrary unbiased linear estimator for h_i. Thus

$$\xi_i = \sum_{j=1}^{2N-1} \alpha_{ij} y_j \qquad i = 1, \ldots, N \quad . \tag{B-2}$$

The unbiased requirement further implies

$$E[\xi_i] = \sum_{j=1}^{2N-1} \alpha_{ij} \sum_{k=1}^{N} a_{jk} h_k = h_i \tag{B-3}$$

which, in turn, requires that the α_{ij} must satisfy

$$\sum_{j=1}^{2N-1} \alpha_{ij} a_{jk} = \delta_{ik} \tag{B-4}$$

where δ_{ik} is the Kronecker delta. If we desire a minimum variance estimator, we must minimize

$$\text{var}[\xi_i] = \sum_{j=1}^{2N-1} \alpha_{ij}^2 \sigma^2 \tag{B-5}$$

with respect to α_{ij} subject to Eq. (B-4).

Using a set of LaGrange multipliers to include the constraints,

$$\frac{\partial}{\partial \alpha_{ij}} \left\{ \text{var}[\xi_i] - 2\sigma^2 \sum_{k=1}^{N} \lambda_{ik} \left(\sum_{j=1}^{2N-1} \alpha_{ij} a_{jk} - \delta_{ik} \right) \right\} = 0 \qquad \begin{matrix} i = i, \ldots, N \\ j = 1, \ldots, 2N-1 \end{matrix} \tag{B-6}$$

or

$$2\sigma^2 \alpha_{ij} - 2\sigma^2 \sum_{k=1}^{N} \lambda_{ik} a_{jk} = 0 \qquad \begin{matrix} i = 1, \ldots, N \\ j = 1, \ldots, 2N-1 \end{matrix} \quad . \tag{B-7}$$

In addition, there is the constraint equation

$$\sum_{j=1}^{2N-1} \alpha_{ij}\, a_{jk} = \delta_{ik} \quad . \qquad \text{[Eq. (B-4)]}$$

Thus

$$\alpha_{ij} = \sum_{k=1}^{N} \lambda_{ik}\, a_{jk} \quad . \qquad \text{(B-8)}$$

If we multiply this result by $a_{j\ell}$ and sum over j,

$$\begin{aligned} \sum_{j=1}^{2N-1} \alpha_{ij}\, a_{j\ell} &= \sum_{j=1}^{2N-1} \sum_{k=1}^{N} \lambda_{ik}\, a_{jk}\, a_{j\ell} \\ &= \sum_{k=1}^{N} \lambda_{ik}\, c_{k\ell} \\ &= \delta_{i\ell} \end{aligned} \qquad \text{(B-9)}$$

where

$$c_{k\ell} = \sum_{j=1}^{2N-1} a_{jk}\, a_{j\ell} \quad . \qquad \text{(B-10)}$$

As long as the $(a_{i1}, \ldots, a_{iN})$ are linearly independent, it is clear from Eq. (B-9) that the solution for the λ_{ik} is given by the matrix equation

$$[\lambda_{ik}] = [c_{ik}]^{-1} = [c^{ik}] \qquad \text{(B-11)}$$

where c^{ik} is the element in the i^{th} row and k^{th} column of $[c_{ik}]^{-1}$. Consequently, from Eqs (B-2), (B-8), and (B-11), the minimum variance unbiased linear estimator for h_i is the linear combination of the samples given by

$$\begin{aligned} \zeta_i &= \sum_{j=1}^{2N-1} \sum_{k=1}^{N} c^{ik}\, a_{jk}\, y_j \\ &= \sum_{j=1}^{2N-1} d_{ij}\, y_j \end{aligned} \qquad \text{(B-12)}$$

where

$$d_{ij} = \sum_{k=1}^{N} c^{ik}\, a_{jk} \quad . \qquad \text{(B-13)}$$

To find the variance of this estimate, we substitute Eqs. (B-4), (B-8), and (B-11) into Eq. (B-5).

$$\text{var}\,[\xi_i] = \sum_{j=1}^{2N-1} \alpha_{ij}^2 \sigma^2$$

$$= \sigma^2 \sum_{j=1}^{2N-1} \alpha_{ij} \sum_{k=1}^{N} \lambda_{ik} a_{jk}$$

$$= \sigma^2 \sum_{j=1}^{2N-1} \sum_{k=1}^{N} c^{ik} \alpha_{ij} a_{jk}$$

$$= \sigma^2 \sum_{k=1}^{N} \delta_{ik} c^{ik}$$

$$= \sigma^2 c^{ii} \quad . \tag{B-14}$$

We may note that in the problem under consideration,

$$a_{jk} = \begin{cases} s_{j-k+1} & k \leqslant j \leqslant N + k - 1 \\ 0 & \text{otherwise} \end{cases} \quad . \tag{B-15}$$

Thus Eq. (B-10) becomes

$$c_{k\ell} = \sum_{j=k}^{N+k-1} s_{j-k+1}\, s_{j-\ell+1}$$

$$= \sum_{m=1}^{N} s_m\, s_{m+k-\ell} \tag{B-16}$$

the autocorrelation function of the input signal. Should this be an impulse,

$$c_{k\ell} = N\, \delta_{k\ell} \tag{B-17}$$

then

$$c^{k\ell} = \frac{1}{N}\, \delta_{k\ell} \tag{B-18}$$

and the weights for the terms in the linear regression formula will be

$$d_{ij} = \sum_{k=1}^{N} \frac{1}{N}\, \delta_{ik}\, s_{j-k+1}$$

$$= \frac{1}{N}\, s_{j-i+1} \quad . \tag{B-19}$$

It is thus clear that the minimum variance unbiased linear estimate for h_i is the cross correlation of the filter input with the noisy output given by

$$\zeta_i = \frac{1}{N} \sum_{j=1}^{N+i-1} s_{j-i+1}\, y_j \quad . \tag{B-20}$$

The corresponding variance can be computed from Eqs. (B-14) and (B-18)

$$\text{var}\,[\zeta_i] = \sigma^2/N \quad .$$

If the input does not have an impulse for an autocorrelation function, a modified form of the cross correlation is used. The pertinent coefficients are to be found in Eq. (B-13) which requires the inversion of the c_{ik} matrix.

APPENDIX C
WEAKENING THE DIFFERENTIAL BIAS ASSUMPTION

In this appendix, we show that the differential bias assumption can be weakened to a condition on the sum of the individual biases, if the probability density of the noise has a certain general property. Specifically, we assume that $p_n(n)$ is upper bounded by a function of the form $Ae^{-\alpha|n|}$ where A and α are any positive constants. Then we show that the moment generating functions obtained under the differential bias assumption can also be obtained under the more general condition

$$\sum_{i=1}^{k} |\delta_i| \geq k\delta$$

for all k, where δ is a constant and the $\{\delta_i\}$ are the differential biases of the incorrect branches involved.

First, from Eq. (13)

$$\gamma_i^{(1)}(t) = e^{tR} \int_{-\infty}^{\infty} p_n(x)\, p_n(x+\delta)^t\, dx \qquad t \geq 0 \quad .$$

Thus, from the hypothesis above, assuming that δ_i is positive (the case of δ_i negative follows in a similar manner),

$$\gamma_i^{(1)}(t) \leq A^{1+t} e^{tR} \left[\int_{-\infty}^{-\delta} e^{\alpha x} e^{\alpha(x+\delta)t}\, dx \right.$$

$$\left. + \int_{-\delta}^{0} e^{\alpha x} e^{-\alpha(x+\delta)t}\, dx + \int_{0}^{\infty} e^{-\alpha x} e^{-\alpha(x+\delta)t}\, dx \right]$$

$$= \frac{A^{1+t} e^{tR}}{\alpha} \left\{ \frac{e^{-\alpha\delta}}{1+t} + \frac{e^{-\alpha\delta t}}{1-t} \left[1 - e^{-\alpha\delta(1-t)}\right] + \frac{e^{-\alpha\delta t}}{1+t} \right\} \qquad t \geq 0$$

$$= \frac{2\, e^{tR} A^{1+t}}{\alpha(1-t^2)} \left[e^{-\alpha\delta t} - t\, e^{-\alpha\delta}\right]$$

$$\leq \begin{cases} \dfrac{2\, e^{tR} A^{1+t} e^{-\alpha\delta t}}{\alpha(1-t^2)} & 0 \leq t \leq 1 \\ \dfrac{2\, e^{tR} A^{1+t} e^{-\alpha\delta}}{\alpha(t^2-1)} & 1 < t \end{cases}$$

for $\delta > 0$ and the sign of the exponent is reversed if $\delta < 0$. Thus, in either case, the dependence on $|\delta|$ is exponential. When we consider the moment generating function of the sum of the metric on many incorrect branches as in Eq. (13), we take the product of the moment generating functions. Thus the required moment generating function is bounded by an expression that is exponential in the sum of the magnitude of the corresponding individual biases. In particular, the bound is of the form

$$\gamma_i^{(k)}(t) \leqslant \begin{cases} f_1(t) \exp\left[-\alpha t \sum_{i=1}^{k} |\delta_i|\right] & 0 \leqslant t \leqslant 1 \\ f_2(t) \exp\left[-\alpha \sum_{i=1}^{k} |\delta_i|\right] & 1 < t \end{cases}$$

Thus if $\sum_{i=1}^{k} |\delta_i| > k\delta$ for all k,

$$\gamma_i^{(k)}(t) \leqslant \begin{cases} f_1(t)\, e^{-\alpha t k \delta} & 0 \leqslant t \leqslant 1 \\ f_2(t)\, e^{-\alpha k \delta} & 1 < t \end{cases}$$

as before.

APPENDIX D
AVERAGE REFLECTION FROM DEPTH N

In this section, we make a calculation to indicate roughly the size of the effect one is trying to observe in the geophysical model described in Sec. II-E. In particular, we consider the magnitude of a reflection from a discontinuity at depth N. However, in order not to specialize the result to a particular sequence of impedance values, we compute the average reflection over the ensemble of all such sequences. In addition, the result is confined to the initial return, since this is the one used to make the initial decision on an impedance and thus determines whether the estimate will require correction.

Assume first that each impedance value is chosen independently and that the impedance at depth n, Z_n is Z_A or Z_B with probability one half. Assume also that $Z_1 = Z_A$. Then there are four possibilities for discontinuity at depth N:

	Z_{N-1}	Z_N
(1)	Z_A	Z_A
(2)	Z_A	Z_B
(3)	Z_B	Z_A
(4)	Z_B	Z_B

The first and the last give no reflection, while the other two do so. We thus consider (2) and (3) for reflections.

Suppose that $Z_{N-1} = Z_A$ and $Z_N = Z_B$. Since Z_1, Z_{N-1}, and Z_N are determined, there are $N - 3$ impedance values to be chosen at random. But for K sections there are K + 1 transitions between them, and thus there are $N - 2$ locations for possible reflection. In the case under current consideration, Z_1 and Z_{N-1} are both Z_A. Thus, if there are n transitions from A to B, there are n transitions back from B to A. These 2n transitions can be arranged among the $N - 2$ potential transition locations in $\binom{N-2}{2n}$ ways. Thus the probability of n transitions from A to B, assuming that Z_1 and Z_{N-1} are both Z_A, is $\binom{N-2}{2n} 2^{-(N-3)}$.

If there are n A to B transitions, and n B to A transitions for a signal moving in the direction of increasing depth, there are the same number of each in the direction of decreasing depth. Hence the transmission coefficient for an input pulse along a path to discontinuity at depth N from A to B with n other A to B transitions along the way is

$$T = T_{AB}^{2n} T_{BA}^{2n} \Gamma_{AB}$$

where T_{AB} is the transmission coefficient for a discontinuity from A to B, T_{BA} is the same quantity for the reverse case, and Γ_{AB} is the reflection coefficient for an A to B junction. Thus, over the ensemble of impedance value sets, the average transmission coefficient is

$$\overline{T} = \sum_{n=0}^{\frac{N}{2}-1} \binom{N-2}{2n} T_{AB}^{2n} T_{BA}^{2n} \Gamma_{AB} 2^{-(N-3)}$$

for N even. If this sum is carried out by using the binomial expansion,

$$\overline{T} = 2^{-(N-2)} \left[\left(1 + \frac{4r}{(1+r)^2} \right)^{N-2} + \left(1 - \frac{4r}{(1+r)^2} \right)^{N-2} \right] \frac{(1-r)}{(1+r)}$$

where $r = Z_A/Z_B$. The cases of N odd and the reversed discontinuity at depth N follow in a similar manner and give essentially the same result.

Since r is positive, the first term in the square brackets is the most significant for large N. Thus the return is exponentially decreasing with N, for N large.

ACKNOWLEDGMENTS

I should like to express my sincere thanks to Professor R. M. Fano, who not only provided the original motivation for this study but also patiently gave much encouragement and guidance. I should also like to express thanks to Professor R. G. Gallager for checking much of the mathematical detail and for many useful suggestions. Professor J. Weizenbaum's help with the SLIP language and the programs he provided made it easy to implement the storage technique used in the simulation. Thanks are also due to Professor J. M. Wozencraft and Mr. H. L. Yudkin for their helpful comments.

Further, I am extremely grateful to Lincoln Laboratory and to the Research Laboratory of Electronics for their support throughout the course of my graduate study. In addition, I should like to thank Project MAC for support in terms of computer time.

BIBLIOGRAPHY

1. R.M. Fano, "A Heuristic Discussion of Probabilistic Decoding," Trans. IEEE, PTGIT IT-9, 64 (1963).
2. C. E. Shannon and W. Weaver, Mathematical Theory of Communication (University of Illinois Press, Urbana, 1949).
3. W.W. Peterson, Error Correcting Codes (Technology Press and Wiley, New York, 1961).
4. J.M. Wozencraft, "Sequential Decoding for Reliable Communication," Technical Report 325, Research Laboratory for Electronics, M. I. T. (9 August 1957).
5. B. Reiffen, "Sequential Encoding and Decoding for the Discrete Memoryless Channel," Technical Report 231, Lincoln Laboratory, M. I. T. (12 August 1960), DDC247612.
6. R.M. Fano, "Class Notes for Advanced Topics in Information Theory," M. I. T. (1963).
7. S. S. Wilks, Mathematical Statistics (Wiley, New York, 1962).
8. W.M. Ewing, W.S. Jardetzky, and F. Press, Elastic Waves in Layered Media (McGraw-Hill, New York, 1957).
9. A. D. Bennet, "Study of Multiple Reflections Using a One-Dimensional Seismic Model," Geophysics 27, 61 (1962).
10. J. S. Steinhart and R. P. Meyer, Explosion Studies of Continental Structure (Carnegie Institute, Washington, D. C., 1961).
11. R. G. Gallager, "Class Notes for Advanced Topics in Information Theory," M. I. T. (1963).
12. G. H. Hardy, J. E. Littlewood, and G. Polya, Inequalities (Cambridge University Press, London, 1952).
13. F. J. Corbato, et al., The Compatible Time-Sharing System (M. I. T. Press, Cambridge, 1963).
14. J. Weizenbaum, "Symmetric List Processor," Commun. ACM 9, No. 6, 524 (1963).
15. A.W. Kaercher, "Random Number Generation: Normal Distribution – BOXNO," SHARE Distribution No. GC 0009 (April 1962).

JOINT SERVICES DISTRIBUTION LIST

Department of Defense

Dr Edward M. Reilley
Asst Director (Research)
Ofc of Defense Res & Eng
Department of Defense
Washington, D.C. 20301

Dr James A. Ward
Office of Deputy Director (Research and Information Rm 3D1037
Department of Defense
The Pentagon
Washington, D.C. 20301

Director
Advanced Research Projects Agency
Department of Defense
Washington, D.C. 20301

Mr Charles Yost, Director
For Materials Sciences
Advanced Research Projects Agency
Department of Defense
Washington, D.C. 20301

Defense Documentation Center
Attn: TISIA
Cameron Station, Bldg 5
Alexandria, Virginia 22314

Director
National Security Agency
Attn: C3/TDL
Fort George G. Meade, Maryland 20755

Department of the Army

Chief of Research and Development
Headquarters, Department of the Army
Attn: Physical Sciences Division P&E
Washington, D.C. 20310

Research Plans Office
U.S. Army Research Office
3045 Columbia Pike
Arlington, Virginia 22204

Commanding Officer
Foreign Service & Technology Center
Arlington Hall
Arlington, Virginia

Commanding General
U.S. Army Materiel Command
Attn: AMCRD-RS-PE-E
Washington, D.C. 20315

Commanding General
U.S. Army Strategic Communications Command
Washington, D.C. 20315

Commanding General
U.S. Army Materials Research Agency
Watertown Arsenal
Watertown, Massachusetts 02172

Commanding Officer
U.S. Army Ballistics Research Laboratory
Attn: V.W. Richards
Aberdeen Proving Ground
Aberdeen, Maryland 21005

Commandant
U.S. Army Air Defense School
Attn: Missile Sciences Division, C&S Dept.
P.O. Box 9390
Fort Bliss, Texas 79916

Commanding General
U.S. Army Missile Command
Attn: Technical Library
Redstone Arsenal, Alabama 35809

Commanding General
Frankford Arsenal
Attn: SMUFA-1310 (Dr Sidney Ross)
Philadelphia, Pennsylvania 19137

U.S. Army Munitions Command
Attn: Technical Information Branch
Picatinney Arsenal
Dover, New Jersey 07801

Commanding Officer
Harry Diamond Laboratories
Attn: Mr Berthold Altman
Connecticut Avenue and Van Ness Street N.W.
Washington, D.C. 20438

Commanding Officer
Harry Diamond Laboratories
Attn: Dr R.T. Young
Electron Tubes Division
Connecticut Avenue and Van Ness Street N.W.
Washington, D.C. 20438

Commanding Officer
U.S. Army Security Agency
Arlington Hall
Arlington, Virginia 22212

Commanding Officer
U.S. Limited War Laboratory
Attn: Technical Director
Aberdeen Proving Ground
Aberdeen, Maryland 21005

Commanding Officer
Human Engineering Laboratories
Aberdeen Proving Ground
Maryland 21005

Director
U.S. Army Engineer Geodesy,
Intelligence and Mapping
Research and Development Agency
Fort Belvoir, Virginia 22060

Commandant
U.S. Army Command and General Staff
College
Attn: Secretary
Fort Leavenworth, Kansas 66207

Dr. H. Robl, Deputy Director
U.S. Army Research Office (Durham)
P.O. Box CM, Duke Station
Durham, North Carolina 27706

Commanding Officer
U.S. Army Research Office (Durham)
Attn: CRD-AA-IP (Richard O. Ulsh)
P.O. Box CM, Duke Station
Durham, North Carolina 27706

Commanding General
U.S. Army Electronics Command
Attn: AMSEL-SC
Fort Monmouth, New Jersey 07703

Director
U.S. Army Electronics Laboratories
Attn: Dr S. Benedict Levin, Director
Institute for Exploratory Research
Fort Monmouth, New Jersey 07703

Director
U.S. Army Electronics Laboratories
Attn: Mr Robert O. Parker, Executive
Secretary JSTAC (AMSEL-RD-X)
Fort Monmouth, New Jersey 07703

Superintendent
U.S. Army Military Academy
West Point, New York 10996

The Walter Reed Institute of Research
Walter Reed Army Medical Center
Washington, D.C. 20012

Director
U.S. Army Electronics Laboratories
Fort Monmouth, New Jersey 07703
Attn: AMSEL-RD-DR NE SS
X NO PE
XE NP PR
XC SA PF
XS SE GF
NR SR ADT
FU#1

Commanding Officer
U.S. Army Electronics R&D Activity
Fort Huachuca, Arizona 85163

Commanding Officer
U.S. Army Engineers R&D Laboratory
Attn: STINFO Branch
Fort Belvoir, Virginia 22060

Commanding Officer
U.S. Army Electronics R&D Activity
White Sands Missile Range
New Mexico 88002

Director
Human Resources Research Office
The George Washington University
300 N. Washington Street
Alexandria, Virginia 22314

Commanding Officer
U.S. Army Personnel Research Office
Washington, D.C.

Commanding Officer
U.S. Army Medical Research Laboratory
Fort Knox, Kentucky

Department of the Air Force

Director
Air University Library
Maxwell A.F. Base, Alabama

Commander
Air Force Office of Scientific Research
Washington 25, D.C.
Attn:-SREE

Department of The Air Force
Headquarters-United States Air Force
Washington 25, D.C.
Attn: AFTAC/TD-1

Dr. Harvey E. Savely, SRL
Air Force Office of Sci. Res.
Office of Aerospace Research, USAF
Washington 25, D.C.

Mr. C.N. Hasert
Scientific Advisory Board
Hq, USAF
Washington 25, D.C.

APGC (PGBAP-1)
Elgin Air Force Base
Florida 32542

AFETR
(AFETR Tech. Library MU-135)
Patrick Air Force Base
Cocoa, Florida

Air Force Cambridge Res. Lab.
L.G. Hanscom Field
Bedford, Massachusetts 01731
Attn: CRDM, Mr. Herskovitz

Commander, AFCRL
Attn: C.P. Smith (CRBS)
L.G. Hanscom Field
Bedford, Massachusetts

Dr. L. C. Block
AFCRL (CROV)
L. G. Hanscom Field
Bedford, Massachusetts

AFCRL
Office of Aerospace Res., USAF
Bedford, Mass.
Attn: CRDA

Mr. Rocco H. Urbano, Chief
AFCRL, Appl. Math. Branch
Data Sciences Laboratory
Laurence G. Hanscom Field
Bedford, Massachusetts

AFCRL (CRFE-Dr. Nicholas Yannoni)
L.G. Hanscom Field
Bedford, Massachusetts

S. H. Sternick
Aerospace Comm. - Attn: ESNC
Waltham Federal Center
424 Trapelo Road
Waltham, Massachusetts 02154

Rome Air Dev. Center (RAWL, H. Webb)
Griffiss Air Force Base
New York 13442

Systems Engineering Group
Deputy for Systems Eng'g., SEPRR
Directorate of Tech. Pubs. and Specs.
Wright-Patterson AFB, OHIO 45433

Aeronautical Systems Division
Attn: ASRPE, Mr. Robt. Cooper
Wright-Patterson AFC, Ohio 45433

Aeronautical Systems Division
Attn: ASRPP-20 (Mr. Don R. Warnock)
Wright-Patterson AFB, Ohio 45433

AFAL
AVR (L)
Wright-Patterson AFB
Ohio 45433

Dr. H. H. Kurzweg
Director Research - OART
NASA
Washington, D.C. 20546

Systems Engineering Group (RTD)
Attn: SEPIR
Wright-Patterson AFB, Ohio 45433

AFAL (AVTE)
Wright-Patterson AFB
Ohio 45433

Mr. Roland Chase
National Aeronautics & Space Administration
1512 H Street, N.W.
Washington 25, D.C.

Professor Arwin Dougal
University of Texas
EE Department
Austin, Texas

Honorable Alexander H. Flax
Asst Secretary of the Air Force (R&D)
Office of the Secretary of the Air Force
Washington 25, D.C.

Professor Nicholas George
California Institute of Technology
EE Department
Pasadena, California

Dr. Lowell M. Hollingsworth
AFCRL
L.G. Hanscom Field
Bedford, Massachusetts

Dr. Zohrab Kaprielian
University of Southern California
University Park
Los Angeles 7, California

JOINT SERVICES DISTRIBUTION LIST (continued)

Dr. John M. Ide
National Science Foundation
Washington 25, D.C.

Lt Col Edwin M. Myers
Headquarters USAF (AFRDR)
Washington 25, D.C.

Professor Wm. H. Radford
Director, Lincoln Laboratories
Lexington, Massachusetts

Brig Gen B.G. Holzman, USAF (Ret.)
Electronics Research Center, NASA
30 Memorial Drive
Cambridge, Mass.

Dr. R. L. Sproull
Director, Advanced Research Projects
Agency
Washington 25, D.C.

Brigadier General J. T. Stewart
Director of Science & Technology
Deputy Chief of Staff (R&D)
USAF
Washington 25, D.C.

Mr. James Tippett
National Security Agency
Fort Meade, Maryland

Dr. H. Harrison
NASA (Code RRE)
Fourth and Independence Streets
Washington, D.C. 20546

AEC
Civ of Tech Info Ext
P.O. Box 62
Oak Ridge, Tenn.

AFRST (SC/EN)
Lt Col L. Stone
Rm 4C 341
The Pentagon
Washington, D.C. 20301

U.S. Atomic Energy Commission
Library
Gaithersburg, Md. 20760

ARL (ARD/Col R.E. Fontana)
Wright-Patterson AFB,
Ohio 45433

Office of Research Analyses
Attn: Col K.W. Gallup
Holloman AFB, NMex 88330

AFCRL (CRXL)
L.G. Hanscom Fld
Bedford, Mass 01731

Frank J. Seiler Rsch Lab
Library
USAF Academy, Colo 80840

ARL (AROL)
Wright-Patterson AFB,
Ohio 45433

Office of Research Analyses
Library
Holloman AFB, NMex 88330

LOOAR (Library)
AF Unit Post Office
Los Angeles, Calif 90045

Churchill Research Range
Library
Fort Churchill
Manitoba, Canada

Los Alamos Scientific Lab
Attn: Technical Library
Los Alamos, NMex 87544

Battelle Memorial Institute
Technical Library
505 King Avenue
Columbus, Ohio 43201

John Crerar Library
35 West 33rd St.
Chicago, Ill.

Linda Hall Library
5109 Cherry St.
Kansas City, Mo.

National Science Foundation
Library
1951 Constitution Ave., N.W.
Washington, D.C. 20550

JOINT SERVICES DISTRIBUTION LIST (continued)

Johns Hopkins University
Applied Physics Lab Library
White Oak
Silver Spring, Md. 20910

Stanford Research Institute
Library
820 Mission St.
South Pasadena, Calif. 91030

Southwest Research Institute
Library
8500 Culebra Road
San Antonio, Texas

ARPA, Tech Info Office
The Pentagon
Washington, D.C. 20301

DDR&E (Tech Library)
Rm 3C 128
The Pentagon
Washington, D.C. 20301

Industrial College of the
Armed Forces
Attn: Library
Washington, D.C.

AFIT (MCLI)
Tech Library
Wright-Patterson AFB
Ohio 45433

AUL 3T-9663
Maxwell AFB, Ala 36112

USAFA (DLIB)
USAF Academy, Colorado 80840

AFSC (Tech Library)
Andrews AFB
Washington, D.C. 20331

ASD (Tech Library)
Wright-Patterson, AFB
Ohio 45433

BSD (Tech Library)
Norton AFB, Calif 92409

ESD (ESTI)
L. G. Hanscom Field, F172
Bedford, Mass 01731

RTD (Tech Library)
Bolling AFC, D.C. 20332

AFFTC (Tech Library)
Edwards AFB, Calif 93523

AFMDC (Tech Library)
Holloman AFB, NMex 88330

AFWL (WLIL, Tech Library)
Kirtland AFB, NMex 87117

APGC (Tech Library)
Eglin AFB, Fla 32542

AEDC (Tech Library)
Arnold AFS, Tenn 37389

RADC (Tech Library)
Griffiss AFB, N.Y. 13442

Director
National Aeronautical Establishment
Ottawa, Ontario, Canada

CIA
OCR/LY/IAS
IH 129 Hq
Washington, D.C. 20505

National Defense Library
Headquarters
Ottawa, Ontario, Canada

Technical Library
White Sands Missile Range
NMex 88002

NASA/AFSS/1 FOB6
Tech Library, Rm 60084
Washington, D.C. 20546

Space Systems Division
Los Angeles Air Force Station
Air Force Unit Post Office
Los Angeles, California 90045
Attn: SSSD

U.S. Regional Science Office/LAOAR
U.S. Embassy
APO 676
New York, N.Y.

Ames Rsch Center (NASA)
Technical Library
Moffett Field, Calif 94035

High Speed Flight Center (NASA)
Technical Library
Edwards AFB, Calif 93523

Goddard Space Flight Center (NASA)
Greenbelt, Md. 20771

Geo. C. Marshall Space Flight
Center (NASA)
Redstone Arsenal, Ala 35808

Lewis Research Center (NASA)
Technical Library
21000 Brookpark Road
Cleveland, Ohio

Aerospace Corp (Tech Library)
P.O. Box 95085
Los Angeles, Calif 90045

Rand Corporation
1700 Main St.
Santa Monica, Calif 90401

Carnegie Institute of Technology
Science & Engineering Hunt Library
Schenley Park
Pittsburgh, Pa. 15213

California Institute of Technology
Aeronautics Library
1201 East Calif St.
Pasadena 4, Calif

AVCO Research Lab
Library
2385 Revere Beach Parkway
Everett, Mass 02149

Dr. G. E. Knausenberger
c/o Hq. Co. Munich Post
APO 09407
New York, N. Y.

Commander
Space Systems Division (AFSC)
Office of the Scientific Director
Inglewood, California

Commander
Aerospace Systems Division
AFSC
Office of the Scientific Director
Wright-Patterson AFB, Ohio

Commander
Aerospace Research Laboratories (OAR)
Office of the Scientific Director
Wright-Patterson AFB, Ohio

Commander
Air Force Cambridge Research Laboratories
Office of the Scientific Director
L. G. Hanscom Field
Bedford, Massachusetts

Commander
Air Force Systems Command
Office of the Chief Scientist
Andrews AFB, Maryland

Commander
Research & Technology Division
AFSC
Office of the Scientific Director
Bolling AFB 25, D.C.

Commander
Rome Air Development Center
AFSC
Office of the Scientific Director
Griffiss AFB, Rome, New York

Department of the Navy

Dr. Arnold Shostak, Code 427
Head, Electronics Branch
Physical Sciences Division
Department of the Navy
Office of Naval Research
Washington, D.C. 20360

Chief of Naval Research, Code 427
Department of the Navy
Washington, D.C. 20360

Chief, Bureau of Weapons
Department of the Navy
Washington, D.C. 20360

Chief, Bureau of Ships
Department of the Navy
Washington, D.C. 20360
Attn: Code 680

Commander
U.S. Naval Air Development Center
Johnsville, Pennsylvania
Attn: NADC Library

Library
U.S. Navy Electronics Laboratory
San Diego, California 92152

Commanding Officer
U.S. Navy Underwater Sound Laboratory
Ft Trumbull
New London, Connecticut

Director
Naval Research Laboratory
Washington, D.C. 20390

Commanding Officer
Office of Naval Research Branch Office
Navy 100, Fleet P.O. Box 39
New York, New York

Chief of Naval Operations
Pentagon OP 07T
Washington, D.C.

Commanding Officer
Officer of Naval Research Branch Office
495 Summer Street
Boston, Massachusetts 02110

Commander
Naval Ordnance Laboratory
White Oak, Maryland
Attn: Technical Library

U.S. Navy Post Graduate School
Monterey, California
Attn: Electrical Engineering Department